Experimental Investigation of Confined Vortex Flow in a Cylindrical Chamber of Aspect Ratio 1.5

Antonios Ioannou Georgantas

A Thesis

in

The Faculty

of

Engineering

Presented in Partial Fulfillment of the requirements

for the Degree of Master of Engineering at

Concordia University

Montréal, Québec, Canada

November 1983

ABSTRACT

EXPERIMENTAL INVESTIGATION OF CONFINED VORTEX FLOW IN A CYLIDRICAL CHAMBER OF ASPECT RATIO 1.5

Antonios Ioannou Georgantas

The experimental investigation of the confined vortex flow inside a cylindrical vortex chamber of aspect ratio (L/D) equal to 1.5, was carried out. A five-hole, Pitot-static pressure probe was used to perform quantitative measurements of the radial profiles of the velocity components, and of the static pressure along different axial levels of the cylindrical chamber. Three different air input configurations were analysed. In the first configuration, the air was introduced tangentially at the chamber end where the exit nozzle was located. In the second, the air was supplied at the opposite end of the chamber, while all the other geometric parameters were kept constant. Both the bottom and the top air inlets were used in the third configuration, so as to create a double vortex flow structure. The distinct features of the two individual single inlet vortex structures, top and bottom, were clearly exhibited in the double vortex flow pattern. The variation of the relative strengths of the top and bottom air supply was found to control the vertical level of a unique localized inward radial stream that was formed by the interaction of the two single vortices.

ACKNOWLEDGEMENT

The author is deeply indebted to his supervisors Dr. C.K. Kwok and Dr. T. Krepec for their constant enthusiasm and willingness to advise throughout the course of this project.

Thanks are due to the technical staff for the construction of the experimental apparatus, and also to colleagues and staff in the Mechanical Engineering Department for their valuable discussions and suggestions. Special thanks are extended to his friends, Mr. Khalid Abdol-Hamid and Mr. Constantine Athanasoulias for their help during the final stages of the preparation of this manuscript.

The author also wishes to express his gratitude to his family for their encouragement and understanding.

Finally, thanks go to the Natural Science of Engineering Research Council of Canada for their financial support, without which the present work would not have been possible.

TABLE OF CONTENTS

	Page:
ABSTRACT	iii
ACKNOWLEDGMENT	iv
TABLE OF CONTENTS	v
LIST OF FIGURES	viii
LIST OF PLATES	xii
LIST OF TABLES	xiii
NOMENCLATURE	xiv

CHAPTER 1

INTRODUCTION

1.1	General	1
1.2	The Nature of Swirling Flows	1
1.3	Classification of Swirling Flows	2
1.4	Areas of Interest and Practical Devices	9
1.4.1	Geophysical Flows	9
1.4.2	Magnetohydrodynamic (MHD) Applications	9
1.4.3	Advanced Nuclear Rocket Propulsion	11
1.4.4	Fluidic Devices	12
1.4.5	Cyclone Separator	14
1.4.6	Cyclone Combustors	14

CHAPTER 2

SWIRLING FLOWS - LITERATURE REVIEW

2.1	Introduction	20
2.2	General Characteristics	21
2.3	Cyclone Combustors	26

2.4 Confined Vortex Flow 30
2.5 Velocity and Pressure Measuring Techniques 34

CHAPTER 3

FORMULATION OF THE PROBLEM AND METHOD OF APPROACH

3.1 Background of the Present Work 45
3.2 Objectives and Program of Investigations 49

CHAPTER 4

ENGINEERING SPECIFICATIONS FOR THE TRANSPARENT CYCLONE CHAMBER DESIGN AND TESTING PROCEDURE

4.1 Design Specifications 53
4.2 Instrumentation and Measurements 61
4.3 Test Procedure 70
4.4 Data Reduction 71
4.5 Accuracy of Results 71

CHAPTER 5

EXPERIMENTAL RESULTS AND DISCUSSION

5.1 General 74
5.2 Single Vortex: Bottom Air Supply 74
5.2.1 Variations of the Flow Quantities Over the Radius and Height of the Cyclone 76
5.2.2 Effects of the Inlet Velocity 88
5.2.3 Effects of the Exit Nozzle Size 93
5.3 Single Vortex: Top Air Supply 99
5.4 Double Vortex 101

5.5 Some Analytical Considerations 104
5.5.1 Motion Governing Equations 104
5.5.2 Prediction of Static Pressure From the Experimental Tangential Velocity Profiles 106
5.5.3 Results 111

CHAPTER 6

THE AERODYNAMIC STRUCTURE OF THE VORTEX FLOW

6.1 Introduction 116
6.2 Vortex Streamline Construction 116
6.3 Single Vortex Structure: Top Inlet 118
6.4 Single Vortex Structure: Bottom Inlet 121
6.5 Double Vortex Structure 124
6.6 Visualization of the Double Vortex Structure 131
6.6.1 Smoke Visualization 133

CHAPTER 7

7.1 Conclusions 137
7.2 Future Work 139

REFERENCES 141

APPENDIX A: CALIBRATION OF THE ROTAMETERS USED TO MEASURE THE AIR SUPPLY TO THE TRANSPARENT CYCLONE CHAMBER 146

APPENDIX B: COMPUTER PROGRAM FOR DATA REDUCTION 154

LIST OF FIGURES

Fig. 1.1 Vortex flow 5

1.2 Rotating flow 6

1.3 Classification of swirling flows: Fluid Mechanics aspects 8

1.4 Classification of swirling flows: Thermodynamic aspects 10

1.5 Nuclear rocket proposed by Kerrebrock and Meghreblian (6) 13

1.6 Typical vortex valve (7) 13

1.7 Typical cyclone dust separator (7) 16

1.8 Trumpet-shaped swirl burner (4) 16

1.9 Typical cyclone combustion chamber with top air inlet (20) 17

2.1 Schematic of a short combustion cyclone chamber similar to that of Robert's, (2) 28

2.2 Schematic of a double-cyclone furnace (25,26,27) 31

2.3 Aerodynamics of a cyclone chamber (33) ... 35

2.4 Cylindrical-wedge, five-channel pressure probe 42

3.1 Double vortex chamber and gas flow pattern (24) 47

Fig. 4.1 Single Entry vortex chamber. Assembly drawing: Front half-cross section ... 57

4.2 Single Entry vortex chamber. Assembly drawing: Top half-cross section..... 58

4.3 Schematic arrangement of the transparent vortex chamber 60

4.4 Five channel pressure probe 64

4.5 Coordinate system and velocity components 65

4.6 Calibration curves for the 5-channel pressure probe 67

4.7 Typical manometer connections for the 5-channel pressure probe 68

5.1 Tangential velocity profiles 77

5.2 Axial velocity profiles 80

5.3 Annular control volume 84

5.4 Radial velocity profiles 86

5.5 Static pressure profiles 87

5.6 Tangential velocity profiles for different inlet velocities 89

5.7 Axial velocity profiles for different inlet velocities 91

5.8 Static pressure profiles for different inlet velocities 92

Fig. 5.9 Tangential velocity profiles for different exit nozzle sizes..... 94

5.10 Radial position of the maximum tangential velocity versus the exit nozzle radius..... 95

5.11 Axial velocity profiles for different exit nozzle sizes..... 97

5.12 Static pressure profiles for different exit nozzle sizes..... 98

5.13 Axial velocity profiles for single vortex with top inlet..... 100

5.14 Axial velocity profiles for the double vortex configuration of the cyclone chamber..... 102

5.15 Axial component of velocity in the double vortex chamber for two different air flow conditions..... 103

5.16 Localized radial velocity at the merging level of the two vortices..... 105

5.17 Experimental and predicted tangential velocity profiles 112

5.18 Experimental and predicted static pressure profiles for exit nozzle size, D_e=0.3D..... 114

5.19 Experimental and predicted static pressure profiles for exit nozzle size, D_e=0.2D..... 115

6.1 Single vortex structure; top inlet configuration. Air flow rate: 1.98 SCMM, (70 SCFM) 119

6.2 Single vortex structure; bottom inlet configuration. Air flow rate: 2.83 SCMM, (100 SCFM) 122

Fig. 6.3 Double vortex structure; Q_B/Q_T=1.22. Air flow rate: 2.83 SCMM (100 SCFM)..... 125

6.4 Double vortex structure with prevailing bottom flow. Q_B/Q_T=1.5. Air flow rate: 2.83 SCMM (100 SCFM)..... 127

6.5 Double vortex structure. Q_B/Q_T=1. Air flow rate: 2.83 SCMM (100 SCFM)..... 128

6.6 Double vortex structure with top flow prevailing. Air flow rate: 2.83 SCMM (100 SCFM). Q_B/Q_T=0.67..... 129

6.7 Vertical position of the localized radial velocity zone versus the bottom to top flow ratio..... 132

A.1 Top inlet air flow rate; Calibration curve... 149

A.2 Bottom inlet air flow rate; Calibration curve for the combined air flow rate of rotameters B and C..... 153

LIST OF PLATES

Plate:	4.1	Double Entry Vortex Chamber	59
	4.2	Rotameters for the Measurement of the Volumetric Air Flow Rates at the Top and Bottom Inlets.	63
	4.3	Traversing Mechanism and Inclined Manometers.	69
	6.1	Smoke Visualization of the Double Vortex Air Flow Pattern	135
	6.2	Double Vortex Smoke Pattern after Smoke Diffusion	136

LIST OF TABLES

Table; A.1 Calibration of Rotameter A 148

A.2 Calibration of Rotameters B and C 152

NOMENCLATURE

A - area, m^2

A_i - area of a single inlet port, m^2

C - constant

C_p - pressure recovery factor

D - diameter of vortex chamber, m

D_e - diameter of exit nozzle, m

D_o - diameter of single inlet port, m

f - body force per unit volume, Nt/m^3

H - vertical distance between the top and bottom inlets, m

h - vertical distance from bottom inlet, m

K - constant

K_1 - constant, $V_\phi r^n$ (potential vortex)

K_2 - constant, $V_\phi r^n$ (forced vortex)

N - number of experimental points

n - tangential velocity power law exponent

P - pressure, Nt/m^2

P_1 - pressure sensed by the center hole of the probe, Nt/m^2

P_2, P_3 - pressure sensed by the lateral holes of the probe (determine the yaw angle), Nt/m^2

P_4, P_5 - pressure sensed by radial holes of the probe (determine the pitch angle), Nt/m^2

P' - gage pressure, Nt/m^2

P* - normalized pressure, $(Ps - P_{atm}) / ((Ps)_w - P_{atm})$

P_c - pressure at $r = r_{max}$, Nt/m^2

P_s - static pressure, Nt/m^2

P_t - total pressure, Nt/m^2

Q - volumetric air flow rate, SCMM

Q_B - bottom inlet volumetric air flow rate, SCMM

Q_T - top inlet volumetric air flow rate, SCMM

Q_a - net volumetric air flow rate through surface "a", m^3/sec

Q_b - net volumetric air flow rate through surface "b", m^3/sec

Q_c - net volumetric air flow rate through surface "c", m^3/sec

R - radius of the vortex chamber, m

Re - Reynolds number

$(Re)_r$ - radial Reynolds number, $V_r \cdot r/\nu$

r, ϕ, z - cylindrical coordinates

r^* - dimensionless radius, r/R

r_e - radius of exit nozzle, m

r_{max} - radius of maximum tangential velocity, m

T - temperature, ^oK

t - time, sec

S - swirl number, $\frac{De\ D}{4\ D_o^2}$

V - absolute velocity, m/sec

V_r - radial velocity component, m/sec

V_ϕ - tangential velocity component, m/sec

V_z - axial velocity component, m/sec

X_i - $\log r_i$

Y_i - $\log V_{\phi i}$

Z - axial station

Greek Letters

α - yaw angle, degrees

β - pitch angle, degrees

Γ - circulation, $\int_c \vec{V} \cdot d\vec{s}$

Δ - increament

Δh - axial distance between two adjacent measuring stations, m

μ - dynamic viscosity, $\frac{Nt - sec}{m^2}$

ν - kinematic viscosity, $\frac{m^2}{sec}$

ρ - density kg/m^3

Σ - summation

Ψ - stream function, $\int_o^r rV_z \, dr$, $\frac{m^3}{sec}$

Ψ_w - stream function at the side wall, $\int_o^R rV_z \, dr$, $\frac{m^3}{sec}$

ψ - non-dimensional stream function, $\frac{\Psi}{\Psi_w}$

Ω - vorticity $\vec{\nabla} \times \vec{V}$

Subscripts

a - surface "a"

atm - atmospheric

act - actual

B - bottom inlet

b - surface "b"

c - surface "c"

circ - in circulation

e - exit plane

i - experimental point "i"

o - inlet value

max - at maximum tangential velocity

s - static

sc - scale reading

T - top inlet

t - total

w - value at the periphery of the chamber

Superscripts

$\bar{}$ - average quantities

* - dimensionless quantities

$'$ - gage

CHAPTER 1

INTRODUCTION

1.1 General

Swirling flow has become recently a subject of intensive research in the world of technological and scientific developments. In the last three decades numerous applications involving the swirling flow phenomena, have resulted in a widespread interest in this field by many prominent scientists. The range of applications comprises many specialized fields such as high intensity combustion, heat transfer, advanced nuclear rocket propulsion, turbomachinery, fluid controls with specialization in the "Fluidics" technology, magneto-hydrodynamics and meteorology.

In this chapter, an attempt will be made to describe the phenomena related to swirling flows as they are presently understood in view of recent developments.

1.2 The Nature of Swirling Flows

Local vorticity effects are found to be present in almost all types of fluid flows. It is the global vorticity ($\vec{\nabla} \times \vec{V}$), however, that characterizes the swirling

type of flow.

The occurrence of many natural phenomena such as typhoons, whirlwinds, tornadoes hurricanes, waterspouts, whirl-pools etc., demonstrate the character of the swirling type of fluid motion. As simple as it may seem, however, swirling flow is a fluid motion of great complexity. It has velocity components in all three directions and engenders secondary flows when confined within solid boundaries. Its static pressure, density and temperature change as the fluid flows spirally toward its center of rotation.

1.3 Classification of Swirling Flows

The interaction of a swirling type of flow with different physical boundaries results in very diverse flow conditions. That is to say, a unique flow pattern is obtained for every different type of physical boundary. With respect to different geometrical configurations, the swirling flows are classified into three major categories [1]:

a) vortex flows

b) rotating flows

c) curved flows

a) The first class, vortex flows, Fig.1.1, can be subcategorized into "confined" and "free" vortex flows. The confined vortex is contained within solid boundaries while the free vortex moves and expands in a quiescent atmosphere. Confined vortices are usually contained inside cylidrical, conical or spherical chambers and are generated by passing the fluid through tangential inlet ports located at the side wall of the chamber. The fluid enters the chamber, which is usually referred to as "vortex or cyclone chamber", at its periphery and spirals toward its axis of rotation. It escapes the chamber through an exit nozzle that is usually located concentrically at either end of the chamber. As the flow emerges from the exit nozzle, it expands into a conical shape. Its angular momentum is dissipated further downstream as it interacts with the stagnant atmosphere. A free vortex is developed at the exit nozzle of such vortex chamber. Free vortex flow can also be generated by inserting swirl vanes at the exit of an axial flow, or by passing fluid through the annulus created between two concentric tubes being in relative angular motion. Both, the free and the confined vortices, are basically comprised of two elementary types of flow, Fig.1.1:

- forced vortex flow
- potential vortex flow

The tangential velocity fields of these two basic flows can be described in terms of a simple mathematical power law [2,3,4] as:

$$V_\phi r^n = K \qquad (1.1)$$

where, K is a constant and n is the tangential velocity power law exponent. For the case when n is equal to -1 this relationship describes the forced vortex flow in which the tangential velocity varies linearly with the radial distance from the center of rotation. This type of vortex demonstrates a solid body rotation (constant vorticity). When n becomes +1, (an ideal case), the potential type of vortex flow, sometimes referred as "free", is represented. The main characteristic of the potential vortex is that, it conserves the angular momentum as the fluid particles progressively move toward smaller radii of rotation, (a "circulation preserving" flow). Values of the exponent n in a range of $-1 < n < 1$ represent other types of swirling flows where the frictional and other restraining effects do not allow the tangential velocity to maintain its otherwise high values. Usually a typical vortex flow is comprised of these two elementary parts, the forced flow and the potential flow, which combine at a common boundary to form the so-called "Rankine" or "Combined Vortex". The central part of this vortex, exhibits a "solid body" rotation (forced vortex), and constitutes the core of the vortex, while the outer region exhibits a circulation preserving

type of vortex flow (potential vortex). The core exists in the center of the overall vortex as a physical solution to the potential vortex singularity at the center of rotation.

b) The second class of swirling flows, the rotating flow, Fig.1.2, is essentially a forced type of vortex flow with constant vorticity and with no zones where circulation is preserved when the flow is fully developed. The rotating flow is usually generated by the viscous action within the fluid layers when the flow boundaries rotate with a uniform angular velocity. With respect to the geometric confinement, rotating flow is subcategorized into:

- internal flow
- external flow

Internal flow is usually generated inside a simple or an annular rotating tube, while external rotating flow is formed on a variety of rotating surfaces such as free disks, cylinders, spheres, cones, etc.

c) Finally, the third class of swirling flows, the curved flow, is basically the boundary flow of fluid past concave or convex walls, or the fluid flow through

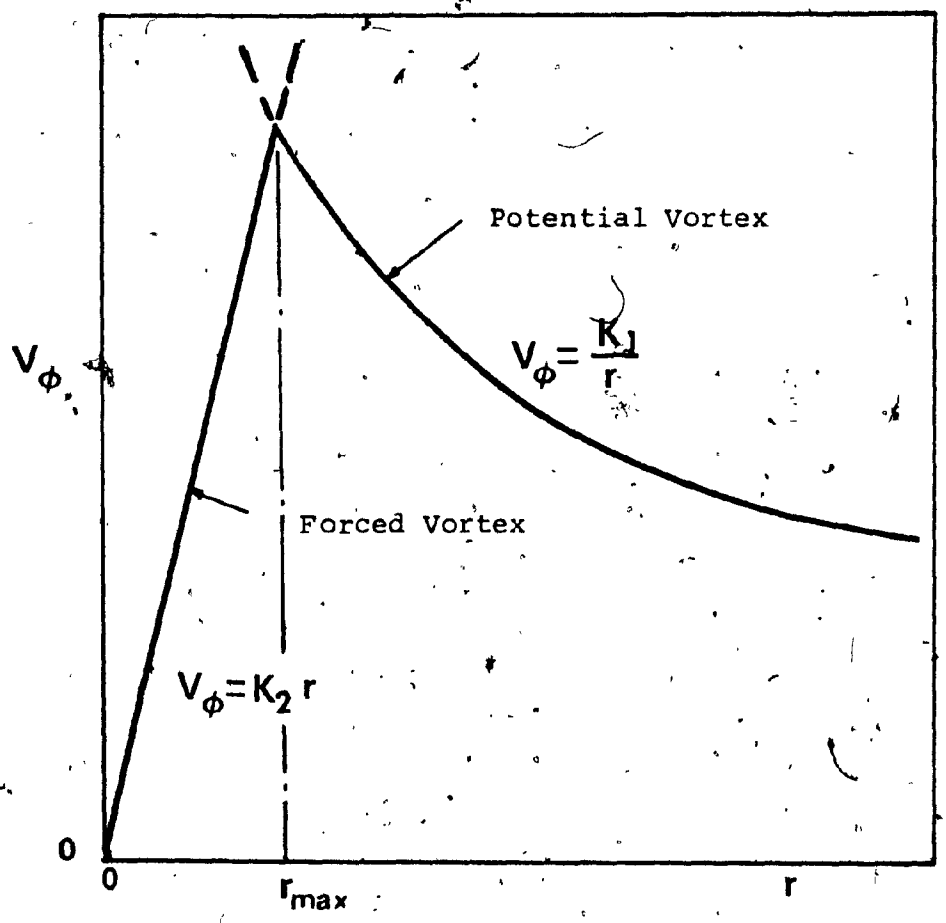

Fig. 1.1 Vortex flow

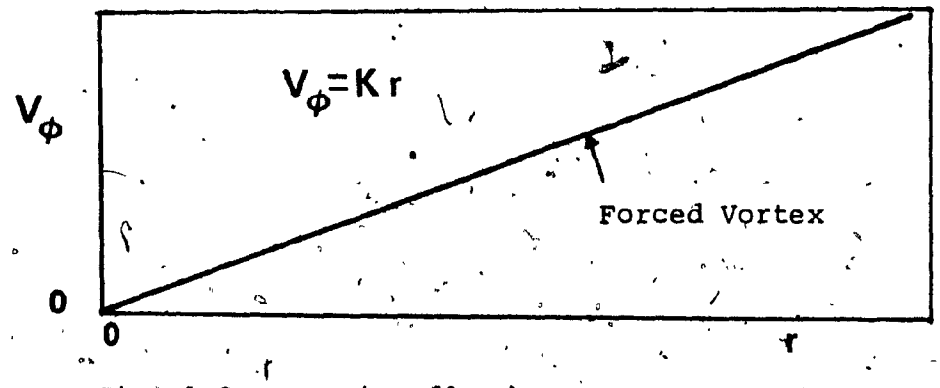

Fig. 1.2 Rotating flow

helically-formed tubes.

The above classification of the swirling flows is summarized in Figure 1.3. A further classification of swirling flows can be made from the thermodynamic point of view [1]. With respect to the energy transfer across the confining boundaries, the flow may be:

- adiabatic, or

- diabatic

In the adiabatic case, heat is not crossing the vortex boundaries, while in the diabatic, thermal energy is being transferred. Chemical energy may be released within the flow by means of an exothermic chemical reaction, in which case the system is referred to as "reacting", while on the other hand, chemical energy may not be released, and in that case, the flow is classified as "non-reacting" or "inert". The flow can be assumed to be isothermal or nearly isothermal in the latter case. The flow, however, can become non-isothermal, although inert, in certain applications where cooling effects are obtained by an energy separation process within the flow, (Ranque-Hilsh tube). The non-reacting flow, furthermore, can be diabatic when a thermal energy difference between the fluid and the

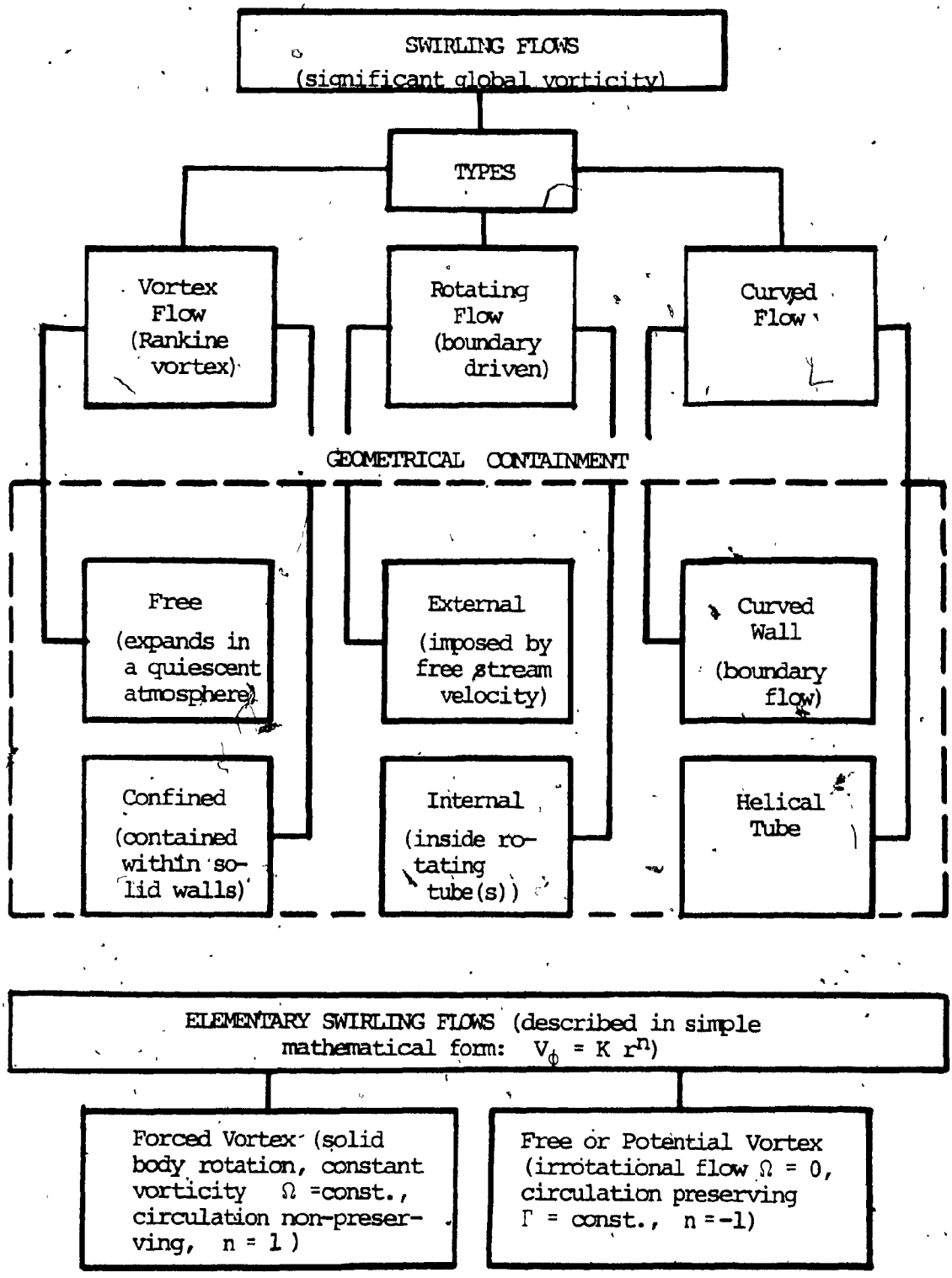

Fig. 1.3 Classification of swirling flows: Fluid Mechanics aspects

confining walls exists. The above thermodynamic classification of the swirling flow is summarized in Figure 1.4.

1.4 Areas of Interest and Practical Devices

For the sake of completness of the present chapter, selected areas of interest related to swirling flows as well as some of the most important applications are discussed in this section.

1.4.1 Geophysical Flows

Large scale atmospheric vortex motions which usually are of destructive nature, have made the study of vortex flow of great importance to meteorologists. The knowledge of the vortex behaviour can be very helpful in the prediction of the path of large scale natural vortices such as tornadoes and hurricanes, basing on velocity, pressure and temperature measurements (from an aircraft) inside the vortex core. Early warnings could ,as a result,be conveyed to populated areas.

1.4.2 Magnetohydrodynamic (MHD) Applications

Magnetohydrodynamic power may be produced as a hot electrically conducting gas is injected tangentially inside

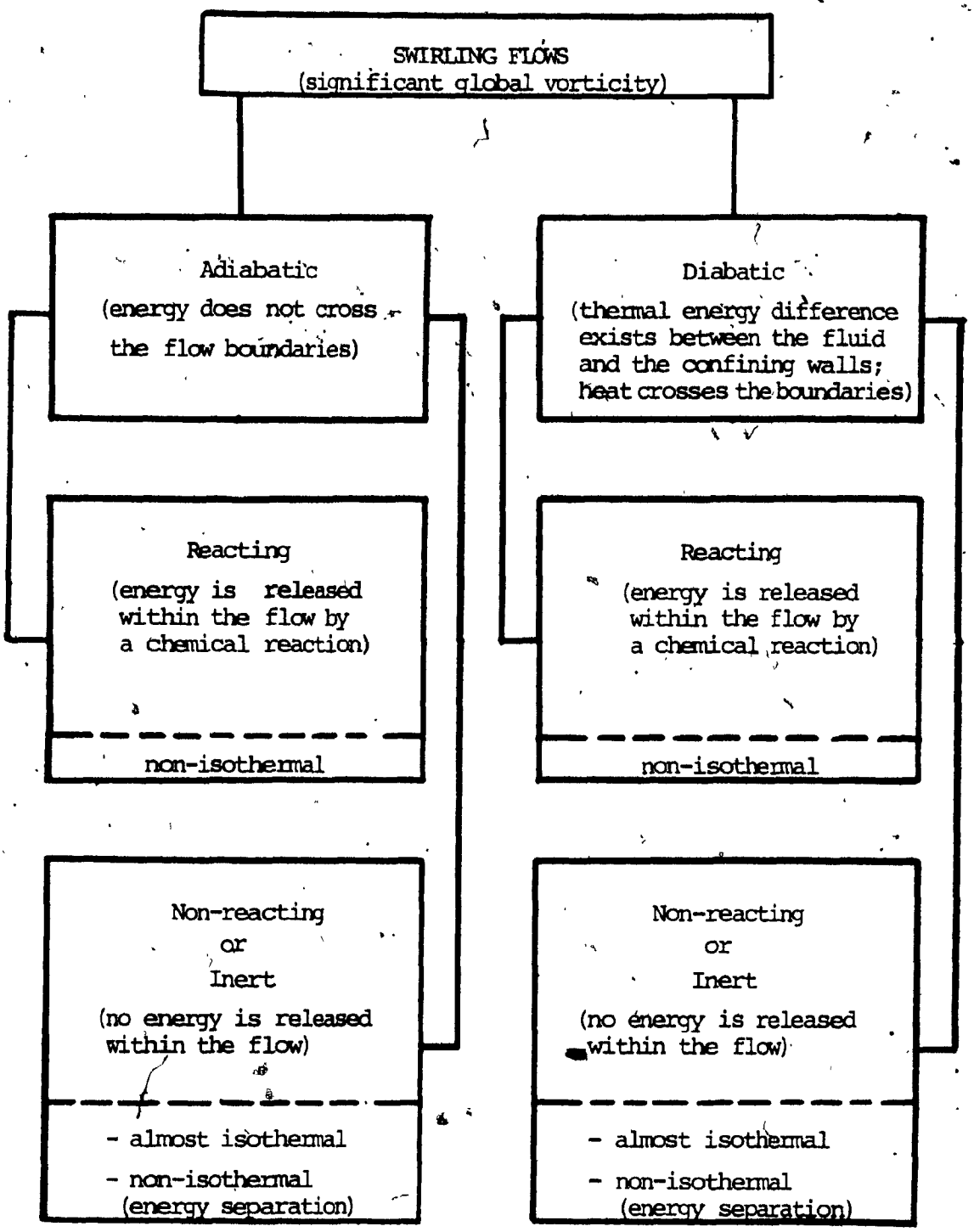

Fig. 1.4 Classification of swirling flows: Thermodynamic aspects

the annulus formed by two concentric electrodes [4,5]. The interaction of the gas flow with a uniform axial magnetic field passing between the two electrodes sets up a radial electric field which in turn causes an electric current to flow. The concept of the vortex generator is more promising, as compared with the classical linear channel, because of the compactness of the arrangement and of the lower flux of gas required to achieve the same relative velocities.

1.4.3 Advanced Nuclear Rocket Propulsion

Around 1961, Kerrebrock and Maghreblian [6] proposed the use of vortex flow in order to suspend an annulus of gaseous nuclear fuel inside the cylindrical chamber of a newly conceived rocket engine, Fig.1.5. The energy released by the fission reaction would be used to heat up a tangentially entering propellant such as hydrogen. Due to the large difference in density between the propellant and the gaseous fuel, the propellant would diffuse radially inward and then it would move axially out of the rocket engine. Fissionable material would also have to be introduced together with the propellant in order to compensate for any fuel losses. A good knowledge of the confined vortex flow pattern, however, would be essential for the proper assesment of the above concept. McCafferty [8,9] in 1968 and 1969 reviewed the evolution of the vortex

containment concepts with regard to the rocket engine application.

1.4.4 Fluidic Devices

With the advent of the Fluidics technology many ingenious devices utilizing the vortex phenomena have been developed. The flow of a fluid can be controlled by such devices without the employment of mechanically moving parts. The most basic of these devices is the "vortex valve", Fig.1.6, which is used to increase the resistance to the fluid passing through the valve by introducing a swirl motion to its inflow by a small tangential "control" flow injected at the outer edge of the valve chamber. Another example of a flow modulating device is the "vortex diode", where a much greater pressure drop is required for the flow in one direction than in the opposite.

A novel instrument used to measure volumetric flow rates is the "vortex flowmeter" [10]. It is basically comprised of a ball, driven by a swirling flow in a thin chamber. The frequency of revolution of the ball is calibrated to provide a measure of the volumetric flow rate.

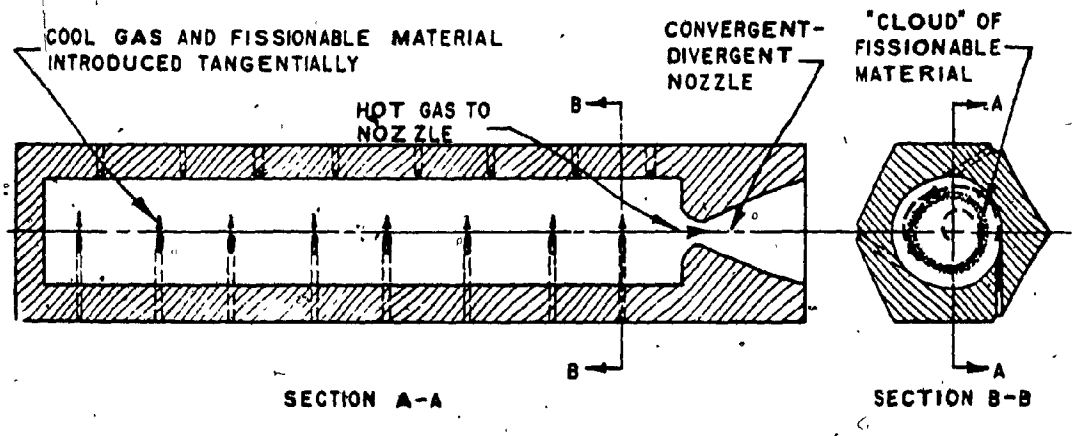

Fig. 1.5 Nuclear rocket proposed by Kerrebrock and Meghreblian (6)

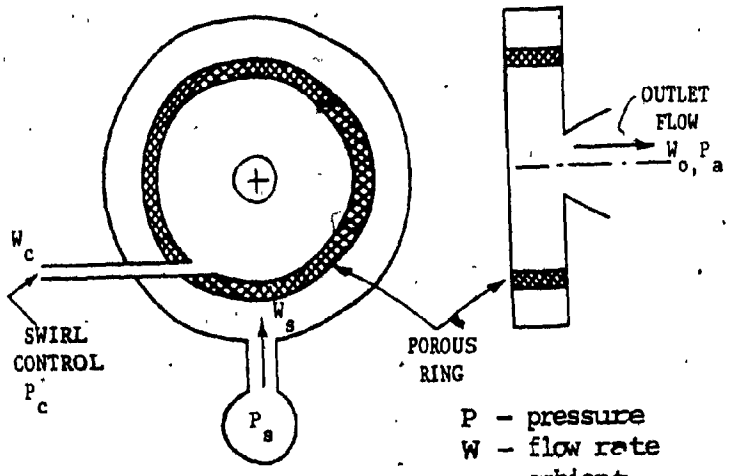

Fig. 1.6 Typical vortex valve (7)

1.4.5 Cyclone Separator

The cyclone separator is considered to be the most useful and the most widespread application of the confined vortex flow, Fig.1.7. It is basically used for the removal of solid particulates from gases. Due to the pressure decrease in smaller cross sectional diameters of the conically shaped chamber, a pressure gradient exists along the side wall, which induces a downward flow of the boundary layer. Particles kept at the wall by the centrifugal force are thus drifted toward the dust collector at the bottom part of the arrangement, Fig.1.7. Particles size in the order of a few microns can be separated by this method. The diameter of the dust collector at the bottom of the separator is of the same order as the exit nozzle diameter.

1.4.6 Cyclone Combustors

Swirling flows have a stabilizing effect upon flames and have been used for many years in high-intensity combustion processes. It has been observed that the introduction of swirl motion enhances the turbulence level and results in a more efficient combustion. High rates of entrainment of the ambient fluid at the recirculation zones result in fast mixing of the fuel with the oxidizer and the

product gases, thus considerably improving the performance of the combustor. The two principal types of combustors using the swirling flow concept are:

a) the swirl burner

b) the cyclone combustion chamber

The first type of combustor, the swirl burner shown in Figure 1.8, is basically comprised of a vortex chamber for generation of swirl and a trumpet-shaped nozzle that exhausts into a furnace. Combustion occurs in a short toroidal recirculation zone formed just outside the burner exit. Oil burners have been widely investigated and recently gas-swirl burners have become also a subject of interest to the fuel technologists [4].

In the second type, Fig.1.9, the major part of the combustion process occurs inside a vortex chamber. Large reverse flow zones engendered by the vortex flow, increase the residence time of the fuel, thus making this type of combustor particularly suitable for the combustion of poor quality low grade coals [2].

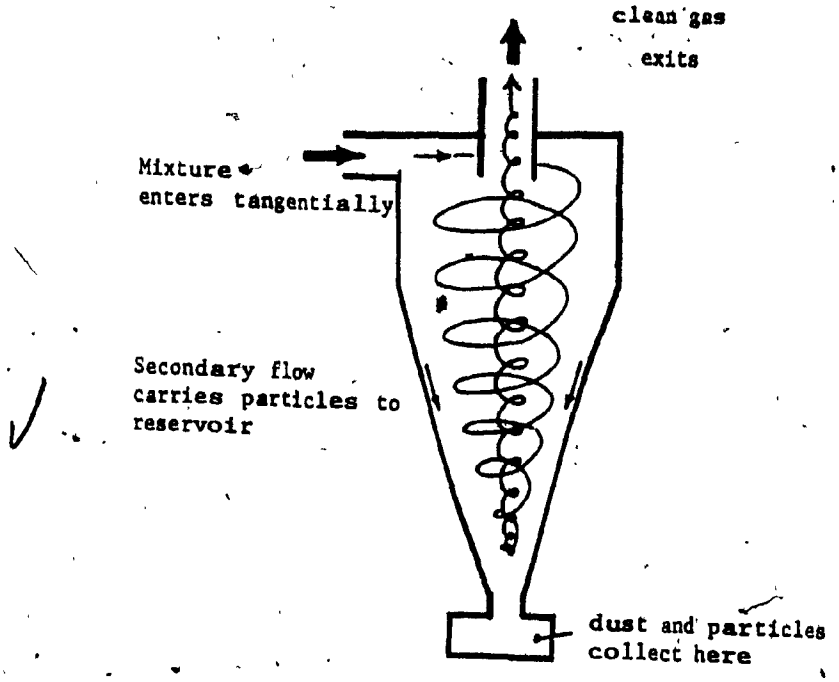

Fig. 1.7 Typical cyclone dust separator (7)

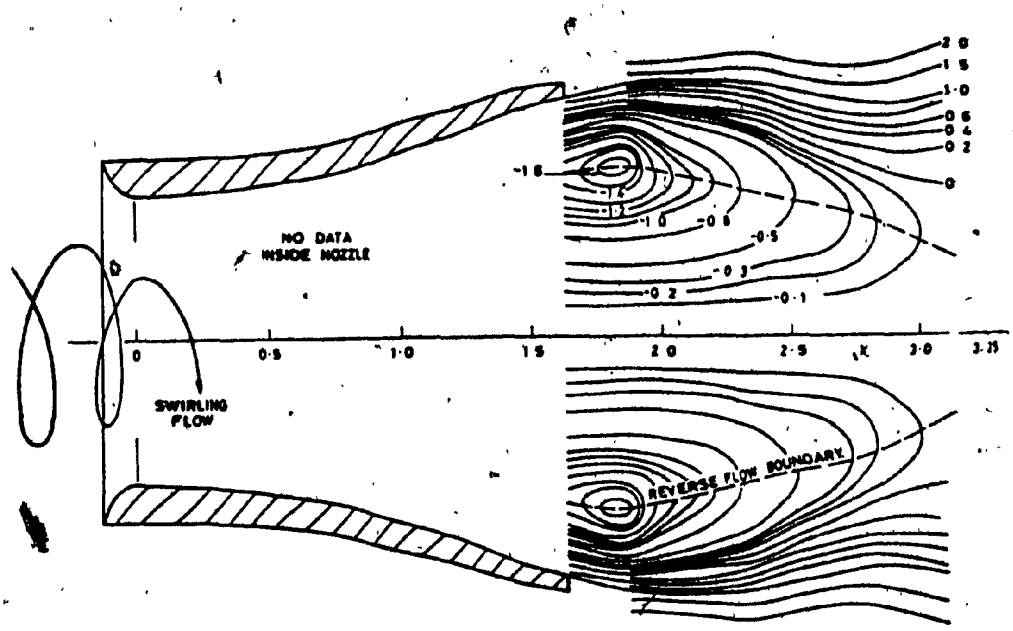

Fig. 1.8 Trumpet-shaped swirl burner (4)

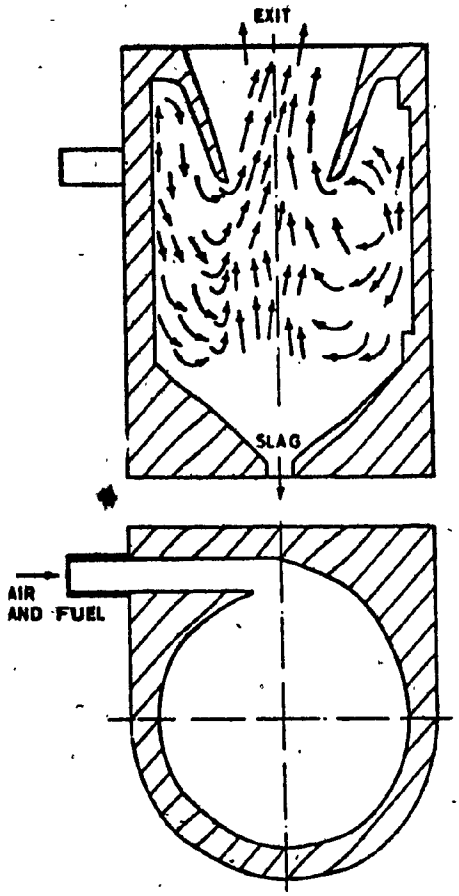

Fig. 1.9 Typical cyclone combustion chamber with top air inlet (20)

1.4.7 Energy Production from Solid Waste Using the Cyclone Incinerator

Solid wastes possess significant heating value, about 12000 kJ/kg [1], and recently, due to the oncoming shortage of hydrocarbon fuels, municipal and industrial disposals have been considered as a viable alternate energy resource. Proposals of procedures for the recovery and use of energy from solid wastes include the incineration in cyclone furnaces using specially designed vortex combustion chambers. This scheme offers a very efficient volume reduction of the waste, about 94% [1], and at the same time offers the prospect of useful heat recovery (mainly by the production of steam). Another scheme proposes the use of the combustion gases to drive specially designed gas turbine engines. Air pollution is, of course, a disadvantage of this proposal, and techniques to minimize this problem must be developed. Presently, proper treatment of the flue gases with electrostatic precipitators tends to diminish this problem.

Solid waste can be also mixed with conventional fuels in order to create more stable combustion conditions. The incineration process can be effected by the conventional stoker-firing, or by the much more efficient techniques of suspension-burning that have been developed

recently and which employ the vortex combustion concept [11,12,23].

CHAPTER 2

SWIRLING FLOWS- LITERATURE REVIEW

2.1 Introduction

Both analytical and experimental studies have been undertaken by many investigators in an attempt to yield more insight into the mechanisms that govern the motion of swirling flows. In the last three decades the number of publications on the subject has been enormous. Studies made in many different areas of application have examined this phenomenon from quite diverse perspectives.

An attempt to make a literature survey that would cover all these areas is not within the scope of the present investigation. However a general review of topics with primary interest to the present work will be considered.

The literature survey will be separated into four parts. In the first part, review of some general aspects of the swirling flow will be made. Next, the suspension burning of solid fuels inside cyclone chambers will be considered. In the third part, the confined vortex flow inside cylidrical chambers of different structural configurations will be reviewed. Finally, an account of

the most common experimental techniques for quantitative measurements in swirling flow systems will be given.

2.2 General Characteristics

With recent advances in the experimental and theoretical techniques for the analysis and modeling of swirling flows, this field has become a science in itself. Despite the great amount of work done in this area, little is still known about these phenomena. Most of the mechanisms that determine the behaviour of the swirling flow in all of its different forms, have not yet been properly described. Many important aspects of this type of flow are incomprehensible and are usually explained in rather loose terms. This is primarily due to the fact that this flow, by its very nature, is a highly complex phenomenon. Instabilities and transitions from laminar to turbulent state are inherent in rotating flows.

Before a breakthrough can be made in this field, advances into some still obscure aspects of the science of fluid mechanics itself have to be made. Even in more simple fluid mechanics problems such as the theoretical treatment of simple boundary layers, proper analysis is still very much unmanageable. That analysis, however, becomes even more complex for diabatic exothermal reacting systems where "thermal" boundary layers also have to be

considered.

With regard to our present understanding of the turbulent combustion processes, even without swirl, J. Swithenbank [13] made certain rather not encouraging remarks (as quoted from reference [1]):

> "
> .... It is widely thought that we understand the industrial combustion processes, and it is this myth which I wish to explode....
>
> .... We do not even know the turbulence level nor its distribution in any industrial combustor. We have no satisfactory theory which accounts for turbulent flame speeds in gaseous systems.... our prediction of convective heat transfer to combustor walls are, to say the least, inaccurate, while the true effects of the unsteady gas temperatures on radiant heat transfer are a long way from comprehension".

It can be inferred from the above, that swirling flows in combustion systems still remain very much an unsolved science.

There is a great deal of controversy with regard to

the significance of experimental work on the subject. The question arises if meaningful data can be obtained by the insertion of probes into the vortex flow, as their presence modifies the fluid flow field. With the development, however, of the Doppler Laser Anemometer for velocity measurements, this problem may be resolved very soon. Meaningful data, even in conflagrant flows, should be forthcoming.

There are several sources of difficulty in the analysis of swirling flows. Murthy [15] among other remarks pointed out that, dimensional parameters can not fully define the fluid rotation. He writes:

> " ....Similarity parameters for confined vortex flows are beset with a great number of difficulties. Such difficulties arise because changes in the geometrical configurations can not simply be accounted for by changes in the geometrical non-dimensional parameters based upon characteristic lengths. ....The occurance of such phenomena is not subject to simple scaling laws".

The above remark indicates that different geometries are difficult to corelate, and as quoted in [1], E.

Soehngen commented :

> " Experimental vortex flows are like their maker; each is one- of- a- kind".

There are many aspects, however, of confined vortex flows related to the experimental and analytical results on which most investigators agree. These were noted by Bank and Gauvin [16,17] and by Reydon and Gauvin [18,19], and the most significant are summarized herein:

(a) The tangential velocity component is predominant and the radial velocity component is relatively very small in the entire vortex flow.

(b) An important axial flow occurs in the annular region adjacent to the wall. Some investigators observed also a substantial axial flow in the maximum tangential velocity region.

(c) The axial velocity may show a reversal near the axis of the vortex chamber.

(d) The tangential velocity component profile is

composed mainly of two regions: a peripheral region of quasi-free vortex and a central region of quasi-forced vortex flow.

(e) The static pressure is relatively high near the vortex flow confining walls and decreases drastically near the axis, where it reaches its minimum".

Reviews related to specialized topics, such as suspension burning and heat recovery from wastes, pulverized fuel vortex combustion, and vortex gas burners have been made by Holman and Razgaitis [1], Roberts [2], and Smithson [4] respectively. Lewellen [7] on the other hand, in his review of "confined vortex flows" gives an almost complete account of our present knowledge of this type of flow. In his work he included a bibliography of more than four hundred papers. Although he resorts mostly into mathematical considerations, his work is complete in most respects and it can be viewed as a fundamental reference for the study of the subject. Syred and Beér [20], gave a lengthy review of combustion in swirling flows. In their work they traced the progress up to date of our understanding and of applying the concept of swirling flows.

2.3 Cyclone Combustors

Vortex flows inside cylindrical chambers have been the subject of interest to many scientists for the last 55 years. Lander [21] was the first to file a British Patent in 1928 on the vortex phenomena related to the physical and chemical processes in cylindrical containers. He made experiments in a water filled cylindrical tank discharging through a small orifice at the bottom end. He observed that solid particles of different sizes when inserted into the tank, were rotating at different radii for a certain speed of rotation. He concluded that the radial drag force of the inward flow was balanced by the centrifugal force, and that made the solid particles to rotate at selected diameters being functions of their sizes.

Harley [22], in a series of studies (1929-1935) attempted to utilize that concept in order to develop a combustion chamber to burn pulverized coal for firing of small boilers. After extensive research, he concluded that high heat release rates and high combustion efficiencies could be obtained by the utilization of the vortex concept in combustion chambers. An attempt was consequently made by U.S. scientists to develop a coal fired gas turbine by using Harley's vortex combustor. This work was, however, stopped as attention was diverted to the possibility of

alternate designs of combustion chambers [2].

The progress in research and developement of low-grade coal vortex combustion chambers, led to many advances in the field of swirling flows during the years after this concept was first introduced by Lander [21]. The first full-scale cyclone chamber was built at the Colument Station of the Commonwealth Edison System in September 1944 [1]. The chamber had a 2.44-meter (8-foot) diameter and was 3.35-meters (11-feet) high. The specific output of that system was very high. It reduced the weight and volume of the furnace, as compared to other systems with the same power output, by 22% and 33% respectively. Due to the success of this first vortex application in a combustion system, many other configurations were studied. Presently there are more than 600 large-scale cyclone combustors built in the U.S. alone.

Recent research on the subject of vortex combustion includes the work of Robert [2], who performed experimental and theoretical studies in a short vortex chamber, (L=0.13 m (0.42 ft), D=0.81 m (2.67 ft)), Fig.2.1, designed to burn pulverized coal. He developed an analytical model to determine the equilibrium state of spherical particles inside the chamber when introduced tangentially at the periphery of the chamber. To simplify his analysis he assumed a 2-Dimensional flow field and found that spherical

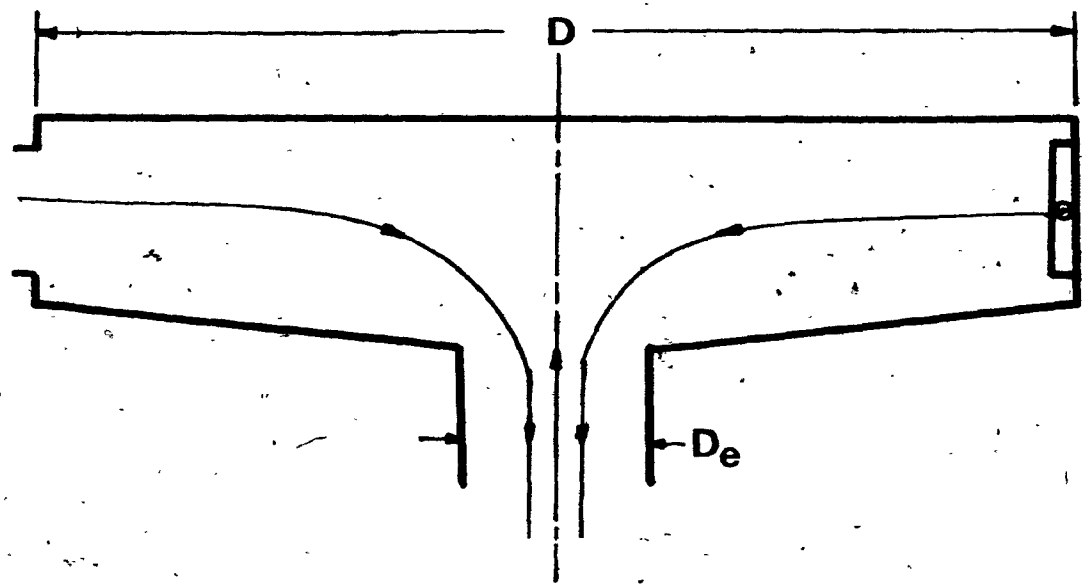

Fig. 2.1 Schematic of a short combustion cyclone chamber similar to that of Robert's (2)

particles up to 80 microns could be retained inside his chamber at combustion conditions. About 70% of the particles (sizes greater than 86 microns) would reside at the periphery of the chamber.

Holman and Razgaitis [1] analysed the effectiveness of a heat recovery system applied in a vortex incineration furnace. Copper tubing that carried water as cooling medium, was wrapped spirally around a cylindrical column that was attached to the exit of a short cylindrical vortex chamber. Industrial refuse was proposed to be used as the fuel, but due to fuel feeding problems, propane was used instead, as in their research, priority was given to the heat recovery concept rather than to the combustion process. Despite few shortcomings, such as large volume of the system, the heat recovery concept in cylindrical cyclone chambers was found to offer a viable option.

Krepec and Kwok [23] used a simplified flow pattern approach, similar to that of Roberts [2], in order to optimize the operating conditions of a double-vortex chamber invented by D. Angus [24]. The experimental proof of the ability of this new concept of double vortex, to retain solid particles in suspension in a very narrow residence zone inside the combustion chamber was given by Georgantas, Krepec and Kwok [25,26,27] for both isothermal and combustion conditions. The schematic of their cyclone

furnace which was built and investigated at Concordia University is shown in Figure 2.2.

2.4 Confined Vortex Flow

The confined vortex is a highly turbulent phenomenon and its nature could only be determined by direct measurement of the velocity and pressure flow fields. In 1952 Kelsall [28] made measurements of radial, tangential and axial velocity components inside a hydrocyclone separator and found that large scale secondary flows existed in that system and that the fluid mass movement occurred mostly along the side and the end walls of the apparatus.

Kelsall's results were later (1962) substantiated by Kendall [29,32] who performed detailed measurements in the boundary layer of the fixed end wall of an otherwise rotating porous cylindical chamber with aspect ratio (L/D) equal to one. Kendall's results showed that the tangential velocity component was essentially constant along the height of the chamber and slightly overshot this value inside the end wall boundary layer. The reason for this being that, inside the boundary layer, a high radial velocity existed, and the angular momentum of a fluid particle was more likely to be conserved inside the boundary layer than outside where the radial velocity was

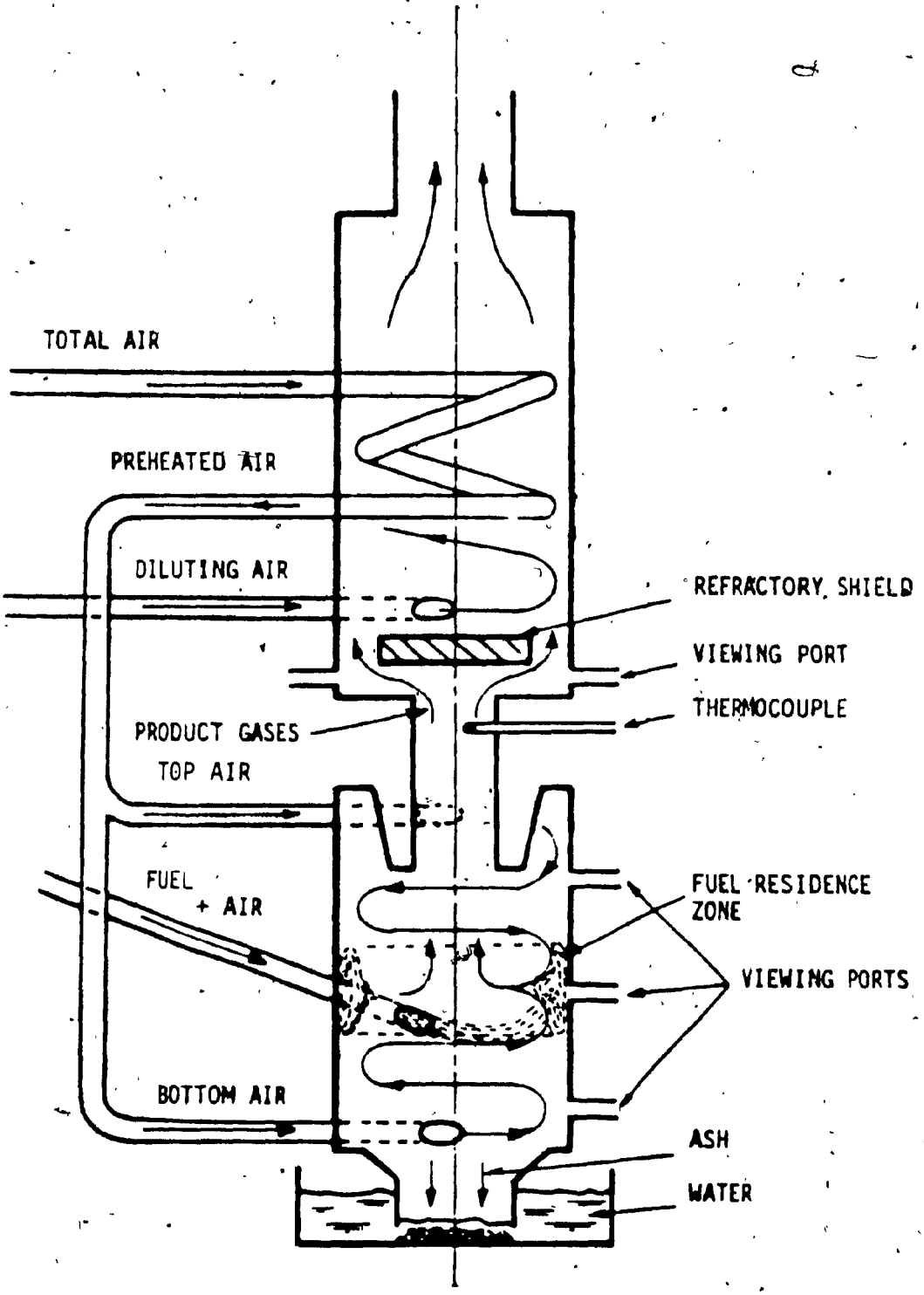

Fig. 2.2 Schematic of a double-cyclone furnace (25,26,27)

virtually zero.

A very detailed experimental study of the velocity components and of the static pressure distribution in a vortex contained in a short cylindrical chamber was done by Savino and Keshock [30]. For their study, a three-hole Pitot-static probe was used which sensed the flow direction as well as the static and dynamic pressures. The axial velocity component was small enough to be neglected, and the total velocity was assumed to be comprised only by the radial and tangential components. All the mass flow was found to occur along the chamber walls, while in the middle level of the chamber a radial reverse zone was observed. The results of that study were subsequently verified by an analytical study made by Kwok, Thinh and Lin [31]. Some investigators have used optical methods to measure the velocity components. Kendall [32] did this by observing the motion of fine particles at various positions within a hydraulic vortex.

Studies conducted in a conically shaped vortex chamber were done by Bank, Raydon and Gauvin, [16, 17, 18, 19]. They used a 5-channel Pitot-static probe in order to measure the absolute velocity and the static pressure distributions within the chamber. The radial velocity component was not reported, however. With regard to the tangential velocity, a combined vortex behaviour was

observed. Angular momentum conservation in the potential vortex part, and solid body rotation near the center were demonstrated. The radial profile of the tangential velocity was found to be virtually constant along the different axial sections of the conical chamber. Subatmospheric pressure and reverse axial velocity were observed in the "core" region of the vortex. An analytical expression describing the radial distribution of the tangential velocity was also obtained.

The most revealing experiments on cyclone chambers were made by Baluev and Troyankin [33]. They made experimental investigations in many structurally diverse cyclone chambers. Specifically, they examined twenty-three chamber versions in which the predominant design parameters were varied; namely, the cyclone chamber height, the number of tangential inlets, the diameter of the exit nozzle and the relative roughness of the walls. The total inflow area, however, was always kept constant, and the air was introduced tangentially at the bottom end of the cylindrical chamber. Their experimental findings provided much insight into the confined vortex gas motion.

Five characteristic annular flow zones inside the chamber were described. Two of these zones carried the

main mass flow of the gas to the exit of the chamber, that was located at the center of the end wall of the chamber, opposite to the air inlet. The other three zones being induced by the flow of the two main flow zones mentioned above, were basically flow entrainment zones and demonstrated a reverse axial flow, Fig. 2.3. An empirical mathematical expression including the most important design parameters was also obtained in order to describe the radial profile of the tangential velocity. Their results, in general, verified and refined the aerodynamic pattern of gas flow previously studied by Lyakhouskii [34], inside similar vortex chambers.

2.5 Velocity and Pressure Measuring Techniques

The accuracy of velocity or pressure measurements in vortex flows has been a subject of discussion for many years. The immersion of probes into the flow field causes localized disturbances and instabilities that could alter the fluid flow field significantly. There are three techniques widely used for swirling flow fields measurements:

- Doppler Laser Anemometry

- Hot-Wire Anemometry

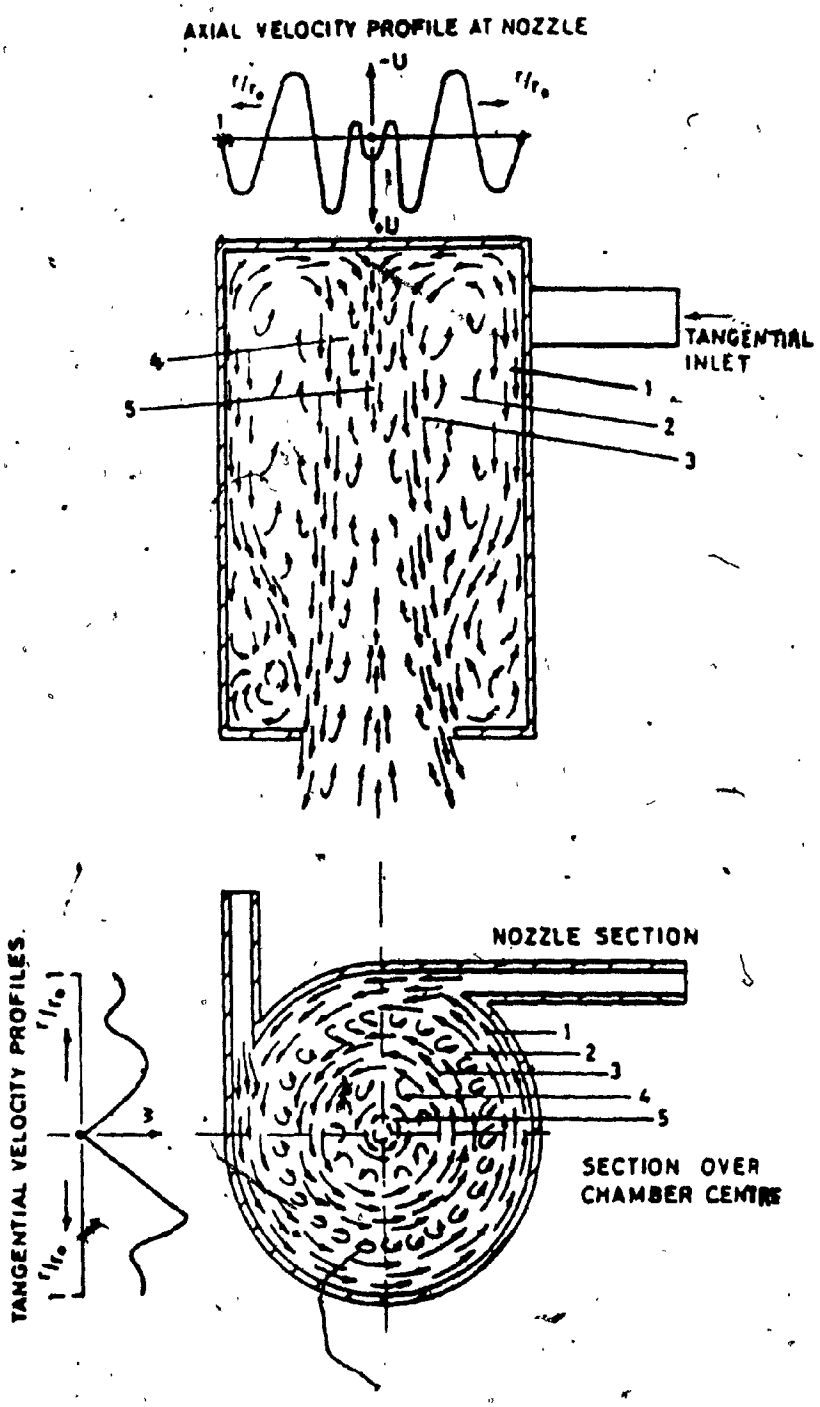

Fig. 2.3 Aerodynamics of a cyclone chamber (33)

- Pitot-Static Pressure Probes

Even though these methods are well recognized and are being used in many flow systems, there are certain drawbacks when applied to swirling types of flow. Each of the above methods will be described separately. The Pitot-static pressure measuring technique, however, was used in the present study and it will be described in more detail.

a) Doppler Laser Anemometry: This is a novel method that has established itself as a valuable flow measuring technique with numerous advantages over more conventional methods. The instantaneous velocity (magnitude and direction) of particles inserted into the flow field, is being measured by detecting the change in frequency (Doppler Shift) of the light waves scattered from the moving particles. The frequency of the scattered light is proportional to the conveyed particle velocity. From the velocity of the particles the velocity of the fluid can then be inferred.

Doppler Laser Velocimetry is basically a non-invasive technique because only light beams are entering the flow field. This makes the method particularly important in flow fields where the immersion of probes would cause a disturbance to the fluid or where

hot, corrosive or otherwise prohibitive fluids are employed. This method is suitable for measurements in mixing flames, rotating machinery, wind or water tunnels, chemically reacting flows and in many other areas where most of the conventional techniques perform poorly.

In certain applications, however, large index of refraction gradients can cause beam motion which results in missed data or spurious velocity components. This disadvantage is by no means degrading the value of this method since the above phenomenon seldom occurs. The advantages of the Doppler Laser Anemometry are:

- no probe presence in the flow field
- no flow calibration is required
- measures flow reversals
- senses only the velocity, independent of temperature, density and composition changes of the fluid.
- provides precise measurements of velocity components.
- has the ability to measure very low velocities

(in the order of micrometers per second [35]).

For the present investigation, this technique was not used because it was assumed that the tagging particles would not exactly follow the gas streamline paths. The particles would have the tendency to separate from the air stream due to the centrifugal force field created by the rotational flow. Instead, the relatively simple arrangement of a 5-channel omnidirectional Pitot-static pressure probe, already present in our laboratories, was used.

b) Hot-Wire Anomometry: This is one of the best methods for measuring the variations of the velocity in a gas or liquid flow with respect to time and space. The sensitive element is usually a thin cylindrical wire suspended between two prongs. The wire is electrically heated, and loses heat to the surrounding fluid. The rate of the convective heat loss is a measure of the local velocity of the fluid.

The theoretical analysis for obtaining a relationship between the heat flux from the probe and the fluid velocity is very complex and the nature of this relation must be established by experimental means. Direct calibration is therefore necessary. The output of the

anemometer is a bridge voltage, the square of which is proportional to the heat loss from the wire and consequently a measure of the fluid velocity. The relation between the velocity and the output voltage can be linearized by electronic means [36].

Sufficient sensitivity, fast response time, minimal disturbing effects on the fluid stream, and measurement of turbulence quantities are the main features of the hot-wire anemometry. The hot-wire velocity measurement technique proves to be particularly important in polluted gas flows.

c) Pitot-Static Pressure Probes: Many researchers have utilized this method for experimental investigations in swirling flows [2, 4, 18, 19, 30, 32]. Some of them were able to develop analytical methods and obtained solutions that agreed well with their experimental findings [4, 18, 19, 30, 31].

The Pitot-static pressure measuring technique is based on the fact that a pressure distribution is created around a body immersed in a fluid that has a relative motion. The pressure variation around the body can be sensed by pressure taps. Based on the principle of momentum exchange, a very simple relation can be employed to translate the total and static pressure readings into local absolute velocity components. Calibration of the

probe is required at a particular flow condition and remains unaffected at different operating conditions.

Total velocity measurements including speed as well as direction, can be made by employing one general purpose probe or more than one single purpose probes. The single probe measures only one quantity, such as flow direction, static or total pressure. It has, however, the additional advantage of being more sensitive to the particular quantity that it measures. This advantage, is outweighed by errors due to sequential positioning for the measurement of all the flow variables.

Due to its simplicity, the Pitot-static pressure method is widely used for the quantitative exploration of many types of flows with speeds as low as 1.5 m/sec. Although, initially developed for subsonic applications, the pressure probe is also suitable for occasional excursions into supersonic regimes. These probes, however, are of very slow response due to the pressure signal lag and to inertia effects associated with the recording instruments (usually manometers). This technique, therefore, can be used basically for steady state flow problems. In turbulent flows time-averaged values are indicated.

The highest pressure that can be sensed by the

Pitot-static probe cannot be greater than the total pressure of the stream. The lowest pressure recorded may, however, be lower than the local static pressure. If P_1 and P_2 are the readings of two different pressure holes, the dynamic pressure can be expressed in most cases as:

$$P_t - P_s = \frac{1}{2}\rho V^2 = K (P_1 - P_2) \qquad (2.1)$$

where K is a constant, the value of which can be calculated from the following probe calibration:

$$P_s = P_2 + K_2 (P_1 - P_2) \qquad (2.2)$$

$$P_t = P_1 + K_1 (P_1 - P_2) \qquad (2.3)$$

then

$$K = 1 - (K_2 - K_1) \qquad (2.4)$$

The flow direction can be a function of the pressure at a single hole. However, such a relation would be highly non-linear and of very poor senstivity. Instead, the pressure difference between two holes which are symmetrically disposed with respect to the plane of symmetry of the probe, Fig. 2.4, is more sensitive to the angular position changes and shows a linear relationship. If P_2 and P_3 are two such pressure readings, the flow direction can be described by:

$$\gamma = C \left(\frac{P_2 - P_3}{1/2\ \rho V^2} \right) \qquad (2.5)$$

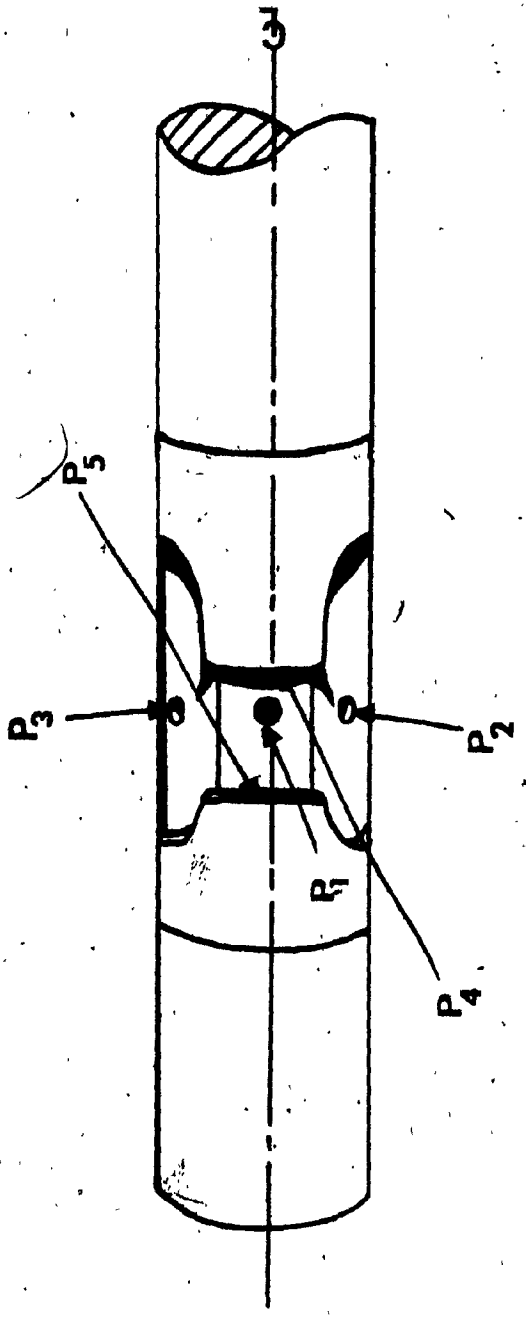

Fig. 2.4 Cylindrical-wedge five-channel pressure probe

where C is a proportionality constant and γ is the angle between the flow direction and the plane of symmetry of the probe. The above relationship however is limited for angles from $+10^{\circ}$ to -10° [37]. For a wider angle range, proper calibration of the probe would be necessary. In a three dimensional flow field, two additional pressure taps are required to completely describe the flow direction, Fig. 2.4. A direct reading of the flow angles is obtained if the probe is rotated with respect to the flow direction until the pressures of the two symmetrically disposed holes are equalized. This is known as the "null-reading" method.

The design of a Pitot-static pressure probe is aimed toward diminishing the effects of the Reynolds number of the measured flow on the readings. At very low speeds or pressures, however, the pressure recovery factor expressed as $Cp=(P_t - P_s)/1/2\rho V^2$, becomes increasingly larger for decreasing Reynolds number. This effect must be accounted for Reynolds numbers less than 40, [37]. The Reynolds number is based on the probe orifice diameter. The accuracy of measurements, on the other hand, is affected in highly turbulent flow fields because the time-averaged pressures sensed by the probe holes do not correspond to the mean velocity of the stream. This is due to the fact that the pressure varies with the square of the velocity and the time-averaged pressure fluctuations about the average pressure, corresponding to the mean velocity, will

not be zero. The increase of the pressure readings due to turbulence was first given by Goldstein [38], and is equal to $1/2\rho\,(\overline{V}_x^2 + \overline{V}_y^2 + \overline{V}_z^2)$, where $(\overline{V}_x, \overline{V}_y, \overline{V}_z)$ indicate turbulent velocity fluctuations about the mean velocity value.

CHAPTER 3

FORMULATION OF THE PROBLEM AND METHOD OF APPROACH

3.1 Background of the Present Work

The work presented here was initiated in order to acquire more knowledge about the vortex structure inside cyclone chambers and, in particular, about the double vortex chamber, developed at Concordia University, Montreal, for suspension-burning of solid fuels. The development work was supported by a grant from the National Science and Engineering Research Council, Canada.

The suspension burning of shredded solid materials creates the prospect of continuous, strictly controlled combustion and provides for high combustion intensities. Several old and new attempts to develop such a combustion technology are described in many related publications. Some of them led to fully developed commercial products being successfully used in several applications (Babcock and Wilcox, Energex [11,12]). Others only showed new possibilities in solid fuel energy extraction thus preparing the ground work for new commercial product developments in that area.

One relatively new approach was recently presented by Derek Angus [24], a Canadian inventor, who proposed a double vortex combustion chamber concept for suspension burning of solid fuels. This is described in the USA patent No 4,002,127, issued in January 1977 under the title: "Cyclone Structure". That concept proposes a cylindrical vortex chamber with two sets of tangential air inlets: one at the top and the other at the bottom of the chamber. A central reentry nozzle is axially placed at one end of the chamber, usually on the top, in case of a vertical arrangement, Fig 3.1. When solid fuel particles are introduced into the chamber, the two converging vortices are supposed to create a narrow distinct residence zone for that fuel close to the side wall of the chamber and at some distance from the end walls of the chamber, depending on the relative strength of the two vortices.

The inventor claimed that a localized inward radial flow is being created at the merging level of the two vortices. That flow subsequently turns into an axial flow as the fluid is discharging at a smaller radius approximately equal to that of the exit nozzle. A quiescent annular zone is claimed to be created around the localized radial flow, and the solid fuel particulates will reside in that particular zone.

When at combustion operating mode, the solid fuel

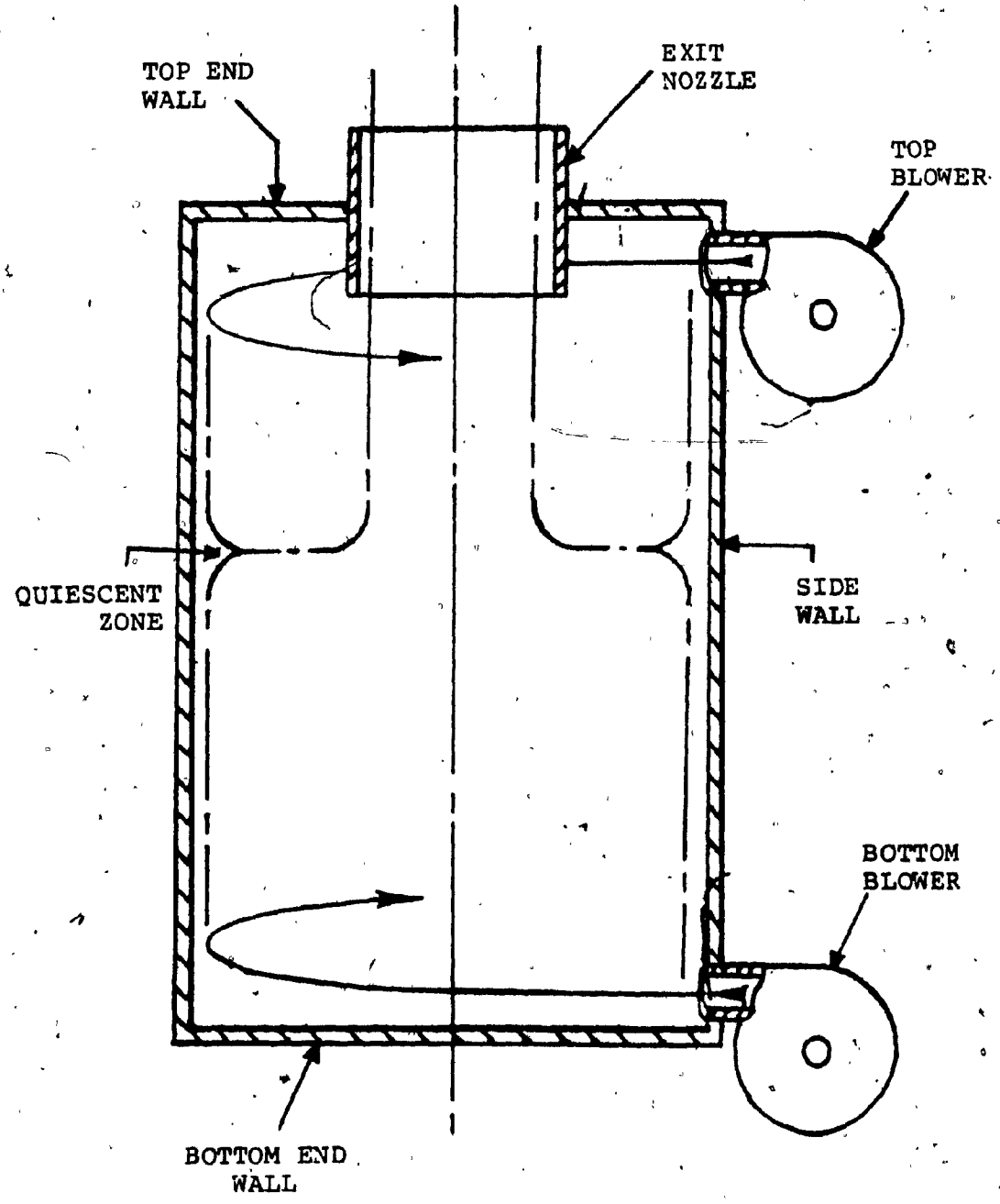

Fig. 3.1 Double vortex chamber and gas flow pattern (24)

particles would break up into smaller sizes and consequently would be conveyed radially inward by the radial drag force. Main combustion will thus take place remote from the side wall. The air flow of the two vortices, near the side wall, will provide a heat transfer shield around the high temperature region and will thus prolong the life expectancy of the combustion chamber. Final combustion would take place as the smallest particles would move axially up toward the discharging tube.

By increasing the strength of the top vortex, the radial inflow zone would be suppresed to a lower level and as a result of the increased distance from the exit nozzle, the residence time of the fuel particles will be increased. The axial level of the fuel residence zone could be adjusted to account for fuels of different burning rates. The axial adjustment of the localized radial flow could be done continuously between the limiting levels by altering the relative strength of the two vortices in a cyclic manner. This provision would prevent local deterioration of the chamber lining. On the other hand, slag deposits formed on the side wall by the cooling effects of the incoming fresh air, would melt and collect at the bottom end of the furnace from where they could be removed by special arrangements.

Slag formation at the side wall would prove advantageous, as small particles would adhere to it and be prevented from escaping from the chamber. This would add to the combustion efficiency and would minimize the pollutant content of the flue gases. Slag collected from the incineration of fuels with high slag content, could be added into the chamber when operating with low slag content fuels in order to profit from these advantages.

Furthermore, it was claimed [24], that the present configuration could be used as a dust separator. As a particulate laden fluid would enter from the bottom inlet of the chamber, the particles would separate from the fluid by the action of the centrifugal force and would be localized at the residence quiescent zone. Consequently, they would be removed out of the chamber by special channeling arrangements at that location.

3.2 Objectives and Program of Investigations

To examine how practical the assumptions made by Angus were, investigations were conducted at the Fluid Control Center of Concordia University. These investigations included the building of a furnace prototype equipped with a double vortex combustion chamber, for tests at the combustion operating mode. In parallel, a transparent model of the combustion chamber was built to

investigate the flow pattern of the air and of the solid fuel particles in order to confirm the assumptions included in the patent [24] and to optimize the combustion chamber design. Because the double vortex chamber, as claimed by Derek Angus [24], could be used also as a dust separator, the investigations would also clarify the possibilities of that application.

The scope in the present work was the investigation of the vortex flow pattern in the transparent model for the single and double configuration, in order to provide enough information for determining the motion of solid fuel particles when being inserted into the chamber. It is claimed herein that a stationary fuel residence zone can be created in the double vortex chamber in which the solid fuel particles can be retained against the conveying drag force of the air flow. The main objectives of the investigation were formulated as follows:

"To determine experimentally the air flow pattern at isothermal conditions in the transparent model of the combustion chamber for different flow conditions and for various structural configurations of the model. The possibility of flow visualization in the transparent chamber will also be considered".

The above objective would be accomplished according

to the following schedule:

1. Development of a physical model of the vortex combustion chamber for flow pattern investigations. A transparent vortex chamber of modular design having the following features would have to be constructed:

   a) It should be easily converted into:
      - single vortex chamber with top inlet
      - single vortex chamber with bottom inlet
      - double vortex chamber

   b) It should allow for the insertion of a 5-channel pressure probe in order to perform measurements of the absolute air flow velocity along a radius of the chamber, for at least six different axial levels.

2. Experimental invesigations in the transparent chamber (cold conditions) using a 5-channel pressure probe. The total volumetric air flow rate will be measured using rotameters. Measurements to be made are, for:
   - single vortex chamber with top inlet
   - single vortex chamber with bottom inlet
   - double vortex chamber

For the above schemes the effect of important structural design and flow parameters on the flow pattern should be examined.

The air supply conditions should correspond to the flow conditions in practical applications of the vortex chamber.

3. Development of a software package to convert the Pitot-static pressure measurements into velocity components and to display the experimental results in appropriate form.

4. Theoretical considerations for interpreting the experimental results.

CHAPTER 4

ENGINEERING SPECIFICATIONS FOR THE TRANSPARENT CYCLONE CHAMBER DESIGN AND TESTING PROCEDURE

4.1 Design Specifications

The transparent cyclone chamber had to be designed for measurement as well as for visualization of the aerodynamic structure of the single and multi-vortex air flow. The following requirements were specified:

a) The transparent chamber would be designed as a modular system, that is, it could be altered using exchange parts to cover all the required air flow configurations.

b) The following combinations of the air flow had to be assured without any major change in the vortex chamber structure:

- the air inlet should be available at the top and or, at the bottom end of the chamber.
- the number of inlets at each end of the chamber should be variable from one to four, with the angular spacing being 90°, 180° or 360°.

- the angular position of the inlet tubes should be variable with respect to the radius of the chamber from 90° to 0° in intervals of 18° so that six different configurations, including the extreme ones, could be obtained.

- the total flow area for the four inlets on each end of the chamber should reach a maximum of 9.8% of the cylidrical cross sectional area of the chamber with all inlets having equal flow area.

- the length of the vortex chamber should be 1.0, 1.5, 2.5 or 3.0 times the size of the internal diameter of the chamber .

- the outlet would be made on the top cover, and its diameter should be 0.2, 0.3, 0.5, or 0.7 times the chamber internal diameter.

- several openings at different axial levels for the insertion of a 3-D Pitot-static directional probe should be made in the cylindrical part of the chamber.

c) The vortex chamber internal diameter should be

close to 0.300 m (0.979 ft) in order to match the size of the cyclone furnace vortex chamber, used for experiments at the combustion operating mode.

d) The chamber should consist of a plexiglass cylinder, having at the top and at the bottom ends the air supplying rings and covers. The supplying rings should consist of four equally spaced similar angular segments attached to an aluminum ring. The segments should be manufactured from plexiglass rectangular blocks and machined after being assembled on a steel mounting plate, which would be used particularly for machining of such segments. The cylinder and the supplying rings would be held together using aluminum rings and steel bolts.

e) The air should be properly distributed to individual inlet ports so as to obtain symmetrical flow conditions. The air flow into the chamber could either be directed clockwise or counter-clockwise, by only inverting the air supplying segments. Different configurations of the inlets (with regard to the inlet angle) would be possible. Blank segments would be used to eliminate some of the inlets and reduce the number to 3, 2, or 1. Should the number of inlets at one end of the chamber be less than four, the total inflow area would become less than maximum. Inflow area could be reduced (without blocking the inlet ports) by the use of hollow cylidrical inserts. The

assembly drawings of the cyclone chamber for the single vortex configuration are shown in Figures 4.1 and 4.2.

Such a design would reduce the amount of material needed, as well as the number of parts. For example, to vary the inlet port angle, only the segments would have to be changed. Structurally different chambers would be obtained by the proper selection of individual parts. It was decided to make the first configuration of the vortex chamber according to the following dimensions:

- chamber internal diameter, D=0.300m (0.979 ft)
- chamber height, L= 0.458m (1.468 ft)
- inlet flow through 4 ports at either end of the chamber; total inlet flow area, A= 6.86×10^{-3} m^2 (73.8×10^{-3} ft^2)
- outlet diameter, D_e = 0.149 m (0.49 ft)

The parts were machined and the chamber was assembled successfully. Plate 4.1 shows the double entry vortex chamber configuration. Flow velocity measurements were made at six axial stations, Fig. 4.3 Twenty three radial positions were traversed at each axial station. The

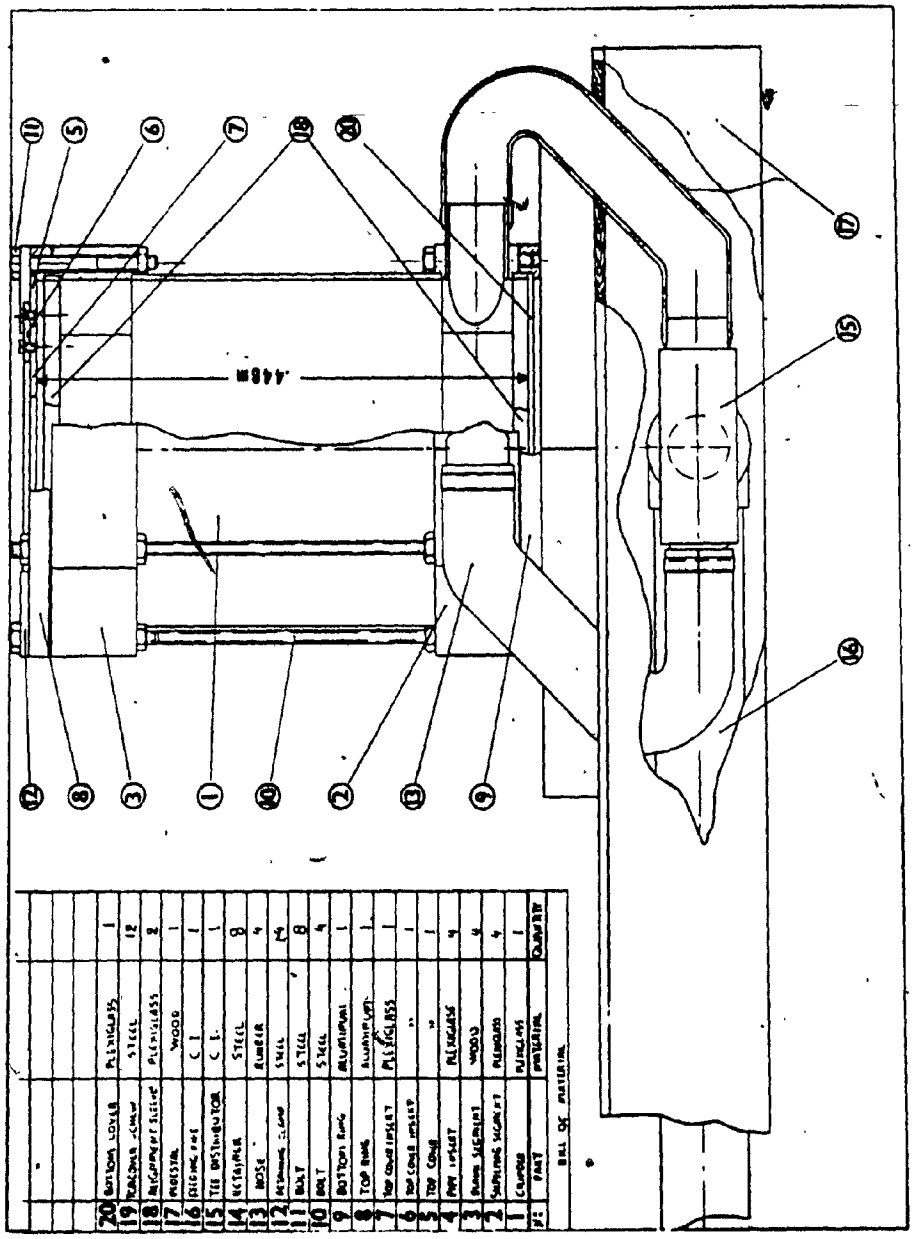

Fig. 4.1 Single Entry vortex chamber.
Assembly drawing: Front half-cross section

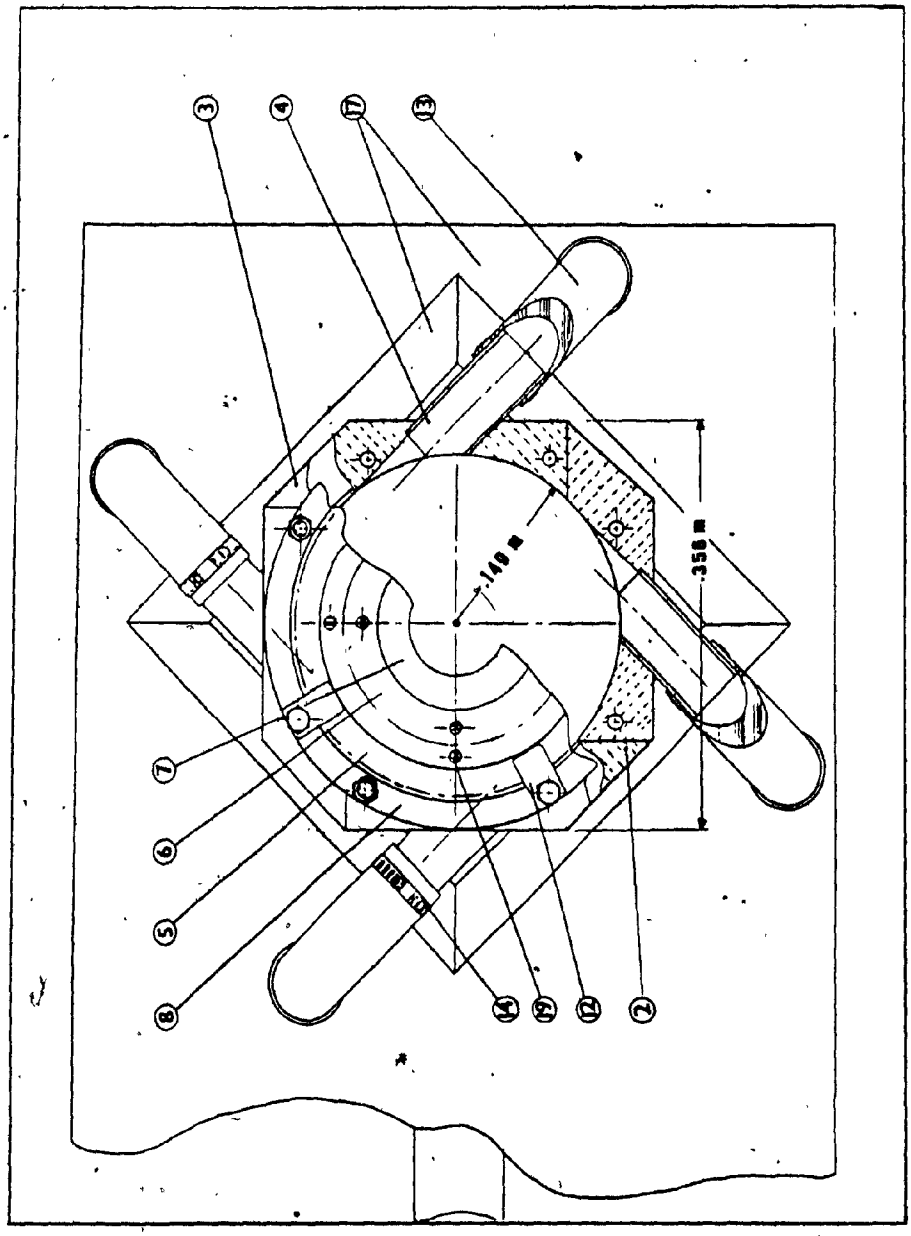

Fig. 4.2 Single Entry vortex chamber.
Assembly drawing: Top half-cross section

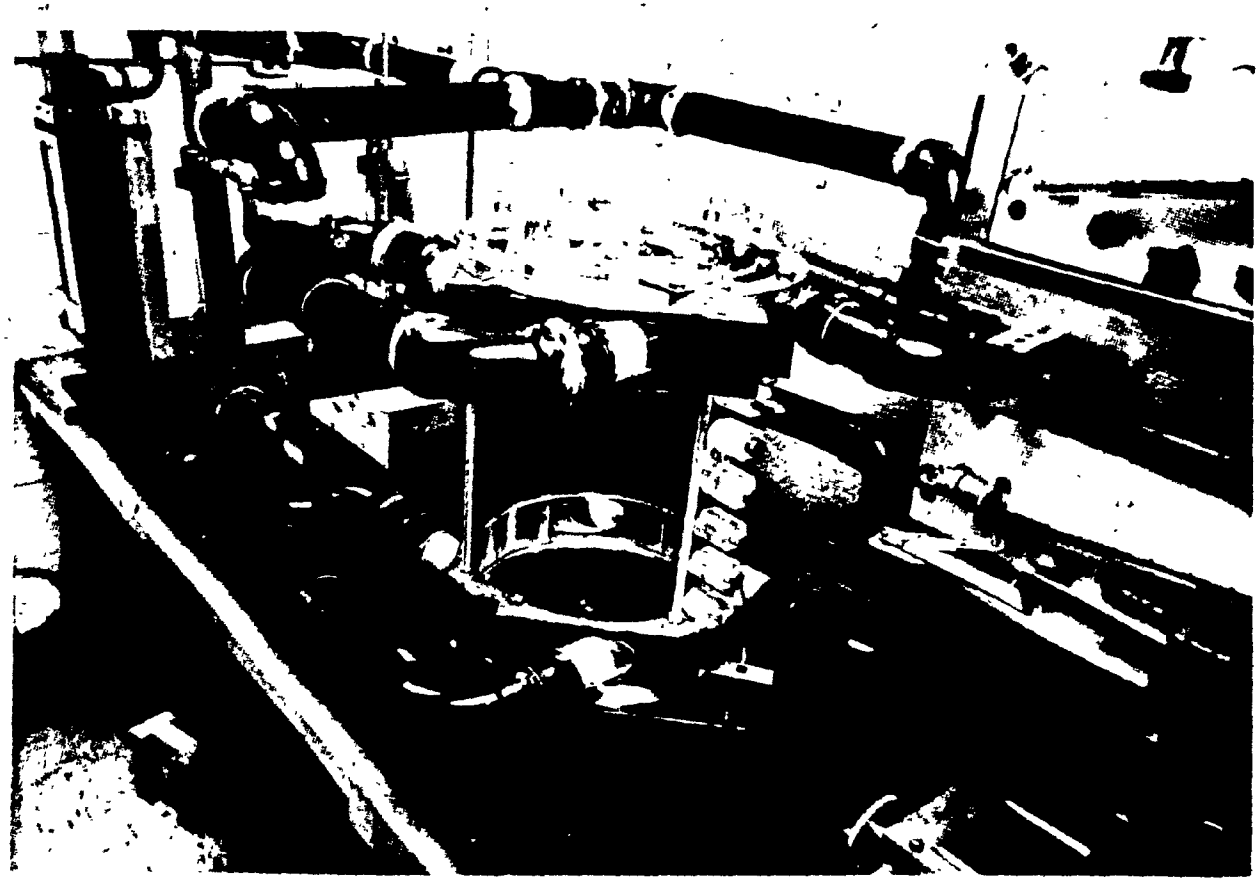

PLATE 4.1 Double Entry Vortex Chamber

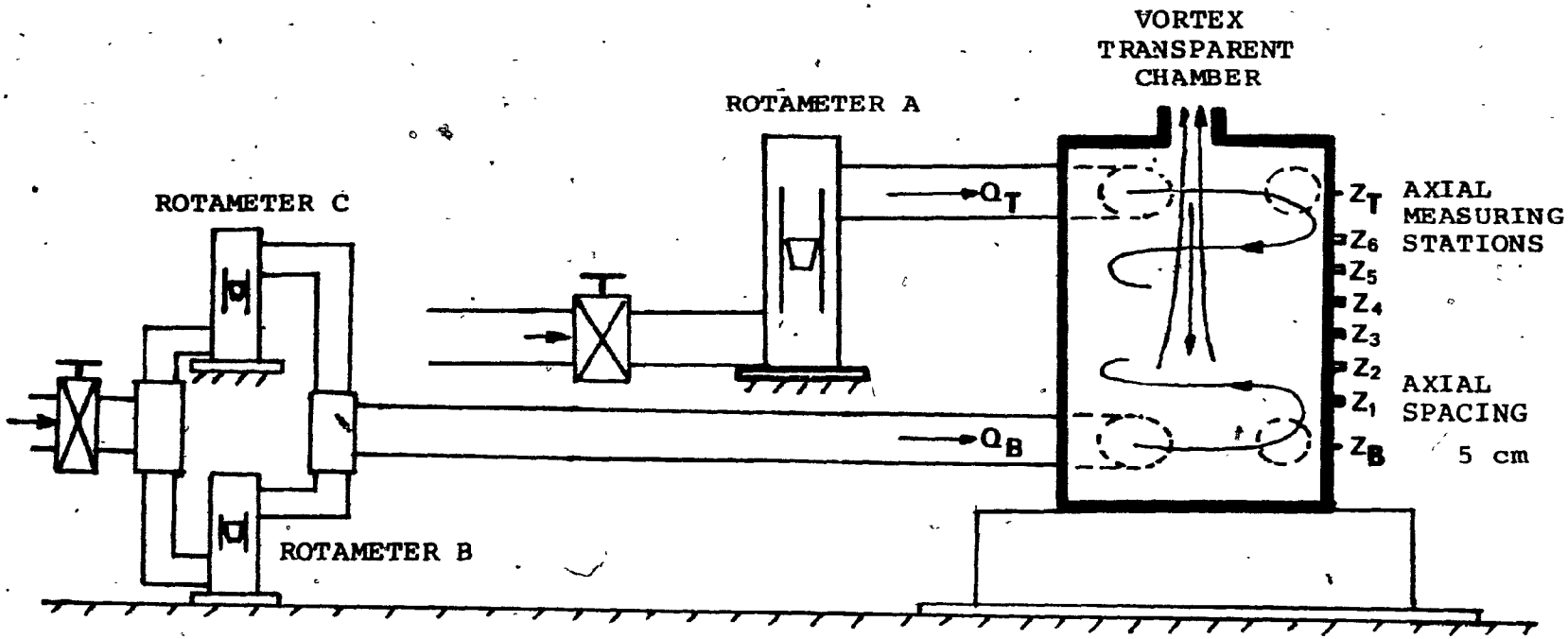

Fig. 4.3 Schematic arrangement of the transparent vortex chamber

nominal aspect ratio of the chamber, (L/D) was 1.5, and the nominal outlet dimensionless diameter, (D_e /D) was 0.3. Four tangential inlets were used of total flow area equal to 6.86×10^{-3} m^2 for the single entry vortex and eight tangential inlets (four at each end) of total flow area equal to $2 \times 6.86 \times 10^{-3}$ m^2 for the double entry vortex configuration. The nominal air flow rate for either case was 2.83 SCMM (100 SCFM) at STP (0 °C, 1 atm). That corresponded to the nominal air flow rate established for the cyclone-furnace.

4.2 Instrumentation and Measurements

Four different kinds of instruments were essential for monitoring the experimental process:

- variable area flowmeters for air flow rate measurements.
- pressure sensing directional probe.
- traversing mechanism to provide a 3-Dimensional adjustment of the probe, and
- pressure-recording instruments to translate the sensed pressures into scale readings.

a) **Variable area flowmeters:** Rotameters were used to measure the air flow rate into the chamber. These instruments had to be calibrated for the operating pressure and temperature and for the molecular weight of the particular fluid to be metered. The rotameters in their operating positions are shown in Figure 4.3 and in Plate 4.2. The calibration curves are included in Appendix A. Side scales were affixed to the rotameters in order to avoid the use of the calibration curves and to shorten the reading procedures.

b) **Pressure probe:** The air flow pattern inside the cyclone chamber was three dimensional, and since the velocity direction could not be predetermined, a pressure probe which would sense both the velocity magnitude and the flow direction, was required. A "United Sensor" probe was used in this study, Fig. 4.4. It employed five pressure sensing holes that would detect the flow direction in a vertical plane; perpendicular to the probe axis, and in a plane along the probe axis intersecting the first one, Fig. 4.5. The flow direction in the vertical plane would be described by the yaw angle, and in the intersecting plane, by the pitch angle, as shown in Fig. 4.5. The angular spacing between a vertical line in the first plane and the intersection line of the two planes would be described by the yaw angle. The probe was furnished with a calibration chart from which it was possible to obtain the

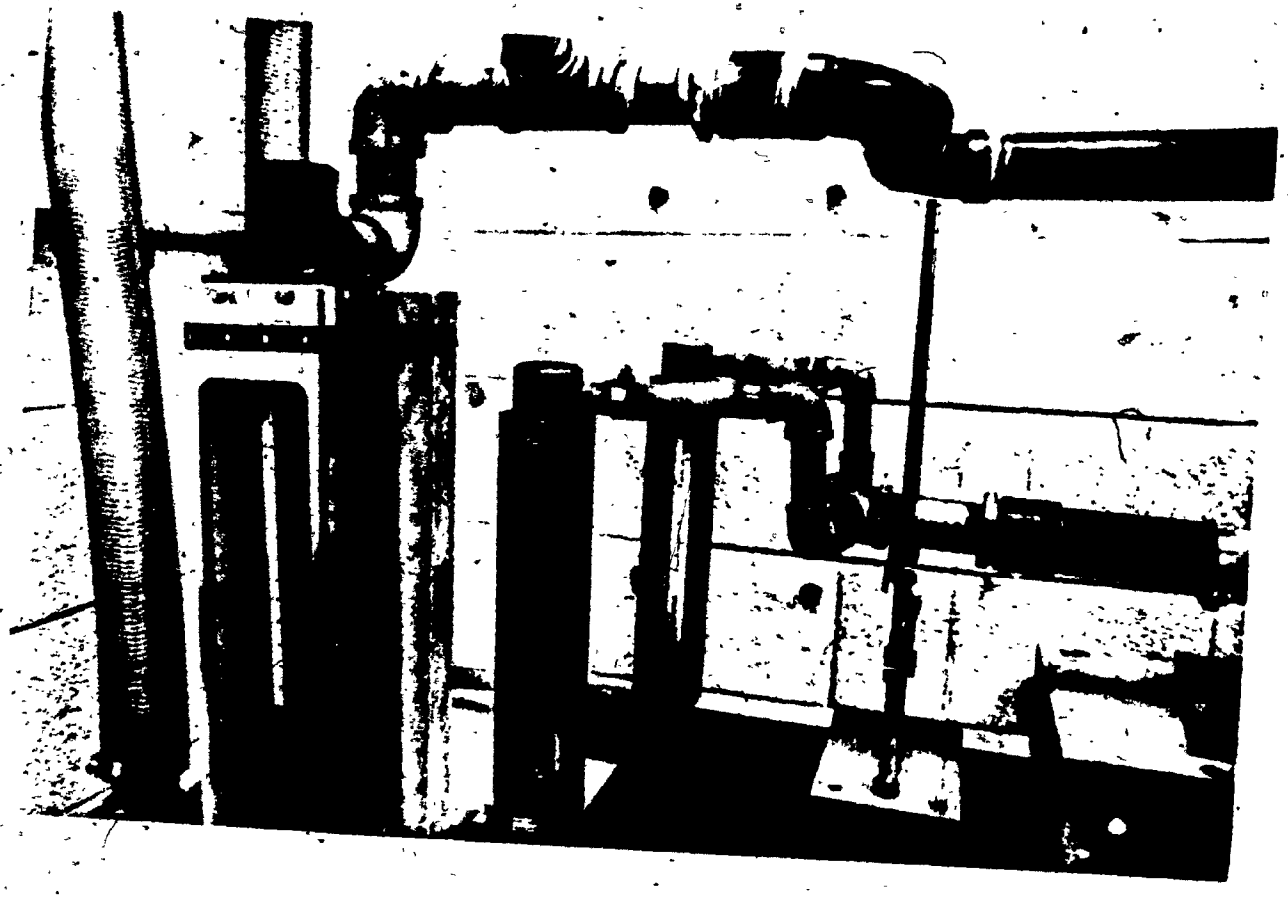

PLATE 4.2 Rotameters for the Measurement of the Volumetric Air Flow Rates at the Top and Bottom Inlets

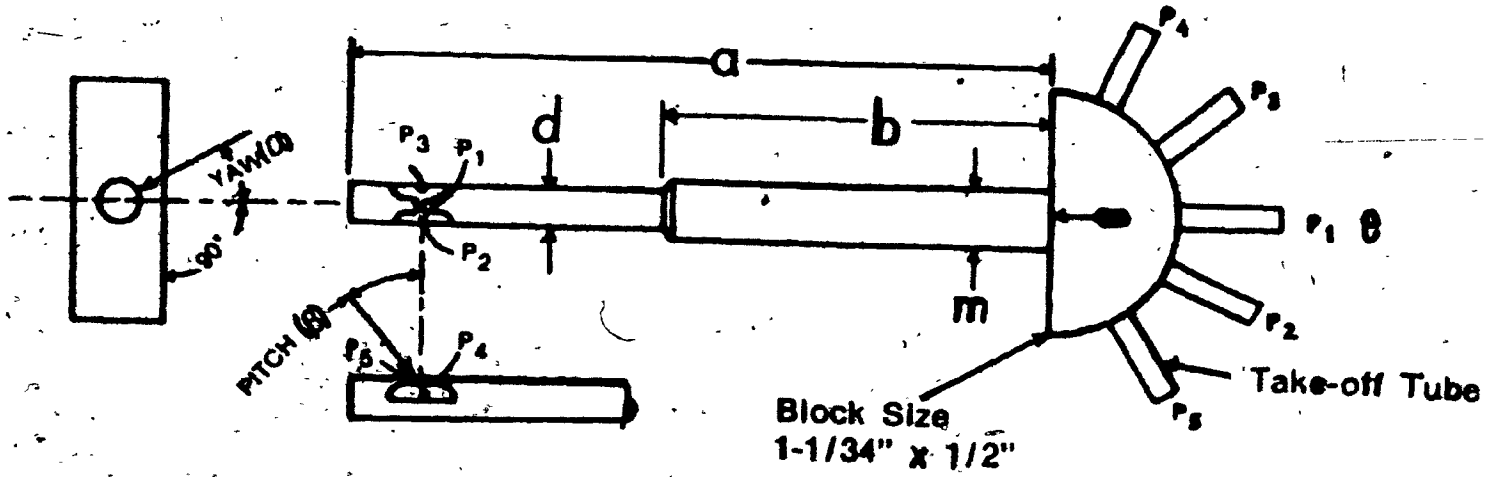

Fig. 4.4 Five channel pressure probe

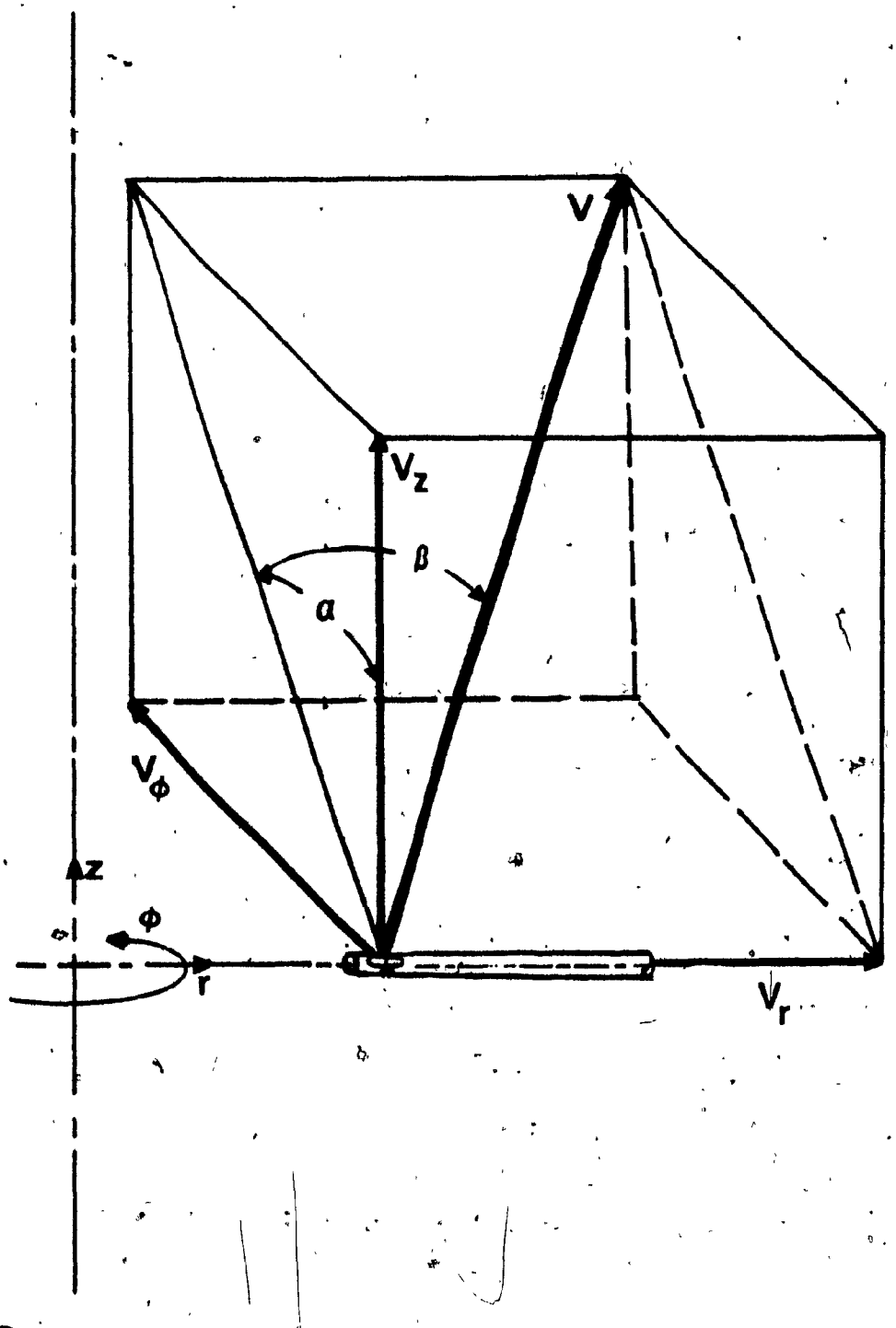

Fig. 4.5 Coordinate system and velocity components

pitch angle and calculate the dynamic and static pressures, Fig. 4.6. Typical manometer connections are shown in Figure 4.7. The choke (USC-1160), intended to average pressures P_2 and P_3, was not essential and was removed in order to decrease the response time of the system.

The following experimental procedure was described by the manufacturer [40]: "Probe is rotated until $P_2 = P_3$, and the yaw angle of the stream is then indicated by the take-off block. Pitch angle is determined by calculating $(P_4 - P_5)/(P_1 - P_2)$ and using the calibration curve A for the individual probe, Fig. 4.6. At this pitch angle the velocity and pressure coefficient $(P_t - P_s)/(P_1 - P_2)$ and total pressure coefficient $(P_1 - P_t)/(P_t - P_s)$ can be read from curves B and C and values of $(P_t - P_s)$ and P_s calculated".

c) **Traversing mechanism:** The traversing mechanism, shown in Plate 4.3, allowed a 3-D movement of the probe, such that all three space adjusements were possible. The linear movement of the mechanism was adjustable within 1.0 mm. An adjustable disc-dial fitted to the probe holder would indicate the yaw angle with an accuracy of 0.5^{o}.

d) **Pressure-recording instruments:** Inclined well-type manometers, shown in Plate 4.3, were used for the

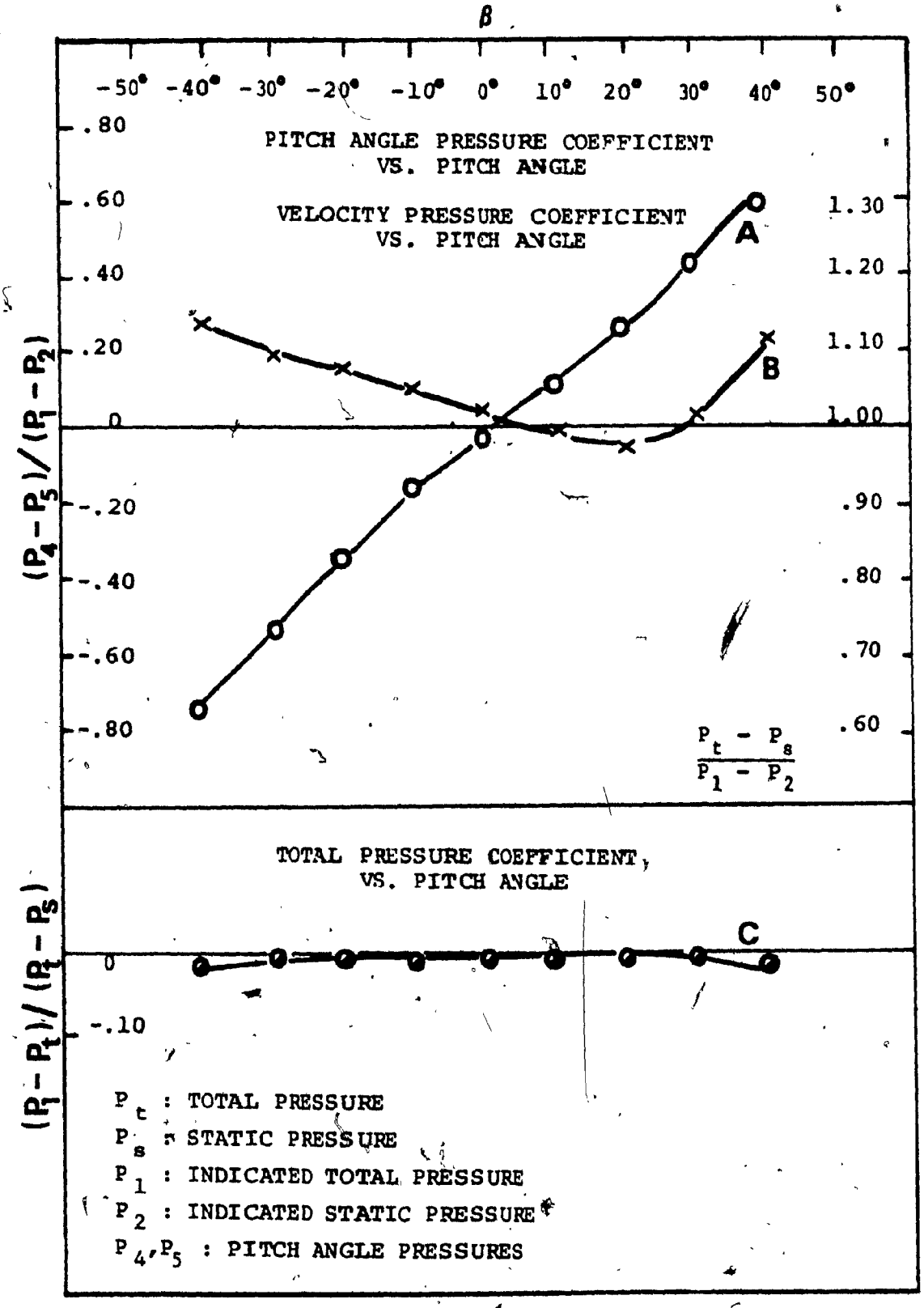

Fig. 4.6 Calibration curves for the 5-channel pressure probe

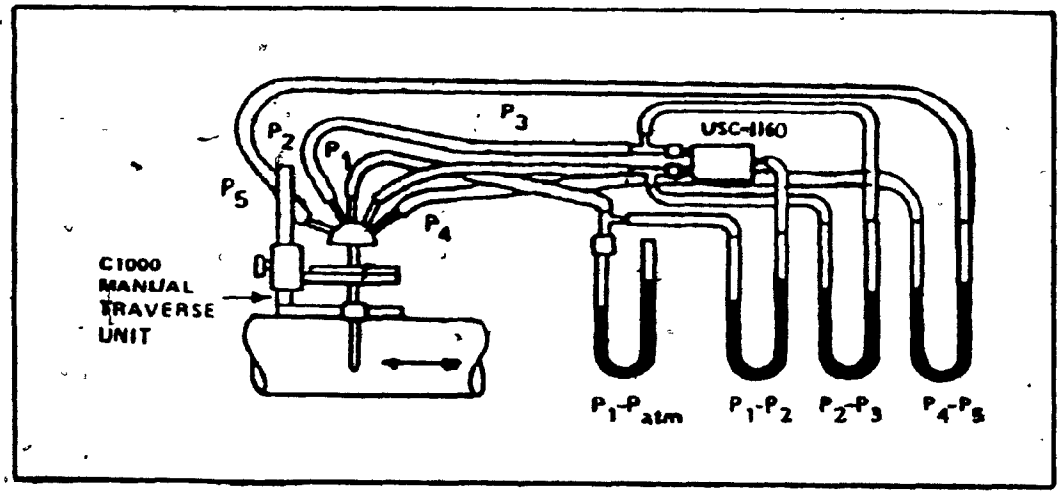

Fig. 4.7 Typical manometer connections for the 5 - channel pressure probe

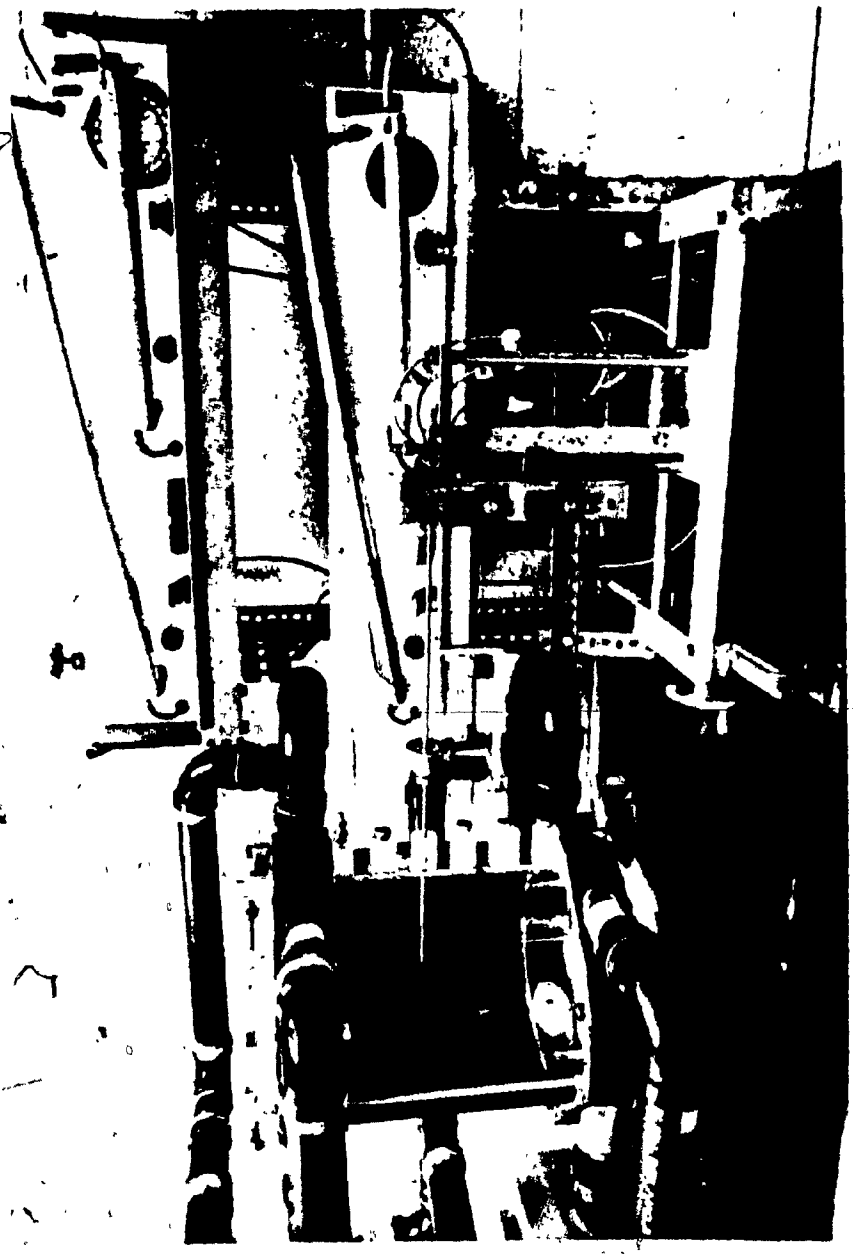

PLATE 4.3 Traversing Mechanism and Inclined Manometers

pressure indication. The manometer liquid was Meriam oil (SP. GR. 0.787), and the scale was calibrated in water equivalent height. Three inclined positions, associated with different sensitivities, were possible. The accuracy of the pressure readings, associated with the first (lowest) inclined position, was within 0.13 mm H_2O.

4.3 Test Procedure

Before allowing any air into the chamber, the radial alignment of the probe was assured by a plumb bob suspended from the central point of the top plate. Then the yaw angle was set to zero reading by using a spirit level to adjust the horizontal position of the take-off block. The air supply of the top and bottom inlets was then set to the desired values and approximately ten minutes were allowed for the system and recording instruments to reach steady state conditions. Then, the radial traverse of the probe at a particular axial station was started. At every radial location the probe was rotated until P_2 and P_3 were equalized and the yaw angle was noted. The pressure differences $P_1 - P_{atm}$, $P_1 - P_2$ and $P_4 - P_5$, were also recorded at that position.

4.4 Data Reduction

After $P_t - P_s$ and P_s were calculated Bernoulli's equation was employed to determine the air flow velocity:

$$V = \sqrt{\frac{2(P_t - P_s)}{\rho}} \qquad (4.1)$$

The absolute velocity was then resolved into radial, tangential and axial componenets:

$$V_r = V\sin\beta \qquad (4.2)$$

$$V_\phi = V\cos\beta \sin\alpha \qquad (4.3)$$

$$V_z = V\cos\beta \cos\alpha \qquad (4.4)$$

To speed-up the data processing, a software package (included in Appendix B), was designed to perform the above calculations. Radial static pressures were also evaluated. Display subroutines (Tektronix, PLOT-10) were employed to plot the static pressure and velocity components along the radial direction.

4.5 Accuracy of Results

The measurements were subject to some error with

respect to positioning and radial alignment of the probe. The fine adjustment and readability of the instruments were essential for obtaining accurate measurements.

The net air flow rate through a cross sectional area of the chamber was calculated by employing the axial velocity profile at any particular section. The percent difference of this calculation and the volumetric flow rate as indicated from the rotameters, was then obtained. It was found that this difference ranged from 5% to approximatelly 30%. Though this criterion is good enough to indicate the accuracy of the axial velocity profile measurements, it is not well suited to reflect the accuracy of the whole experiment. The error is mainly due to the insensitivity of the pressure difference $P_2 - P_3$ to yaw angle changes at low velocity regions.

Errors accumulate when pressure readings are of the same order of magnitude as the accuracy of the recording instruments. Surface tension effects of the manometer liquid are also error-sources at low velocity regimes. On the other hand, the accuracy of the axial velocity measurements at large radii ($r \cong R$) is very critical in calculating the volumetric air flow rates, because velocities are associated with larger flow areas ($\Delta A \cong 2\pi r \Delta r$). The tangential velocity was not subject to errors because it was of relatively greater magnitude and

it was virtually not affected by small misreadings of the yaw angle. The radial velocity in the main part of the chamber where the experimental investigation was carried out, was quite small, since almost all of the radially directed mass inflow was effected along the end walls of the chamber. However in areas close to the axis where this component was appreciable, other effects such as large pitch angles (exceeding the range of the calibration chart supplied by the manufacturer, [40]), would tend to diminish the value of the results.

CHAPTER 5

EXPERIMENTAL RESULTS AND DISCUSSION

5.1 General

The velocity components in the three directions (r, ϕ, z) together with the static pressure, can be used to sufficiently describe the flow field of the vortex configuration inside the cyclone chamber at isothermal conditions. Except for the axial velocity profiles, all three cyclones, namely the top, the bottom, and the double, behave very similarly. In order to explain the effects of the design and flow parameters on the confined vortex structure, detailed results need only be presented for one basic configuration. The single vortex with bottom air-supply was considered for that purpose.

5.2 Single Vortex: Bottom Air-Supply

For this configuration the air was introduced at the bottom end of the chamber and was discharged through the exit nozzle located at the opposite end of the cylindrical chamber. No variation of the inlet flow angle was considered throughout the course of this investigation. The air was introduced into the chamber at a 90^{0} angle with respect to the radius at any particular inlet position,

(pure tangential air-input); four inlet ports were located around the air supply ring at equal arc distances so as to provide symmetrical inlet conditions.

In order to describe the degree of the swirl for the different configurations of the vortex chamber, a suitable swirl number should be used. Murthy [15] in his discussion of swirl numbers for free vortex flows included a confined vortex analogue of this parameter to be equal to $1/2\ (\Gamma/\dot{m})$, where Γ is the circulation around a particular contour, and $\dot{m}$ is the mass flow through that contour. When applied to the present cyclone chamber this expression results in a swirl number equal to $D^2/(4\rho D_o^2)$. The effect of the outlet nozzle size, however, is not included in this expression. A more appropriate definition of the swirl number for the present configuration would be the one given by Syred and Beér [20]:

$$S = \frac{\text{Input Angular Momentum}}{\text{De}/2 \times \text{Exit Linear Momentum}} \qquad (5.1)$$

For the single vortex with four tangential inlet ports, the above expression reduces to:

$$S = \frac{De\ D}{4\ D_o^2} \qquad (5.2)$$

The inlet port diameter was equal to 46.7×10^{-3} m, and that resulted into a swirl number equal to 34.15 [1/m] D_e.

5.2.1 Variations of the Flow Quantities over the Radius and Height of the Cyclone

a) Tangential Velocity

The variation of the tangential velocity component over the radius of the chamber (for an inlet velocity, V_o, equal to 7.41 m/s and an exit diameter, D_e, equal to Ø.3D), is shown in Figure 5.1 for three different axial levels of the chamber. It is evident from these profiles that the swirling flow in the chamber resembles a Rankine vortex flow. The potential vortex which demonstrates a circulation preserving zone, extends from near the side wall of the chamber to the radius corresponding to that of the exit nozzle. The forced vortex part (solid body rotation) then, extends up to the axis of the chamber and constitutes the confined vortex core. Viscosity effects tend to smoothen out the otherwise sharp, transition zone at the common boundary between the potential and forced vortex consituents of the flow. The tangential velocity close to the side wall is equal to the inlet velocity, V_o, as calculated from the rotameter reading ($V_o = Q / \Sigma A_i$).

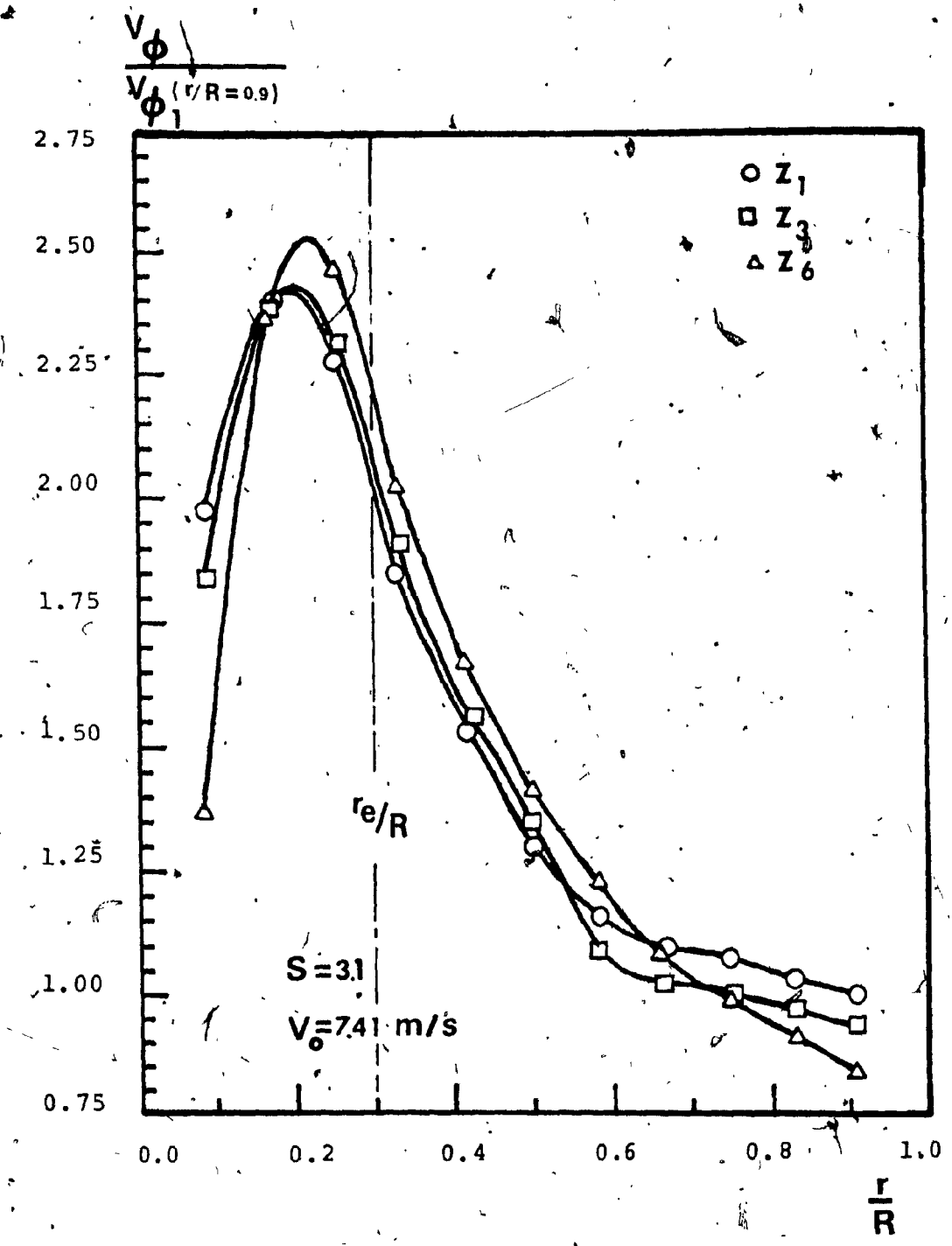

Fig. 5.1 Tangential velocity profiles

It was observed from measurements at different vertical locations, that the tangential velocity was not a strong function of the axial position, and consequently, it could be inferred that the vortex strength was basically constant along the height of the chamber. Along the side wall, however, a slight decrease in the tangential velocity profile was observed while at higher axial stations. This could be attributed to the fact that the flow loses energy due to the dissipative effects of the boundary layer at the side wall. At lower axial levels the forced vortex part of the flow was not well developed. As the flow ascended, however, enough time was allowed for an angular momentum exchange process to take place. As a result, the core at axial level Z_6 was more like a forced vortex flow. Moreover, the slightly greater tangential velocity, for $r > r_{max}$, at that axial level, suggests that the angular momentum of a particle was more likely to be conserved at that level, because the secondary flow was not as pronounced, and the radial flow was not reversed.

Additional measurements made at station 6 in vertical planes 90 degrees apart, verified the symmetry of the flow and confirmed the repeatability of the experiments.

b) Axial Velocity

The axial velocity component profiles basically show

the mode at which the vortex traverses the chamber from the inlet ports to the exit plane. It is evident, from Figure 5.2, that the axial velocity is far from being uniform. Four distinct flow zones are identifiable at all axial levels. Two of these zones, one along the side wall and the other near the axis of the chamber (at a radial distance about equal to the exit nozzle radius) move upward toward the top plate. The other two flow zones, one along the axis within the vortex core and the other located at a radial distance equal to about 0.5R, are reverse axial flows and indicate that a vortex breakdown occurs within the chamber. The axial velocity in these four zones is a function of the vertical position and that implies that the fluid is also being moved radially inward and outward as it flows upwards, i.e. is being recirculated in distinct fluid entrainment zones.

Two axial streams in opposite flow directions are distinguishable within the vortex core region. This core flow pattern develops as the surrounding atmospheric air is drawn into the chamber, due to the subatmospheric pressure along the axis, and is being recirculated back to the atmosphere at a greater radius. This reversed axial flow along the chamber axis was verified qualitatively by visualization. When smoke was introduced at the exit plane level, close to the center line, it was found that the smoke was drawn into the vortex chamber. It can be seen in

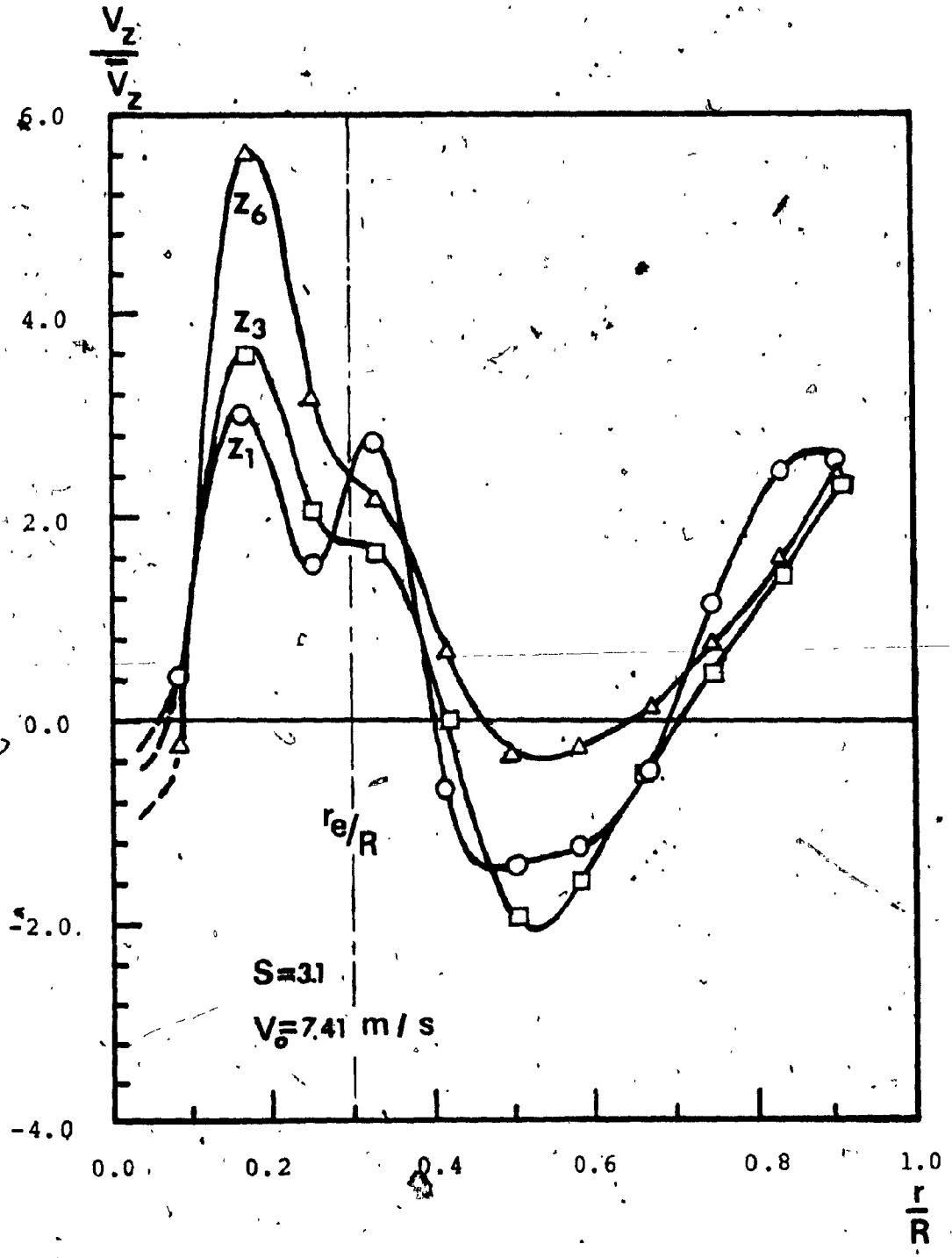

Fig. 5.2 Axial velocity profiles

Figure 5.2 that the radial extension of the core reverse flow is smaller at lower axial levels. That was expected as the atmospheric air drawn into the chamber is progressively returned back into the atmosphere as it moves downward toward the bottom plate. This, in turn, explains why the upward moving core flow is more intensive at axial level 6 than it is at the lower axial levels. The atmospheric air entrainment zone could be seen in Figure 5.2 by extrapolating the axial velocity profiles close to the axis. For the other vortex configurations (section 5.3), however, velocity measurements were made at even smaller radial distances and the above assertion was verified.

The radial distances corresponding to the two flow zones within the core, were approximately the same. Although the reverse atmospheric air flow occupied half of the core radius on its way into the chamber, it only required approximately 15% of the core radius on its way out of the chamber at a greater diameter. The remaing 45% of the core radius was occupied by the air supplied through the inlet ports.

It is remarkable that the maximum axial velocity occurs at the same radial position as the tangential velocity profile. This may be due to the fact that the inner upward zone, flowing between the two reverse flow

zones, loses angular and linear momentum at the same proportions, in order to transfer energy to these two dissipative zones.

C) Radial Velocity

It is generally agreed [7,29,30,31,32,33], that the major part of the radial flow toward the axis of a confined vortex is taking place close to the top and bottom end walls of the chamber. The radial velocity apart from the end wall boundary layers is expected to be comparatively small and results mainly from the recirculation of the fluid in the mass entrainment zones.

The experimental radial velocity profiles obtained in the present investigation did not comply fully with the experimental axial velocity profiles with regard to the continuity equation. This happened because the radial velocity was subject to inaccuracies, as discussed earlier in Chapter 4.

It was, however, possible to obtain quite accurate radial velocity values by using the experimentally obtained axial velocity profiles together with the continuity equation. This was done by considering an annular control

volume bounded by two horizontal planes at two adjacent axial stations at which the measurements were taken, and extending from the periphery of the chamber to a radius r at which the radial velocity had to be calculated, Fig. 5.3. According to the mass conservation law, the fluid entering from sections "a" and "b", would have to exit through the cylidrical surface "c". There was no mass flux considered through surface "d", because the radial velocity was zero at the side wall of the chamber. The net volumetric flow rate crossing surface "a" was determined by performing the following integration:

$$Q_a(r) = 2\pi \int_r^R r V_{za}\, dr \qquad (5.3)$$

Similarly for surface "b":

$$Q_b(r) = 2\pi \int_r^R r V_{zb}\, dr \qquad (5.4)$$

Then, the volumetric flow rate through surface "c" could be expressed as:

$$Q_c(r) = 2\pi \int_r^R r\{ V_{za} + V_{zb} \}\, dr \qquad (5.5)$$

and the average radial velocity between two adjacent measuring stations at a radius r could be determined as:

$$\overline{V}_r(r) = \frac{Q_c(r)}{2\pi r \Delta h} \qquad (5.6)$$

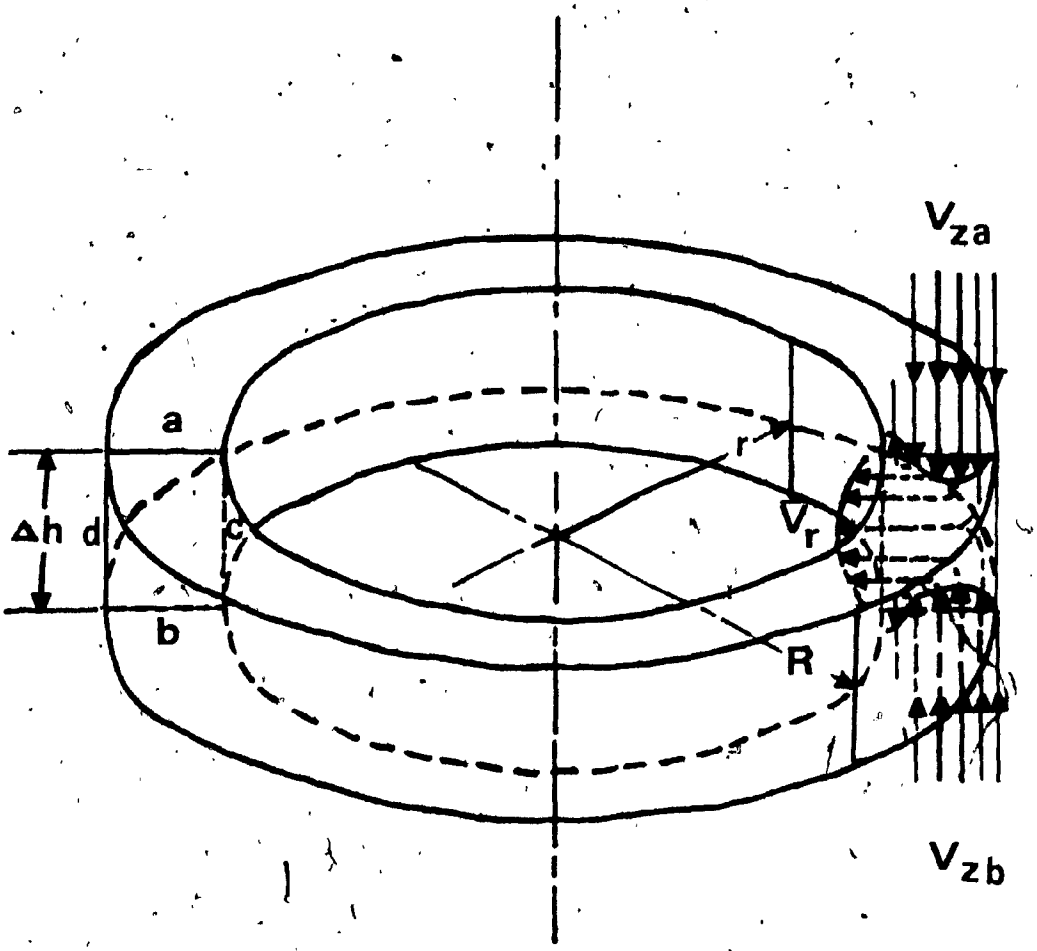

Fig. 5.3 Annular control volume

The above calculations were performed for the five such control volumes, formed between the six axially distributed measuring stations, and the results are shown in Figure 5.4.

The radial velocity profiles clearly show that a recirculation zone composed of two counter-rotating vortices, exists along the height of the chamber. These secondary vortices seem to extend vertically upward almost to the 6th measuring station where no air reverse zones are observed except very close to the center. Secondary vortices seem to exist along the axis of the chamber where the ambient fluid entrainment zone is. The above discussed flow pattern will become very clear when the streamlines in the vertical plane will be presented in Chapter 6.

d) Static Pressure

The static pressure distribution along the radius and height of the chamber is shown in Fig. 5.5., It is evident that the maximum pressure occurs at the side wall of the chamber due to the action of the centrifugal force. The pressure is decreasing at a progressively higher rate as the center of the chamber is approached, and becomes

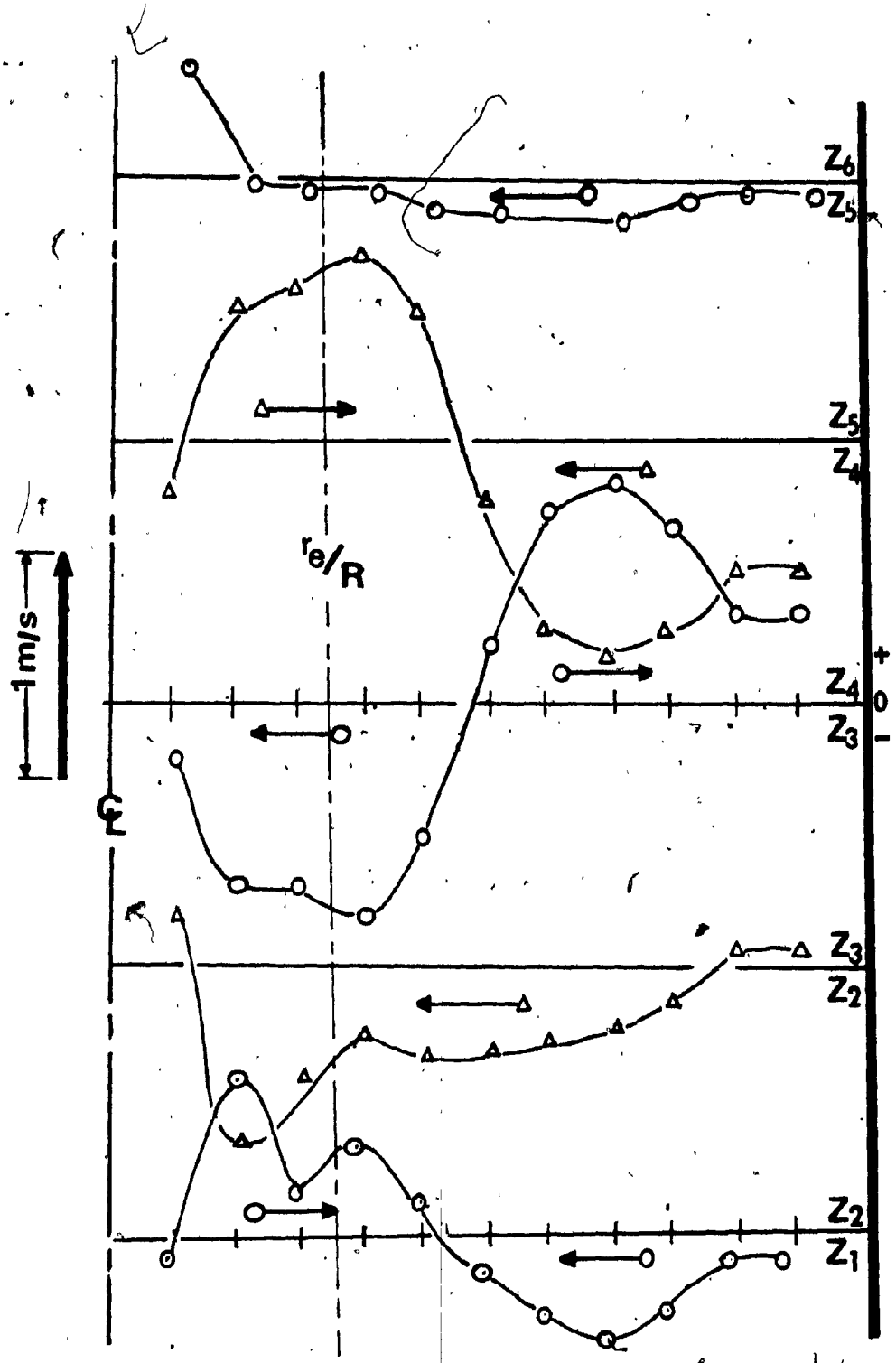

Fig. 5.4 Radial Velocity profiles

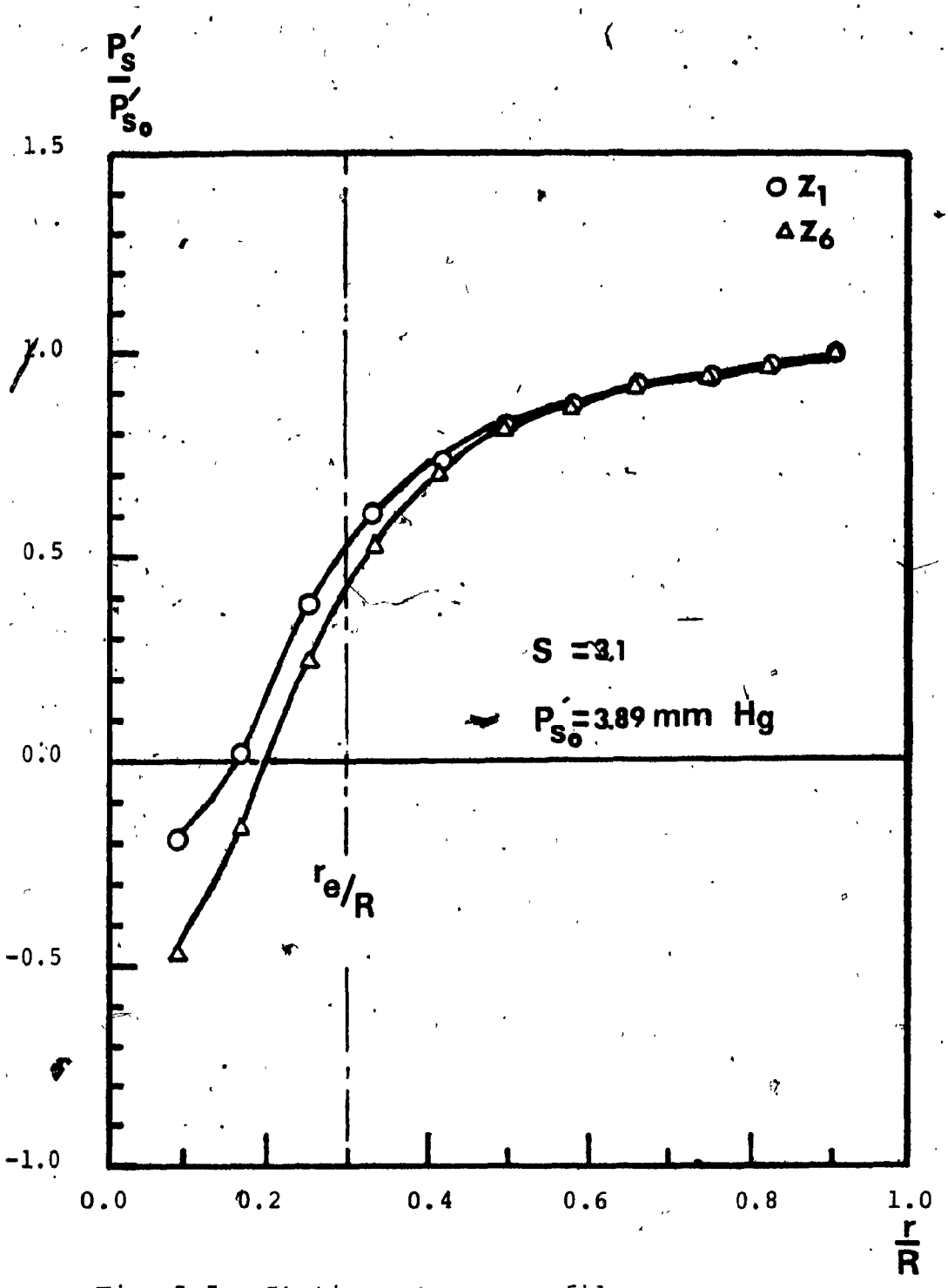

Fig. 5.5 Static pressure profiles

subatmospheric when close to the axis of the chamber. The negative pressure detected complies very well with the reverse axial velocity observed at the center of the chamber.

The gradient of the static pressure along the height of the chamber is very low and this is basically due to the relatively low mass flow rate and to the large diameter of the chamber. However, it was observed that the static pressure at measuring station 1 is slightly higher than the static pressure at measuring station 6.

5.2.2 Effects of the Inlet Velocity

The structural configuration of the vortex chamber (single bottom vortex) was not altered, while the inlet velocity was being varied by changing the mass flow rate at the bottom tangential inlets. Since the tangential velocity was found to be constant in the axial direction as discussed in the previous section, measurements were carried out only at axial station 4. From the results, (shown in Figure 5.6), it can be observed that the tangential velocity is increasing with the inlet velocity (or with the mass flow rate through the chamber). It is, however, interesting to note that the maximum value of the velocity occurs at the same radial position for all the mass flow rates examined.

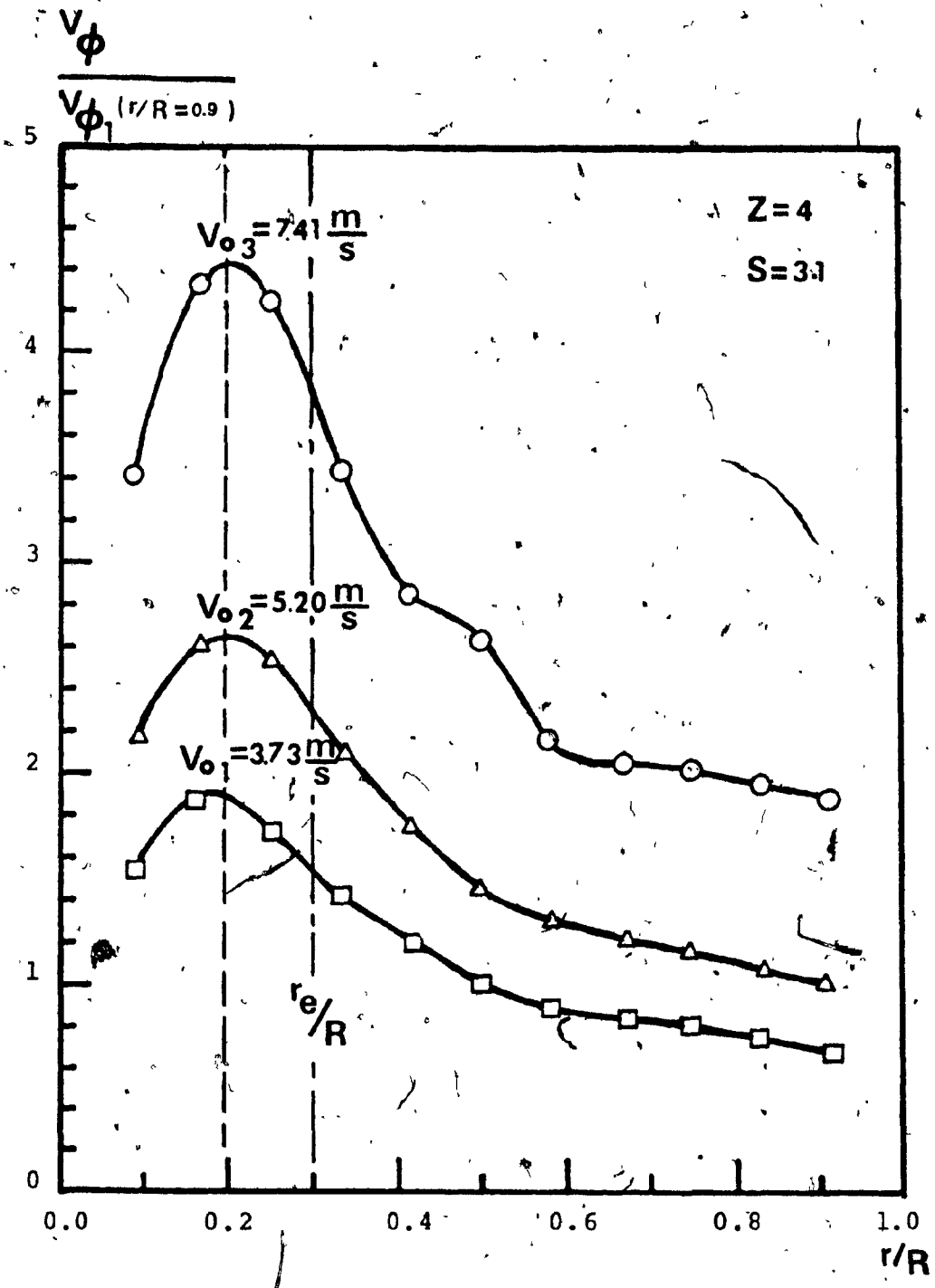

Fig. 5.6 Tangential velocity profiles for different inlet velocities

The inlet velocity could also be varied by changing the inlet flow area while keeping the air mass flow rate constant. In that case, it was also found that the peak value of the tangential velocity occured at at the same radial distance. The only parameter that was likely to affect the location of the maximum tangential velocity was the exit nozzle diameter as will be discussed in the next section.

The effect of the inlet velocity on the axial velocity profile is shown in Figure 5.7. For higher inlet air flow rates the axial velocity increased while the shape of its profile remained virtually identical. That is, the width of the different axial flow zones remained almost constant, while the velocity magnitude varied. There was, however, a minimum value of the inlet velocity, below which the secondary reverse flow zone in the middle-radius distance was not induced. For the present vortex configuration the value of that inlet velocity was found to be close to 2.75 m/sec.

The effect of the inlet velocity on the radial distribution of the static pressure is shown in Figure 5.8. As expected, larger tangential velocities produced larger static pressures close to the side wall of the chamber. It is very interesting to note however, that the static pressure dropped to subatmospheric values. This occurred at the same radial distance for all the different cases. That

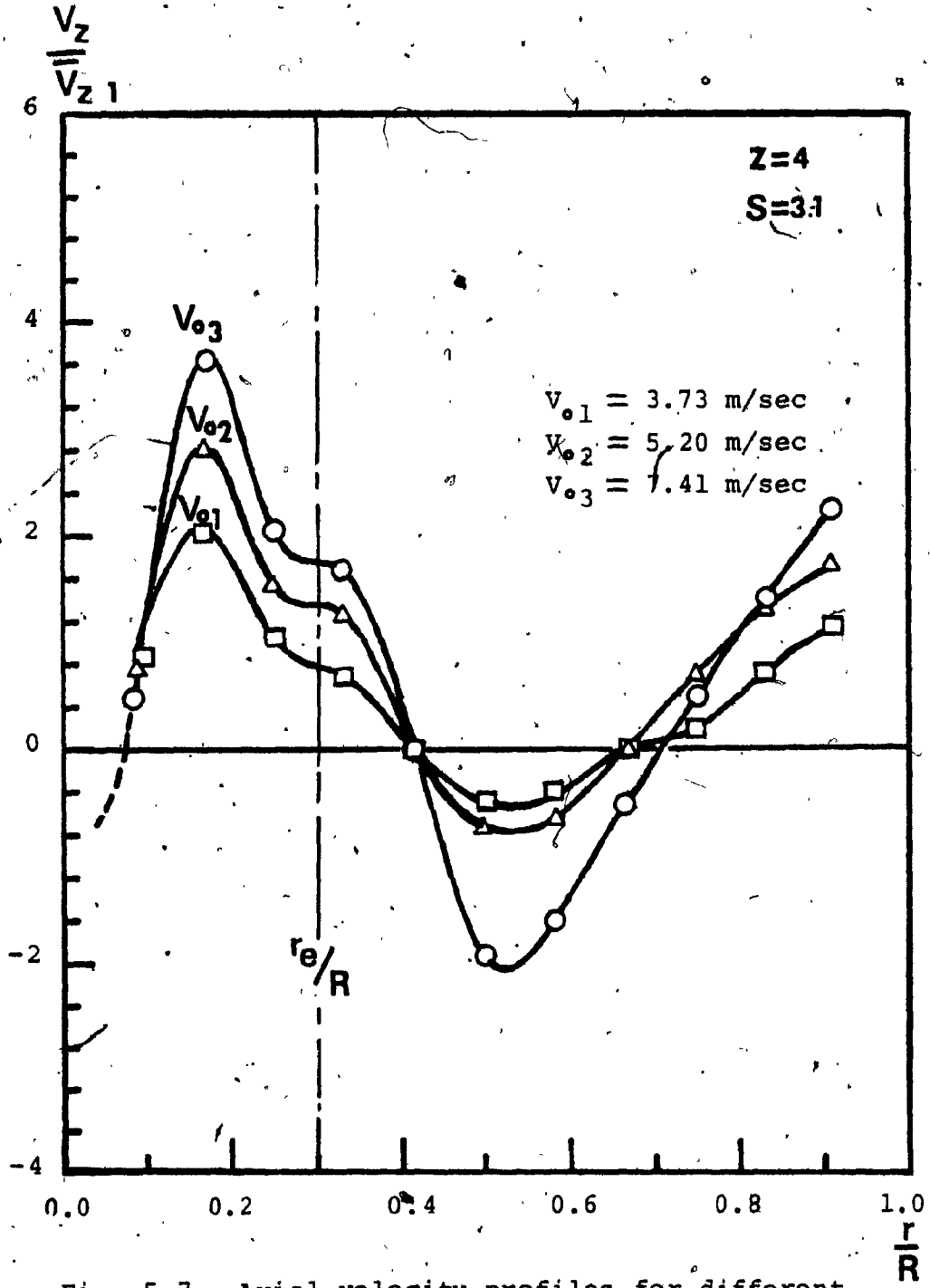

Fig. 5.7 Axial velocity profiles for different inlet velocities

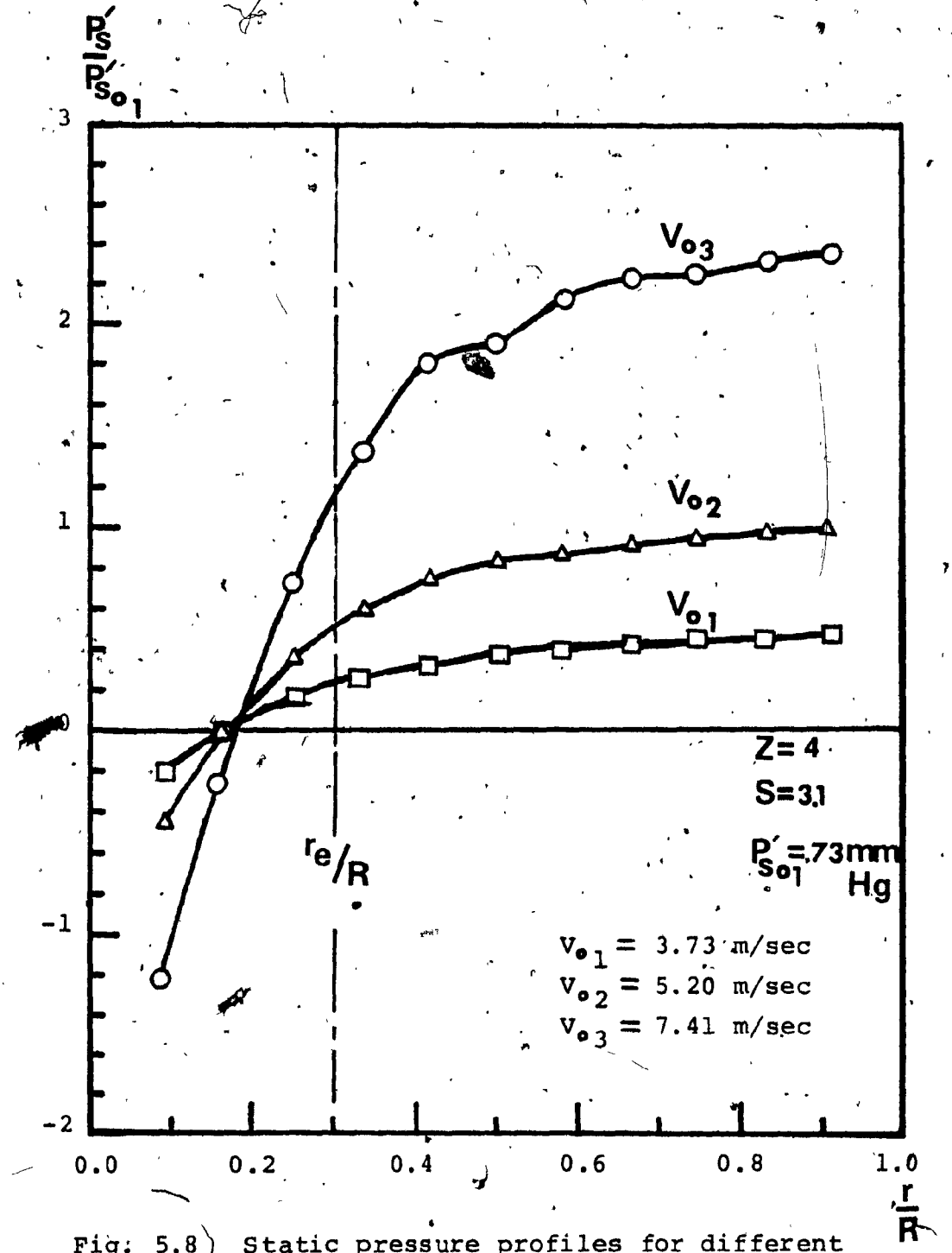

Fig. 5.8 Static pressure profiles for different inlet velocities

distance was almost equal to that for the maximum tangential velocity. This was expected because the static pressure is directly related to the tangential velocity.

5.2.3. Effect of the Exit Nozzle Size

It is generally accepted [4, 16, 17, 18, 19, 20, 33], that the location of the peak of the tangential velocity profile is highly dependent on the exit nozzle diameter. This was also found in the present investigation when different sizes of exit nozzles were used, while the air mass flow rate was kept constant. The results are shown in Figure 5.9. It is interesting to note that the potential vortex part of the flow profile is almost the same for all the different exit conditions.

For the present geometric configuration of the chamber (L/D=1.5), and for an input flow velocity equal to V_o=9.67 m/sec, the relationship between the radial position of the maximum tangential velocity and the exit nozzle radius of the chamber, was found to be almost linear, as shown in Figure 5.10. This relationship is described by the equation:

$$r_{max}=r_e - 0.1R \qquad (5.7)$$

The above equation is expected to hold true also for different inlet velocities, because the radial location of the maximum tangential velocity was found to be independed of the mass flow rate, see Figure 5.6.

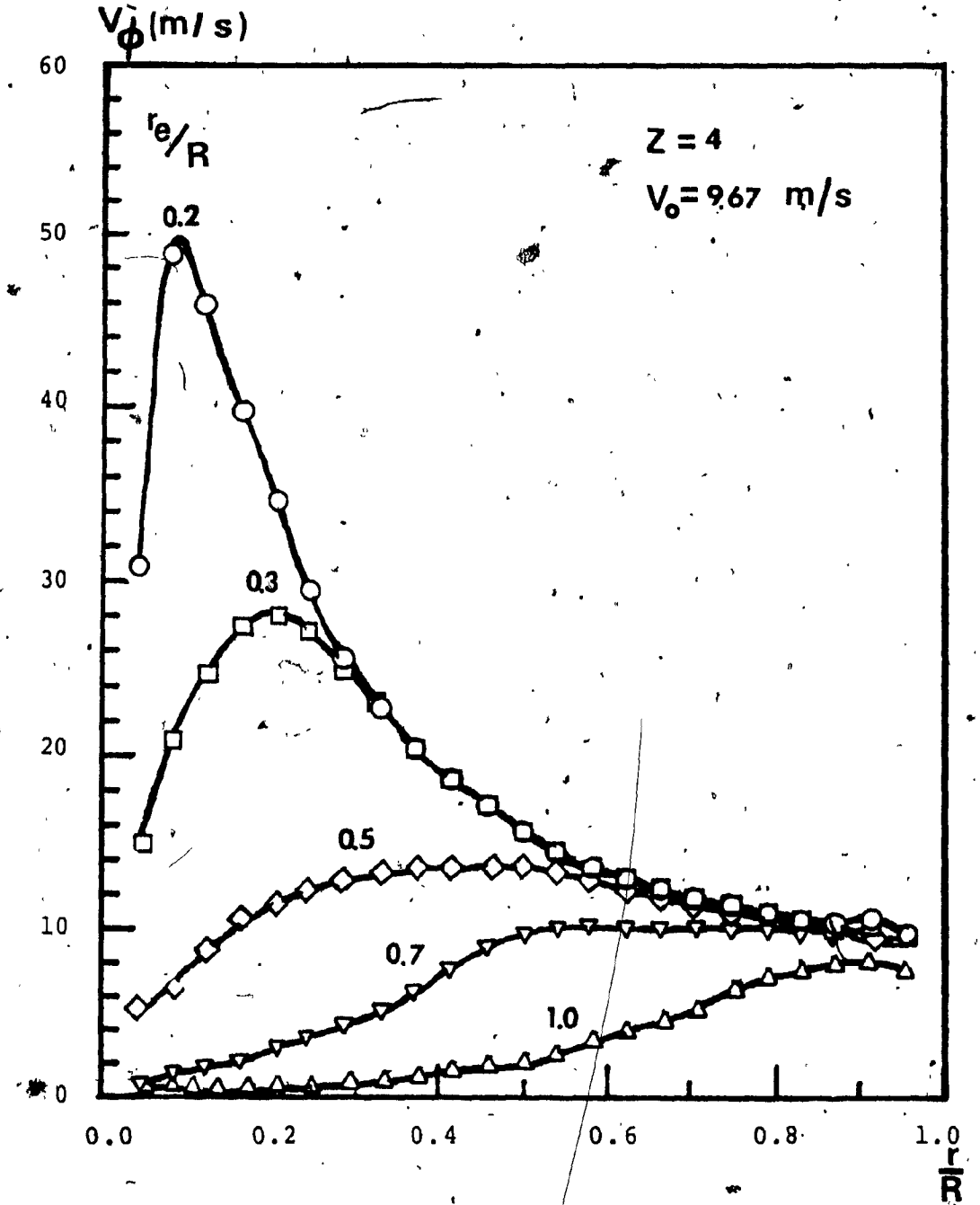

Fig. 5.9 Tangential velocity profiles for different exit nozzle sizes

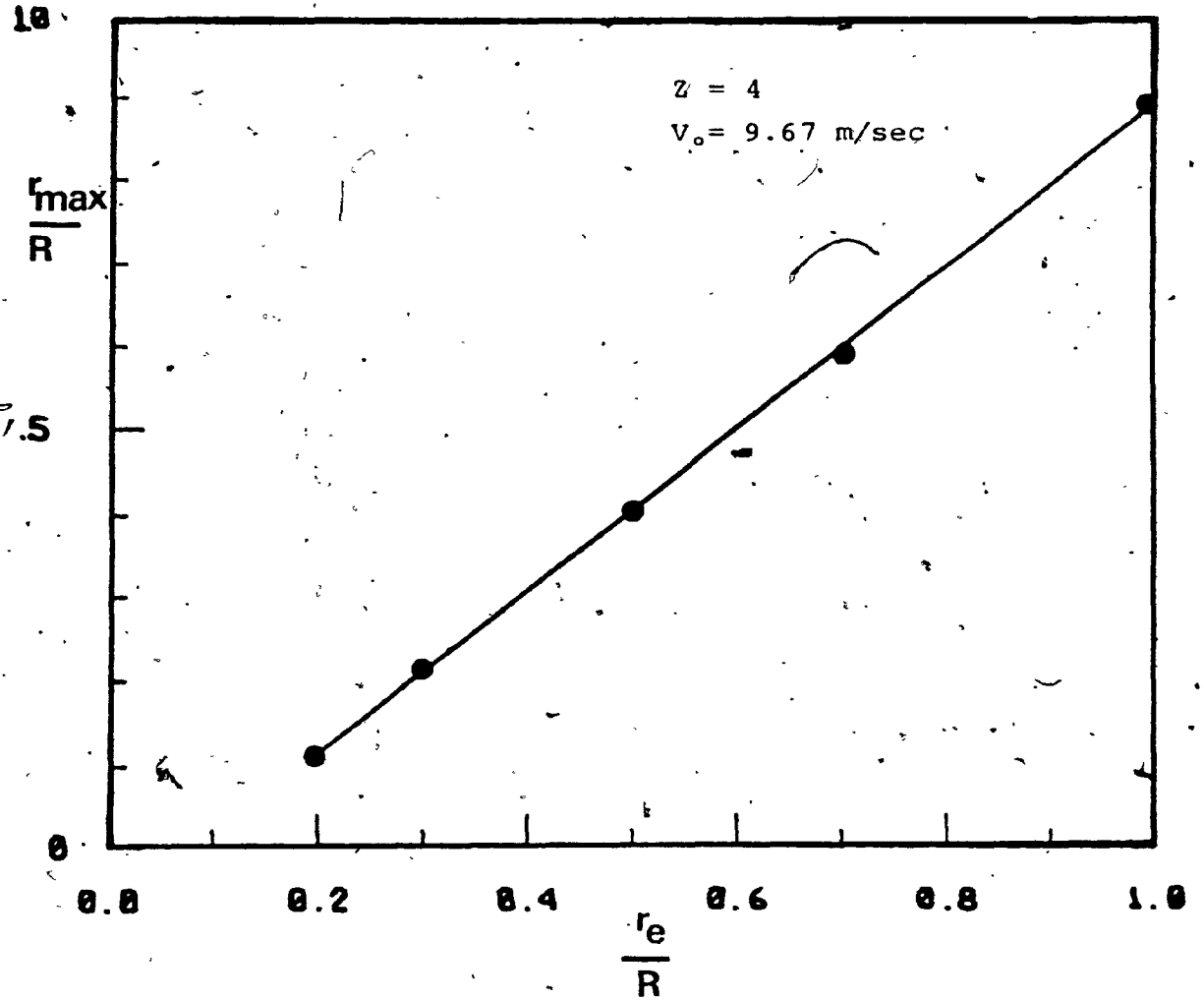

Fig. 5.10 Radial position of the maximum tangential velocity versus the exit nozzle radius

Significant changes, in the axial velocity profiles were also noted as the exit nozzle diameter was being varied. These effects are shown in Figure 5.11. It is striking to note that the maximum of the axial upward stream located closer to the axis of the chamber, was changing its radial position in the same fashion as the peak tangential velocity. The velocity profiles, however, remained unaltered for radii greater than that of the exit nozzle. In the extreme case of very large outlet sizes, only two flow zones were formed. This case is clearly shown for an exit radius equal to 0.7R, where a reverse flow extending from the center of the chamber to about half of the radius, and an upward flow extending from the mid-radius distance to the side wall of the chamber, were formed.

The static pressure within the chamber decreased considerably as the exit nozzle diameter was increased, Fig. 5.12. This was expected because the exit nozzle flow restriction is producing a back pressure within the vortex chamber. The radial position where the static pressure was inverted, was found to be depending on the exit nozzle diameter much the same way as the position of the maximum tangential velocity.

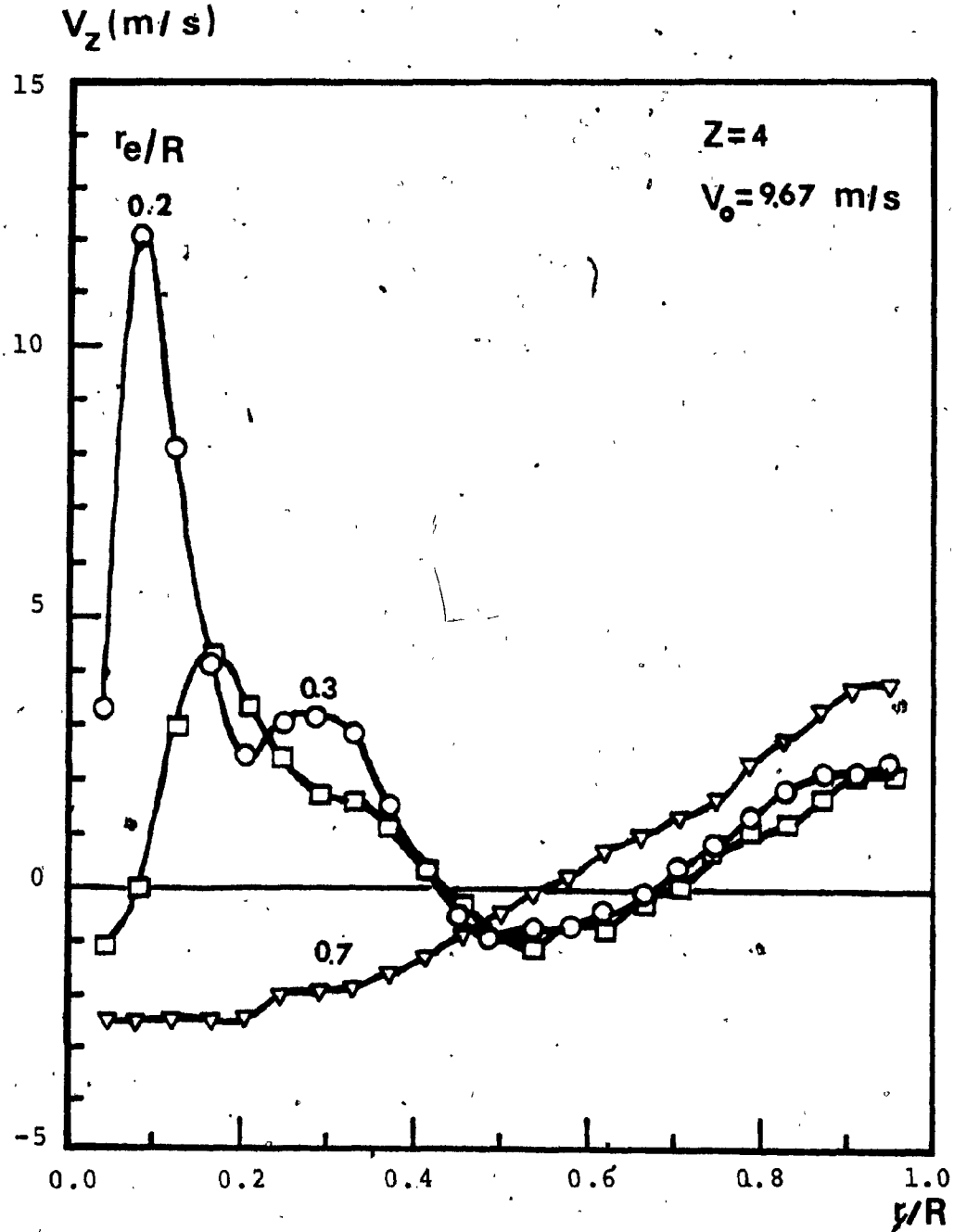

Fig. 5.11 Axial velocity profiles for different exit nozzle sizes

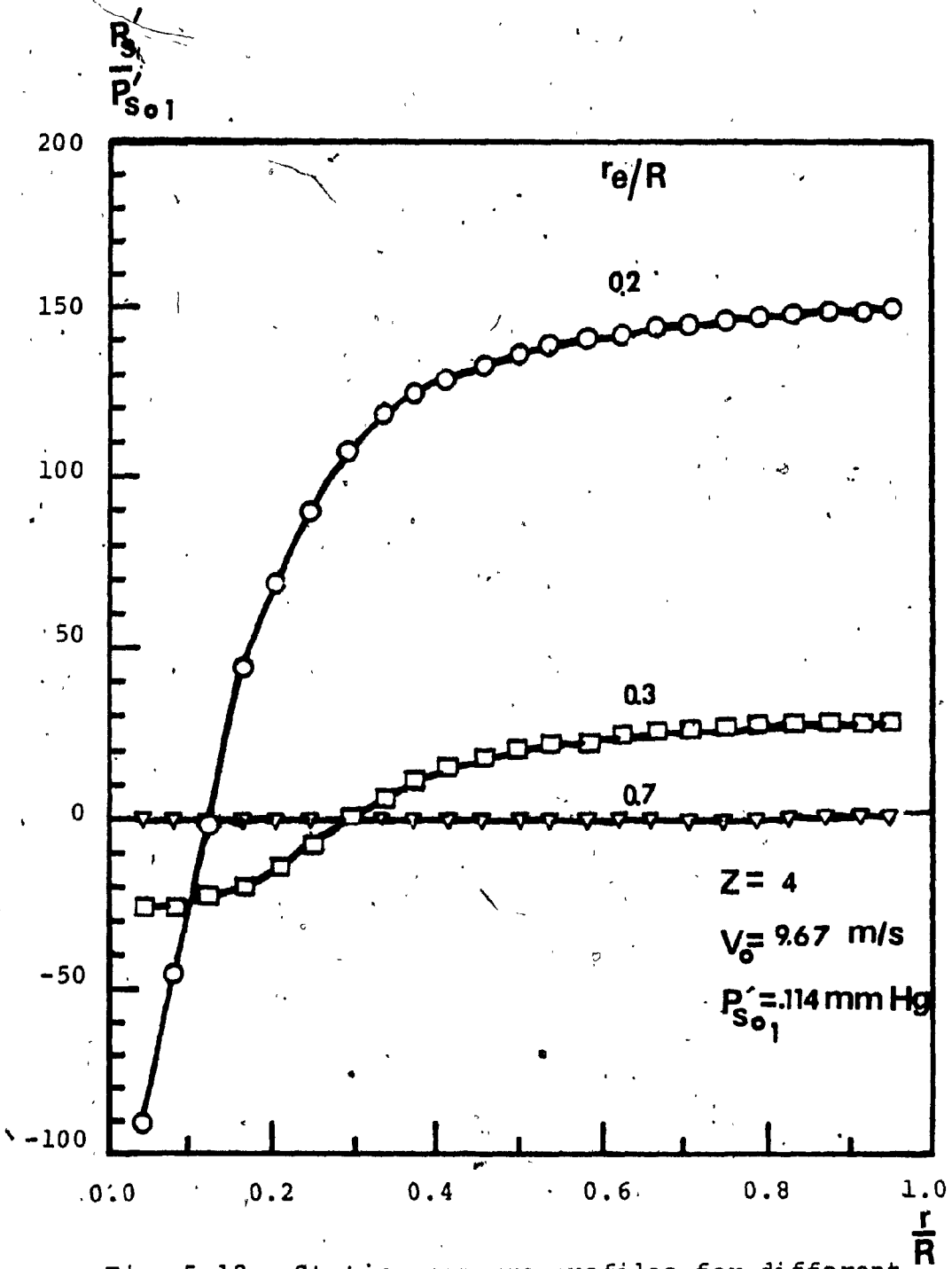

Fig. 5.12 Static pressure profiles for different exit nozzle sizes

5.3 Single Vortex: Top Air Supply

The tangential velocity profile and the static pressure distribution in the radial direction for the single vortex with top air supply were found to be quite similar to their respective profiles obtained in the single vortex with bottom inlet configuration. The axial velocity profiles however were radically different.

The axial velocity profiles for three different axial positions are shown in Figure 5.13. It is observed that the air close to the side wall has a significant downward axial velocity component and exists in almost one third of the radial distance of the chamber. Since this flow eventually has to be diverted upwards again, in order to exit the vortex chamber, another flow stream closer to the axis of the chamber and flowing upwards, is being formed. This second stream occupies a radial distance, which amounts to about two thirds of the chamber's radius. This is expected since mass continuity must be preserved and because the second stream located closer to the center of the chamber, is associated with smaller flow areas. Along the axis of the chamber a reverse flow zone that has a similar characteristic as the axial core flow of the bottom single vortex configuration, is observed.

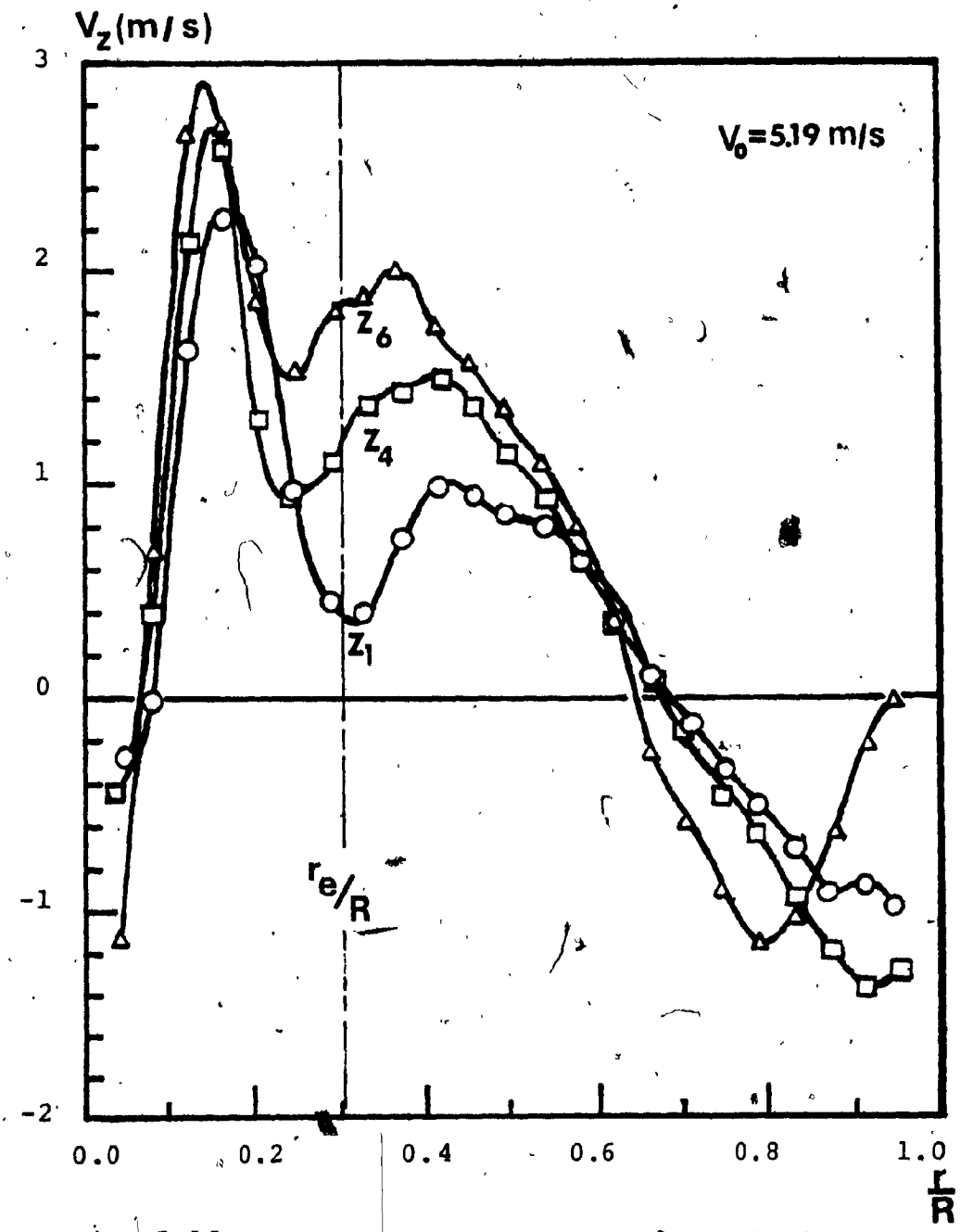

Fig. 5.13 Axial velocity profiles for single vortex with top inlet

5.4 Double Vortex

With regard to the tangential velocity profiles, no particular features different from those already observed in the single vortex flow patterns, were found in the double vortex configuration. The axial flow for comparable strengths of the top and bottom parts of the double vortex, was found to exhibit very similar characteristics to those found in both types of the single vortex pattern. Specifically, in the top part of the chamber the axial velocity resembled the axial velocity of the single vortex with top inlet, while in the bottom part of the chamber, the axial velocity was found to be similar to that of the single vortex with bottom air inlet, Fig. 5.14. When the top vortex was prevailing however, its characteristic axial flow pattern was extending along the whole length of the chamber. The opposite happened as the bottom airflow rate was increased to higher values than that of the top vortex. The axial velocity profiles close to the wall for two particular conditions are shown in Figure 5.15.

The most important feature of the double vortex is related to the radial velocity component. Its radial velocity profile is quite unique at some axial level where the two vortices, the top and the bottom, meet and are diverted radially inwards. As a result, a high localized radial stream is created. By employing the method

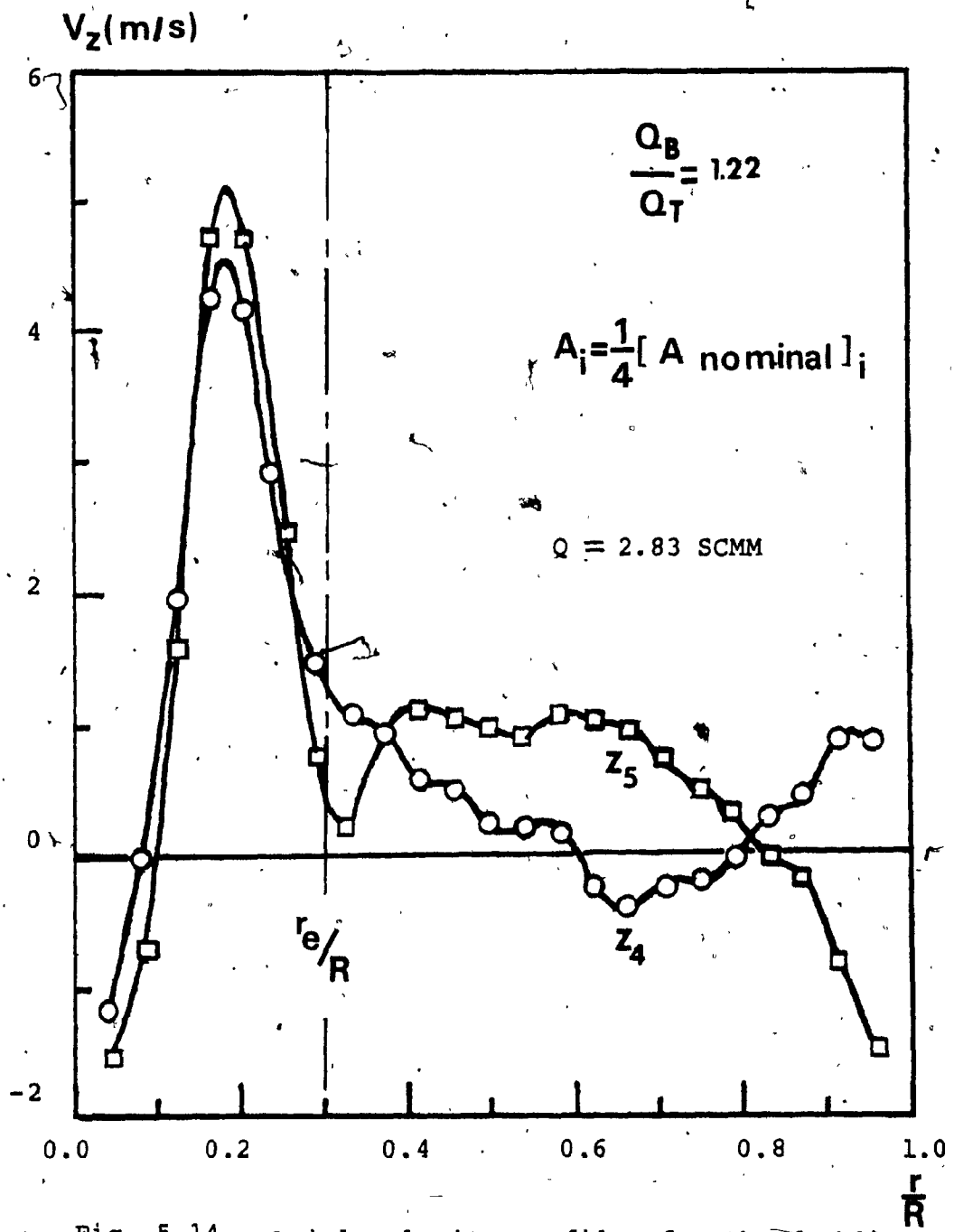

Fig. 5.14 Axial velocity profiles for the double vortex configuration of the cyclone chamber

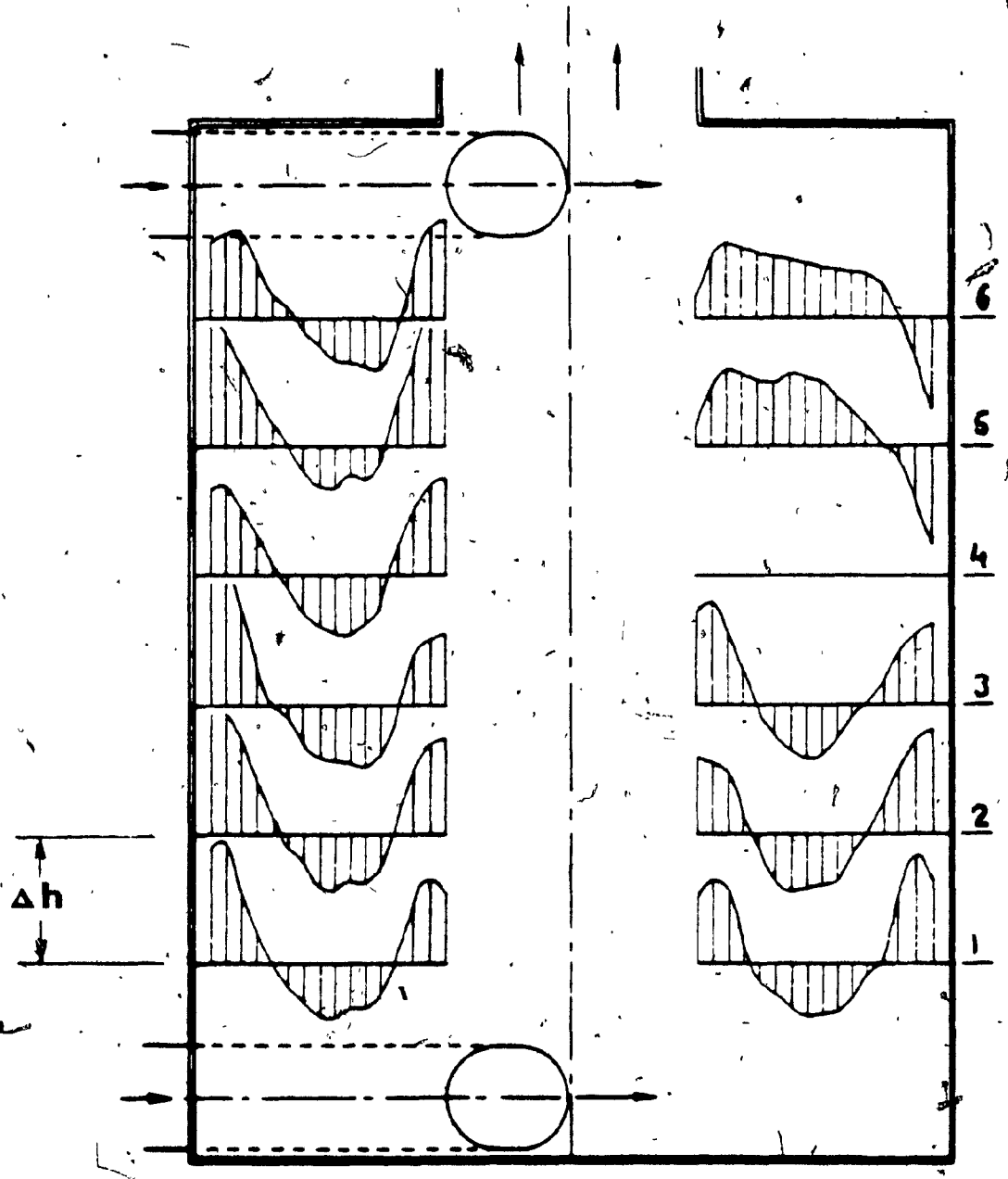

Bottom flow 65% Bottom flow 55%
Top flow 35% Top flow 45%
Q = 2.83 SCMM

Fig. 5.15. Axial component of velocity in the double vortex chamber for two different air flow conditions.

described in section 5.1, the radial velocity at that location was determined and is shown in Figure 5.16. As expected, the radial velocity at this level is quite high when close to the side wall. It decreases rapidly, however, and reaches a value of nearly zero at a radius close to that of the exit nozzle. This implies that the localized radial stream turns into an axial flow at that radial distance.

The above flow pattern agrees very well with the predictions made by the inventor of the double vortex cyclone chamber, D. Angus [24].

5.5 Some Analytical Considerations

5.5.1 Motion Governing Equations

The conservation of linear momentum is expressed by a set of three differential equations (one for each spacial direction) known as the Navier-Stokes equations. More specifically, these equations represent the force equilibrium in the respective three flow directions. In order to describe the general flow of the fluid, the above equations would have to be supplemented by the continuity equation which expresses the mass conservation at any point (or infinitesimal control volume) within the flow field. The complete set of the above equations, in their most

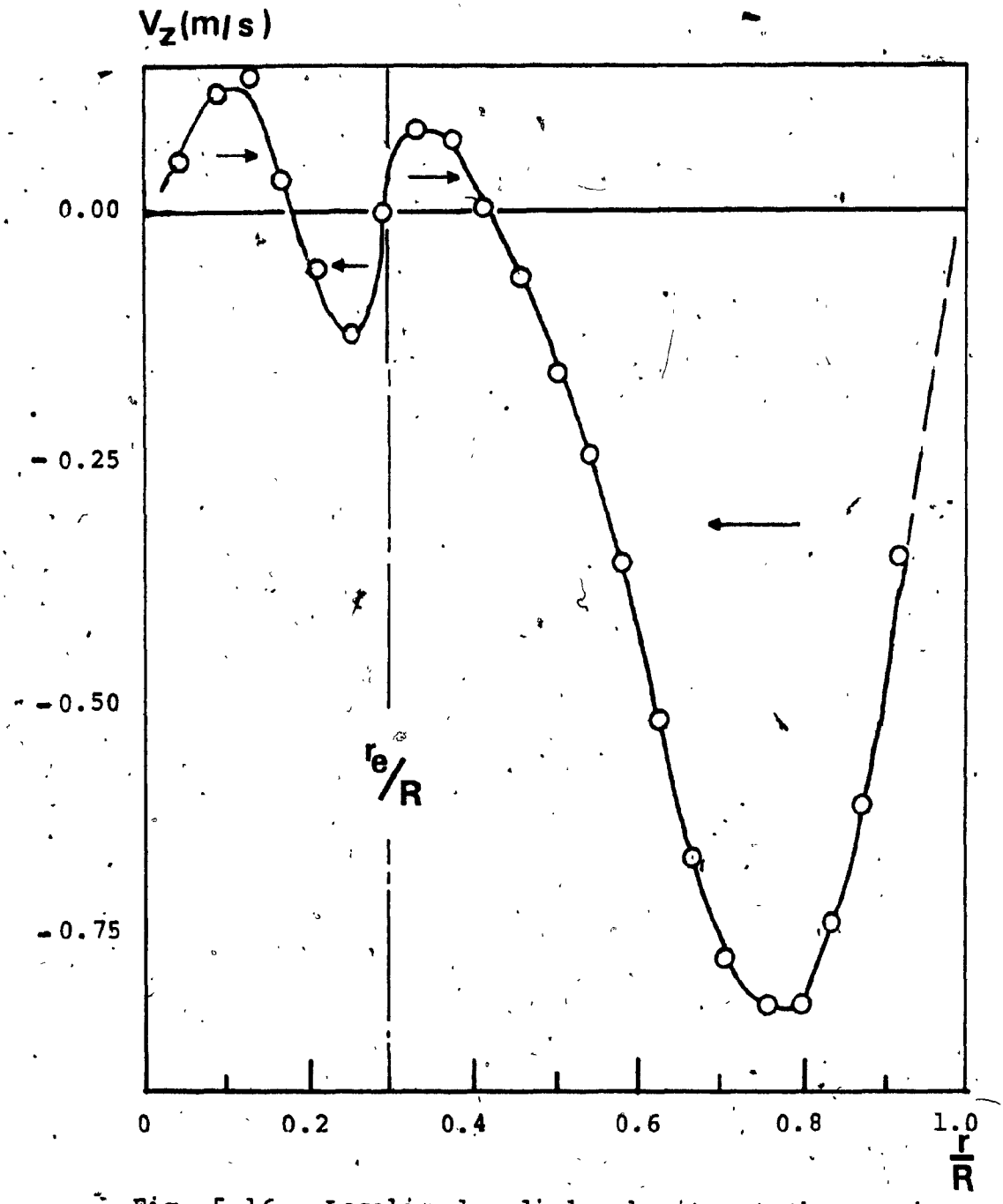

Fig. 5.16 Localized radial velocity at the merging level of the two vortices

general form can be found in reference 39 for cylidrical coordinates.

A closed form solution of the above equations in their full form cannot be obtained. In order to render these equations amenable to mathematical treatment, certain assumptions and simplifications must be made. With the advent of advanced computers, however, solutions of more complex forms of the Navier-Stokes equations can now be approximated very accurately

In the present work no attempt was made to obtain a numerical solution of the momentum and the continuity differential equations. These equations, however, were coupled with the experimental results in order to make predictions of the radial profile of the static pressure.

5.5.2 Prediction of Static Pressure from the Experimental Tangential Velocity Profiles

The momentum equation in the radial direction can be employed in order to obtain a simple relationship between the tangential velocity and the static pressure. The equation can be reduced to a very simple form if we consider that we are dealing with an axisymmetric, steady state flow problem. That implies:

$$\frac{\partial}{\partial_t} = 0, \quad \frac{\partial}{\partial_\phi} = 0 \quad \text{and} \quad \frac{\partial^2}{\partial_{\phi^2}} = 0 \qquad (5.8)$$

Furthermore, constant density, ρ, and kinematic viscocity, ν, can be assumed. All quantities are taken to be represented by their time-averaged values. The radial velocity away from the end wall is expected to be many orders of magnitude smaller than the tangential velocity [4,7,16,28,29] and can be neglected without introducing any serious error. To further simplify the problem, the axial velocity gradients are neglected as compared to gradients in the radial direction. Under the above assumptions we obtain:

$$\frac{dP}{dr} = \rho \frac{V_\phi^2}{r} \qquad (5.9)$$

The flow in the vortex chamber is considered to approximate a "Rankine vortex", and the static pressure distribution for the forced and potential parts can be studied separately.

a) Potential Vortex

The tangential velocity profile in the radial direction for the potential flow is approximated by:

$$V_\phi r^n = K_1 \qquad (5.10)$$

By taking the logarithm of both sides of the equation we obtain:

$$\log V_{\phi} + n \log r = \log K_1 \qquad (5.11)$$

This equation represents a straight line for $X = \log r$ and $Y = \log V$. The expression $B = \log K_1$ gives the Y-axis intersection, and $(-n)$ represents the slope of this relationship. As a result, the power law exponent, n, is readily obtainable from the experimental results. The "best-fit" straight line through the experimental points can be obtained by the linear regression of the respective X and Y values. The value of n and K_1 can then be obtained as follows:

$$n = \frac{N \sum_{i=1}^{N} X_i Y_i - \sum_{i=1}^{N} X_i \sum_{i=1}^{N} Y_i}{N \sum_{i=1}^{N} X_i^2 - \left(\sum_{i=1}^{N} X_i \right)^2} \qquad (5.12)$$

and

$$K_1 = \frac{\sum_{i=1}^{N} Y_i \sum_{i=1}^{N} X_i^2 - \sum_{i=1}^{N} X_i \sum_{i=1}^{N} X_i Y_i}{N \sum_{i=1}^{N} X_i^2 - \left(\sum_{i=1}^{N} X_i \right)^2} \qquad (5.13)$$

By introducing Equation 5.10 into Equation 5.9 and integrating we obtain:

$$\Delta P = -\frac{\rho K_1^2}{2n} \Delta \left(\frac{1}{r^{2n}} \right) \qquad (5.14)$$

Employing the boundary condition:

$$P = P_w \quad \text{at} \quad r = R$$

Equation 5.10 becomes:

$$P_w - P = \frac{\rho K_1^2}{2n} \left\{ \frac{1}{r^{2n}} - \frac{1}{r_w^{2n}} \right\} \qquad (5.15)$$

To non-dimensionalize Equation 5.15, we divide both sides of the equation by P_w. For $P^* = P/P_w$ and $r^* = r/R$ we obtain:

$$P^* = 1 - \frac{\rho K_1^2}{2n P_w R^{2n}} \left(r^{*-2n} - 1 \right) \qquad (5.16)$$

$$r^*_{max} \leq r^* < 1$$

b) Forced Vortex

In the core region the tangential velocity can be approximated by:

$$\frac{V_\phi}{r} = K_2 \qquad (5.17)$$

Introducing Equation 5.17 into Equation 5.9 and integrating we obtain:

$$\Delta P = \frac{\rho K_2^2}{2} \Delta r^2 \qquad (5.18)$$

For the boundary condition:

$$P = P_c \quad \text{at} \quad r = r_{max}$$

Equation 5.18 becomes:

$$P_c - P = \frac{\rho K_2^2}{2} \left(r_{max}^2 - r^2 \right) \qquad (5.19)$$

By non-dimensionalizing we obtain:

$$P^* = \frac{\rho K_2^2 R^2 r^{*2}}{2 P_w} \left(\frac{r_{max}^{*2}}{r^{*2}} - 1 \right) + P_c^* \qquad (5.20)$$

$$0 < r^* < r_{max}^*$$

The position of the maximum tangential velocity and the pressure at the wall are needed for the prediction of the radial profile of the static pressure. As seen in section 5.2.3, however, an empirical relation for the radial position of the maximum tangential velocity was obtained. That relation can be coupled with Equations 5.16 and 5.20 to give the radial profile of the static pressure.

Density variations can be taken into account in the above static pressure prediction if a finite difference grid is assumed where density at a point would be evaluated by employing the state equation using the pressure from the previous radial location.

5.5.3 Results

The tangential velocity power exponent, n, for the potential vortex part of the flow, for many different flow conditions, was calculated and found to be within a range of Ø.75 to Ø.82 with an average value of Ø.78. The tangential velocity profiles for a mass flow rate of 3.68 SCMM and exit nozzle diameters of Ø.2D and Ø.3D, obtained by employing Equation 5.1Ø are shown in Figure 5.17, being superimposed on the experimental velocity profiles.

It is remarkable to note that the flow with respect to its rotation can very well be described by the "combined vortex" assumption. Maximum error, as expected, occurs at the transition from the potential to forced vortex zone, where Equation 5.1Ø overestimates the experimental results. For larger exit diameters, however the forced vortex

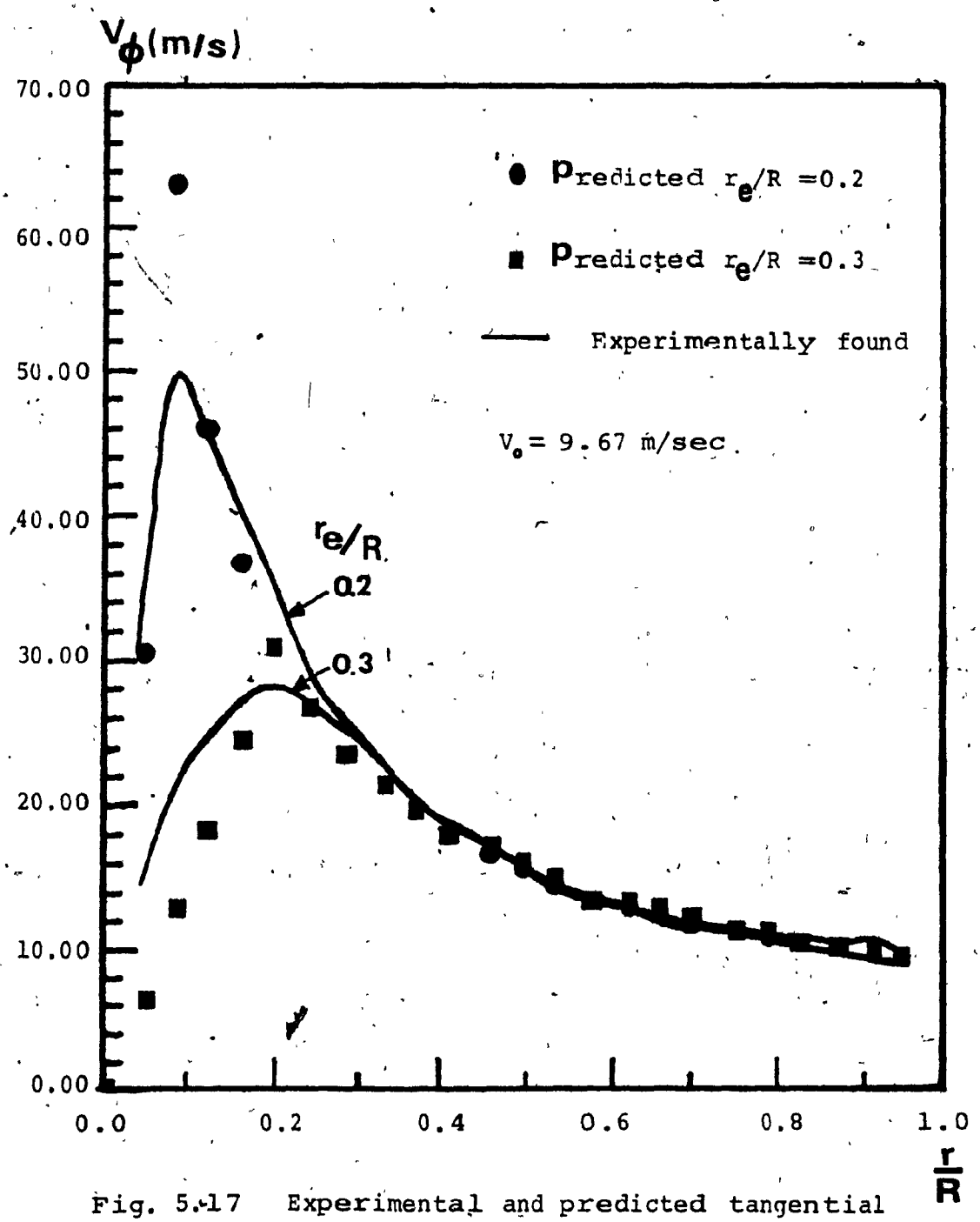

Fig. 5.17 Experimental and predicted tangential velocity profiles

assumption underestimates the experimental results.

The static pressure obtained for the same conditions as for the tangential velocity from the semi-analytical Equation 5.16 and 5.20, are shown in Figures 5.18 and 5.19. From these results it can be concluded that the radial profile of the static pressure can accurately be obtained from the static pressure at the side wall of the chamber, the tangential velocity exponent n, and the location of the maximum tangential velocity. Maximum error was, as expected, close to the vortex transition zone.

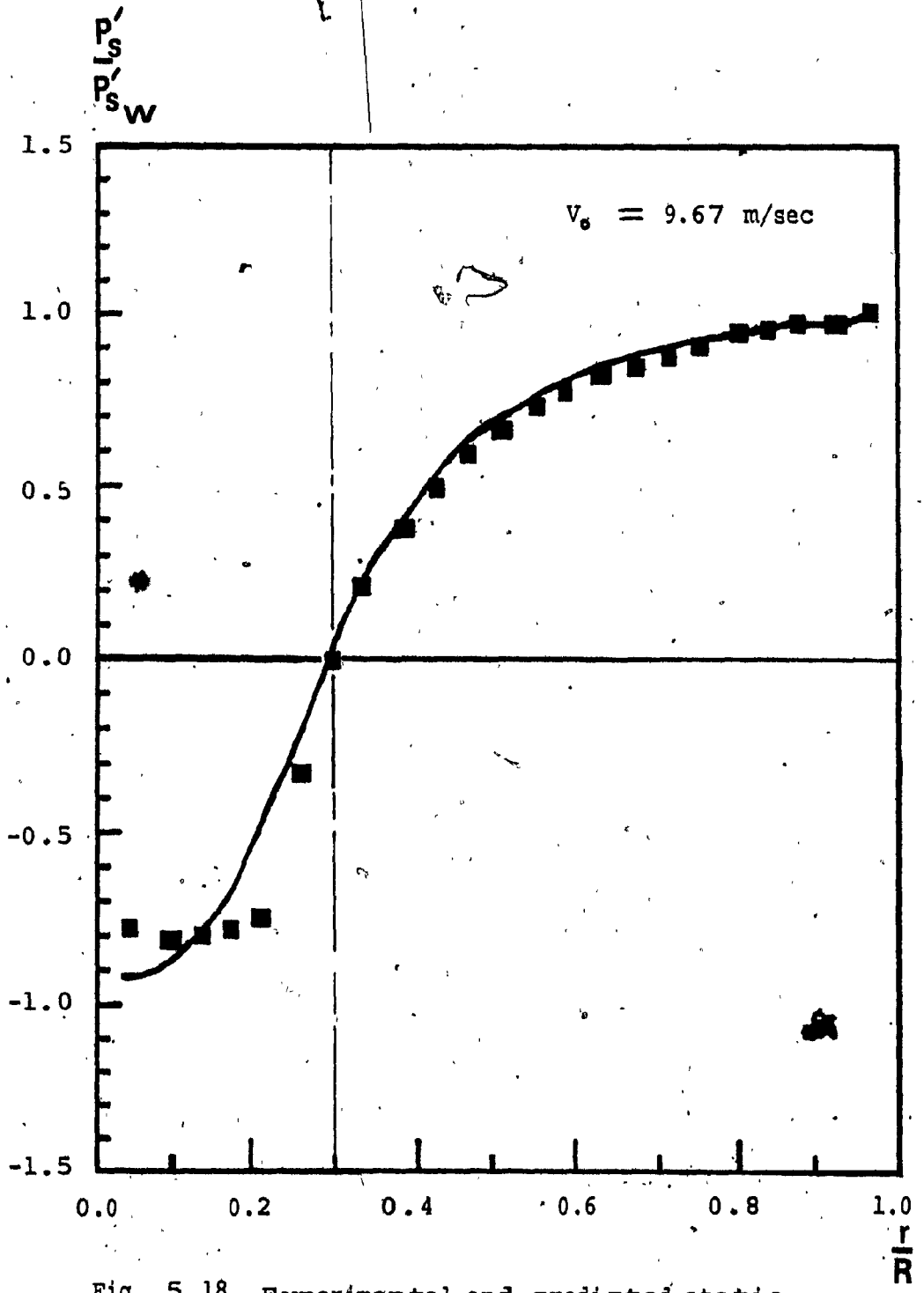

Fig. 5.18 Experimental and predicted static pressure profiles for exit nozzle size D_e=0.3D

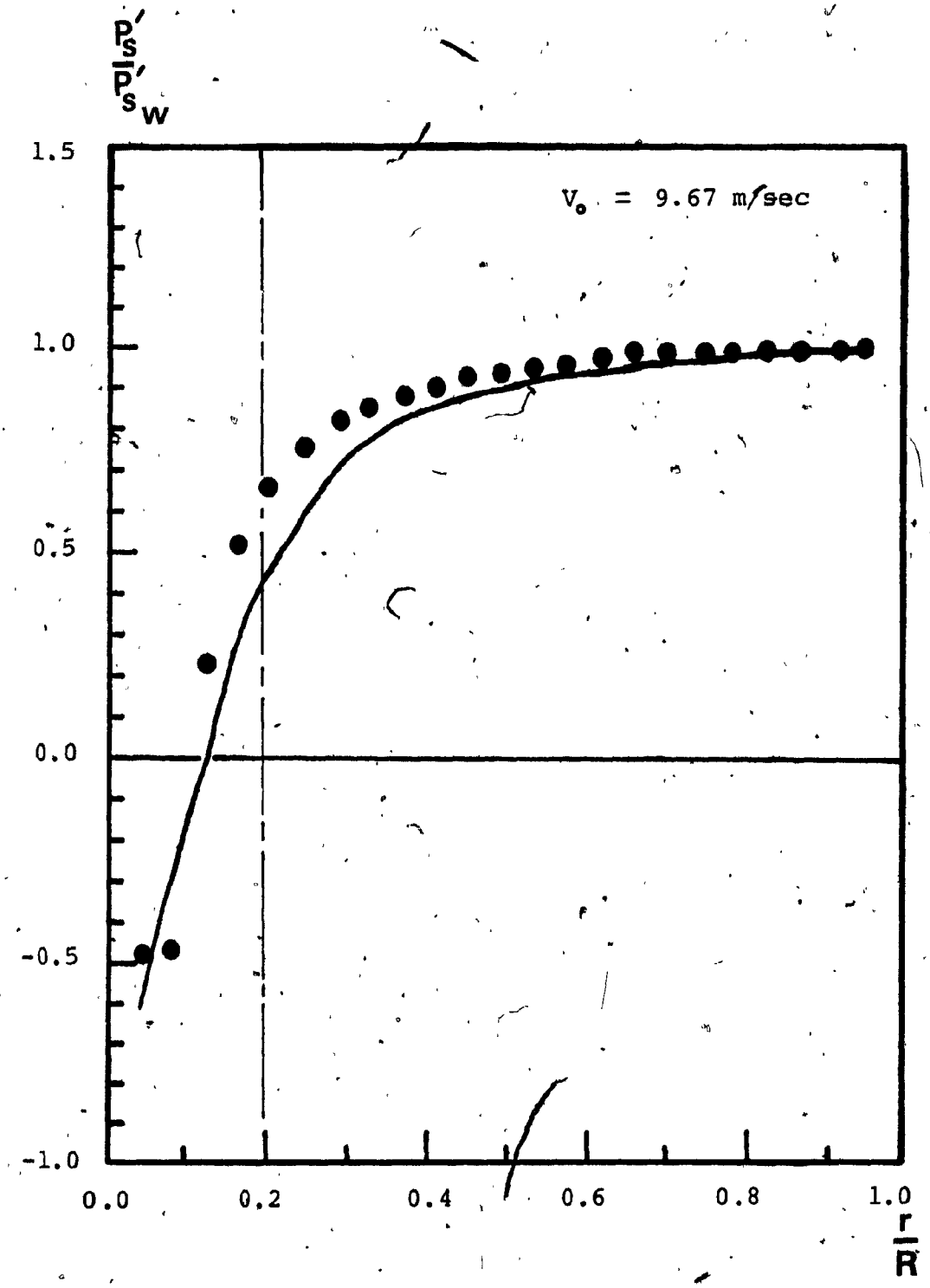

Fig. 5.19 Experimental and predicted static pressure profiles for exit nozzle size $D_e = 0.2D$

CHAPTER 6

THE AERODYNAMIC STRUCTURE OF THE VORTEX FLOW

6.1 Introduction

The double entry vortex consists of two vortices created from two independent air supply sources. An attempt has been made here to analyse its character in terms of the two single vortices, one emerging from the top and the other from the bottom end of the cylidrical chamber. The characteristics of the two single vortices were examined separately first, and then their behaviour was studied as they coexisted in the double vortex arrangement.

6.2 Vortex Streamline Construction

In order to create the "picture" of the vortex flow pattern in a vertical plane containing the axis of the vortex chamber, the streamline pattern of the flow was drawn. The stream function evaluation was based on the experimentally determined axial velocity profiles at the six different levels where measurements were made, (see Chapter 5). In cylindrical coordinates, Fig. 4.5, the stream function is given as [39]:

$$\Psi = \int_0^r r V_z \, dr \qquad (6.1)$$

The above integration is a measure of the volumetric air flow rate between the axis of the chamber and the point where the stream function is evaluated. The stream function, ψ, was non-dimensionalized by dividing it by its value at the side wall of the chamber:

$$\psi = \frac{\Psi}{\Psi_w} \qquad (6.2)$$

where

$$\Psi_w = \int_0^R r V_z \, dr \qquad (6.3)$$

$$Z_B < Z < Z_T$$

Note that ψ_w is an indication of the net volumetric air flow rate through any full cross sectional area of the cylindrical chamber, which in turn is equal to the bottom supply air flow rate. The dimensional value of the stream function was used in the case of the top single vortex, because ψ_w was equal to zero for $Z<Z_T$, (i.e. zero net air flow rate through any cross sectional area).

A computer program was written to calculate the values of r and z coordinates for the points of constant magnitude of the stream function, along the height of the

chamber, (see Appendix B). By proper connection of these points, the streamlines were constructed and the air flow pattern became very evident. The primary and secondary flow zones were clearly identified and the mode in which the air was conveyed from the inlet to the exit of the chamber became apparent.

At the regions close to the top and the bottom ends of the chamber, where measurements were not made, the vortex "picture" was intuitively extrapolated by making logical assumptions based on the adjacent measured vortex structure.

6.3 Single Vortex Structure: Top Inlet

After being introduced tangentially into the vortex chamber through the top inlet, the air separates into two main streams, Fig 6.1. The first stream, indicated by an A, travels directly upward toward the exit nozzle of the chamber, while the second stream, B, being kept close to the side wall by the action of the centrifugal force, moves downward toward the other end of the chamber. After reaching the bottom flat plate, stream B is diverted upward and creates another flow zone which is ascending the chamber at about the mid-radius distance. That stream merges, near the top end wall of the chamber, with stream A, as they both move together toward the exit nozzle.

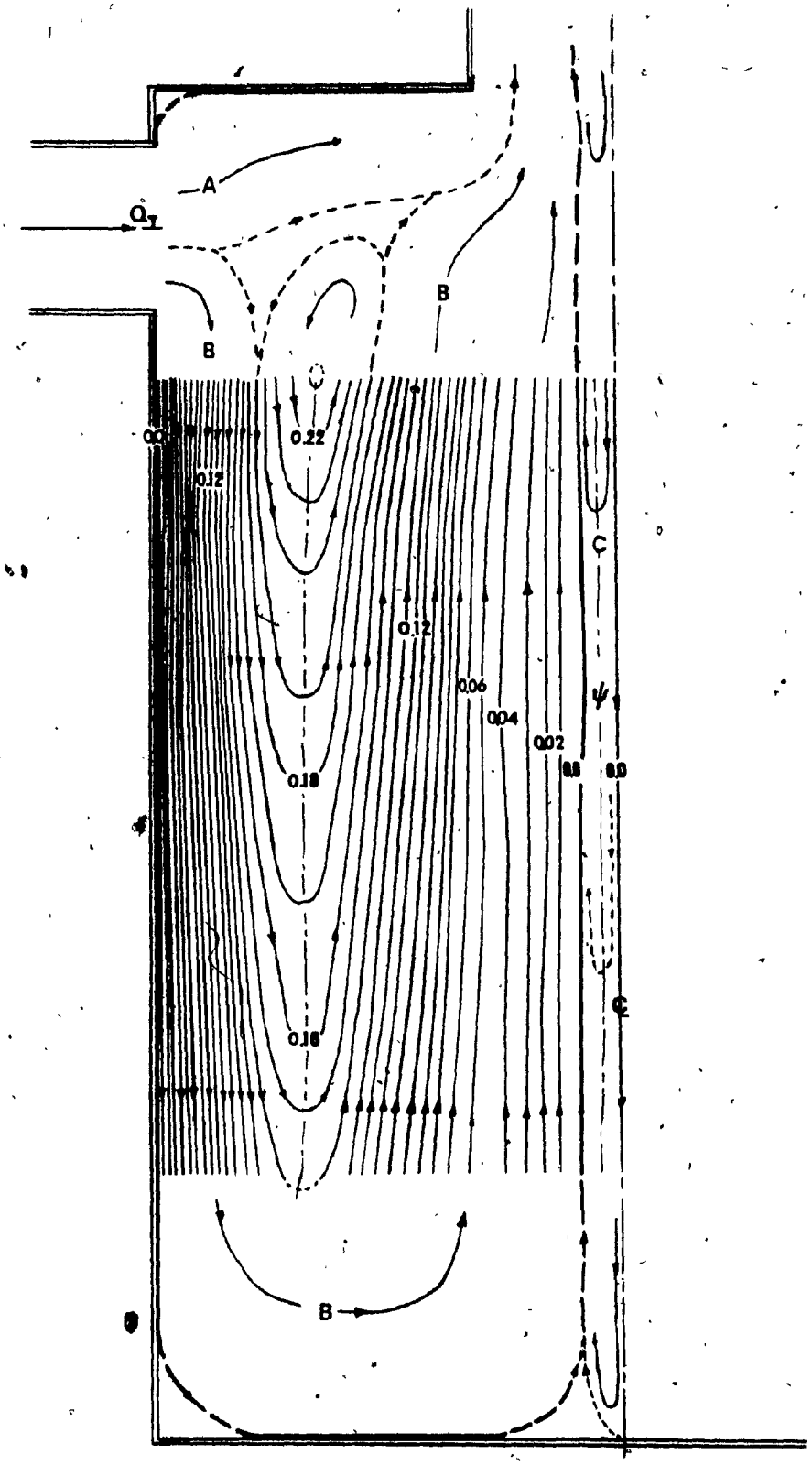

Fig. 6.1 Single vortex structure; top inlet configuration. Air flow rate: 1.98 SCMM (70 SCFM)

In the region between the ascending and descending stream B, a secondary vortex flow is induced due to the presence of two fluid layers of opposite direction moving close to each other. Along the axis in the center of the chamber, a sub-atmospheric pressure region is created, and as a result, ambient air is drawn in through the center of the exit nozzle. The sub-atmospheric region occupies a very narrow cylindrical zone indicated as C in Figure 6.1. The entrained atmospheric air is subsequently merged with the ascending stream B as it moves toward the exit of the chamber.

The whole vortex flow system inside the chamber can be viewed as originating from two separate flow sources, a main and an induced. The air injected through the tangential top inlets can be considered as the main air flow, while the air that finds its way into the chamber through the center of the exit nozzle, emanating from the surrounding atmospheric air, can be considered as the induced air flow. The major part of the chamber, however, is occupied by the main air flow system. The induced air flow exists only in the internal part of the vortex core and it occupies approximately one fourth of the axial flow area of the core (ie. one half of the cylindrical core diameter). The size of the secondary axial flow area of the suction surface as found in Chapter 5, is highly dependent on the size of the exit nozzle diameter. Angular

and linear momentum is being transferred to the induced flow regime, described above, by the main flow system through their common boundary.

6.4 Single Vortex Structure: Bottom Inlet

The bottom inlet vortex structure is generated by similar mechanisms as the top inlet single vortex described in the previous section. After being introduced through the peripheral tangential ports, at the bottom end of the chamber the air is split into two streams, D and E, Fig. 6.2. Stream D is being kept close to the side wall by the centrifugal force, as it travels vertically up toward the top end of the chamber. The second air stream, E, moves in the opposite direction until it reaches the bottom end of the chamber. It is then diverted radially toward the center of the chamber. When it comes close to the central part of the chamber, it is turned through 90 degrees and flows upwards toward the exit nozzle. At the top, this stream meets with the aforementioned stream D and they both move toward the exit of the chamber.

Streams D and E, while ascending in the chamber along independent paths, do not necessarily have the same axial velocities. As a result, counter-rotating secondary flows are induced in order to act as coupling mechanisms for the two streams. These secondary flows are enclosed

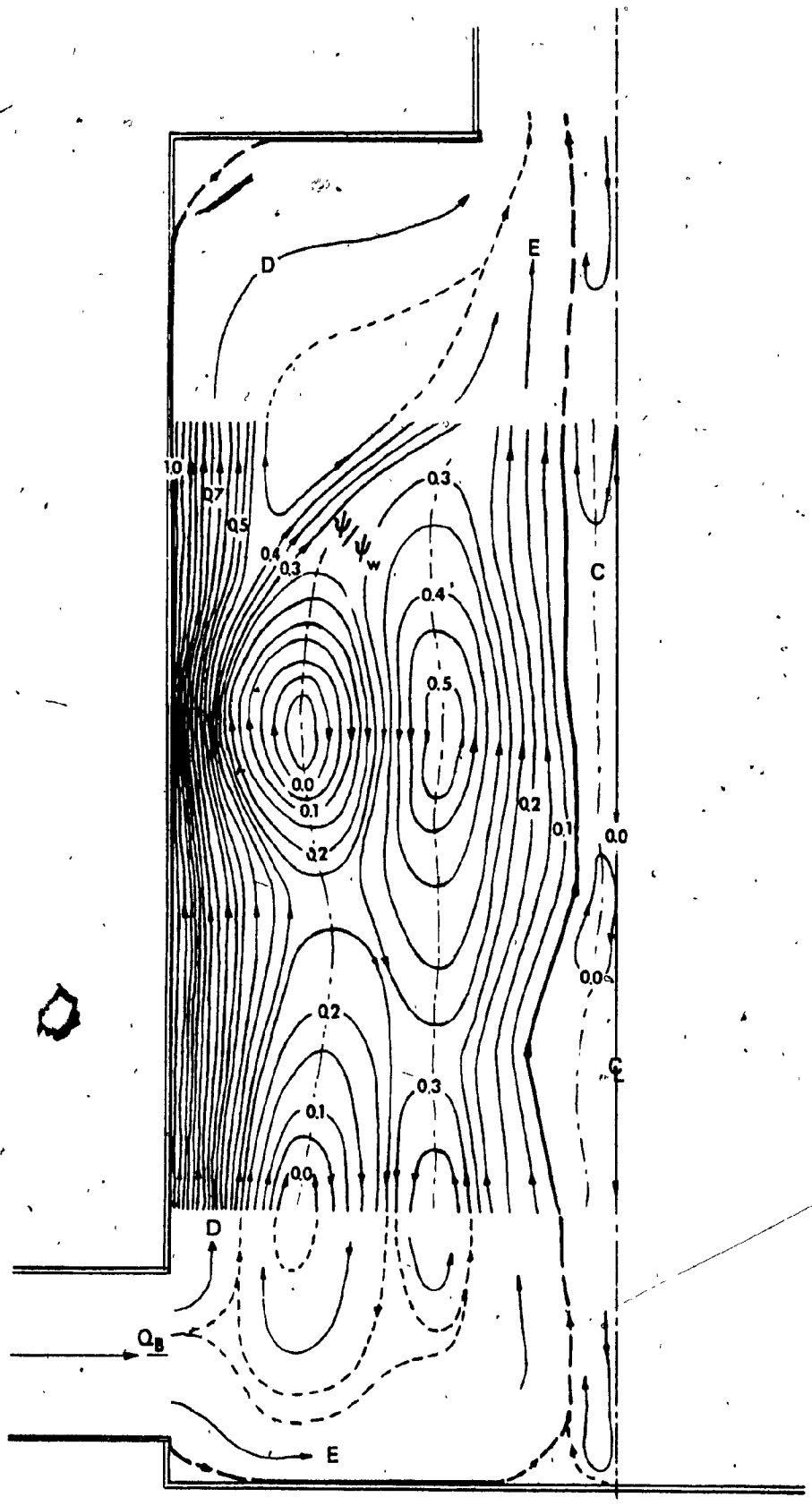

Fig. 6.2 Single vortex structure; bottom inlet configuration. Air flow rate: 2.83 SCMM (100 SCFM)

within a high turbulent toroidal region which extends along the whole length of the cyclone chamber. Since the height of the torus is almost double its width, the secondary flows are separated into two pairs of counter-rotating vortex cores. A slight depression thus results at about the middle-height of the torus. For vortex chambers having aspect ratios (L/D) in the order of 1/2 , one pair of vortex cores would be expected. For slender chambers, however, more than two pairs of secondary vortices would be formed.

The central part of the chamber is occupied by entrained ambient air, and exhibits very similar characteristics to those discussed previously in the description of the aerodynamic flow pattern of the single vortex with top entry.

By inspecting the stream line patterns of the two single vortices it can be concluded that the air entering the chamber at the inlet ports finds its way to the exit nozzle mainly traveling along the side and the end walls of the chamber. The air flow finds easier radial access toward the axis of the chamber at the proximity of the end walls. This can be attributed to the fact that the centrifugal force field is weaker at these flow regions due to the presence of the boundary layers.

6.5 Double Vortex Structure

The double vortex structure, while having its own specific character, can be explained in terms of the two single vortex structures described in the previous sections. The two vortices are clearly identified in the double vortex structure, Fig. 6.3.

A unique flow pattern results as the descending stream B, of the top vortex and the ascending stream D of the bottom vortex meet while they travel in opposite directions along the side wall of the chamber. It can be seen from Figure 6.3, that, as the two streams merge, they are directed radially toward the center of the chamber so as to produce a well defined localized radial velocity field. Then, at about the mid-radius distance of the chamber, the merged streams B and D combine with the stream E and all three zones move vertically up toward the exit nozzle.

It is also observed that the top vortex flow does not extend as much radially toward the axis of the chamber as it did in the single vortex configuration because the central part of the chamber is dominated by the bottom vortex flow as it moves toward the exit of the chamber; the flow of the top vortex is confined inside an annular space

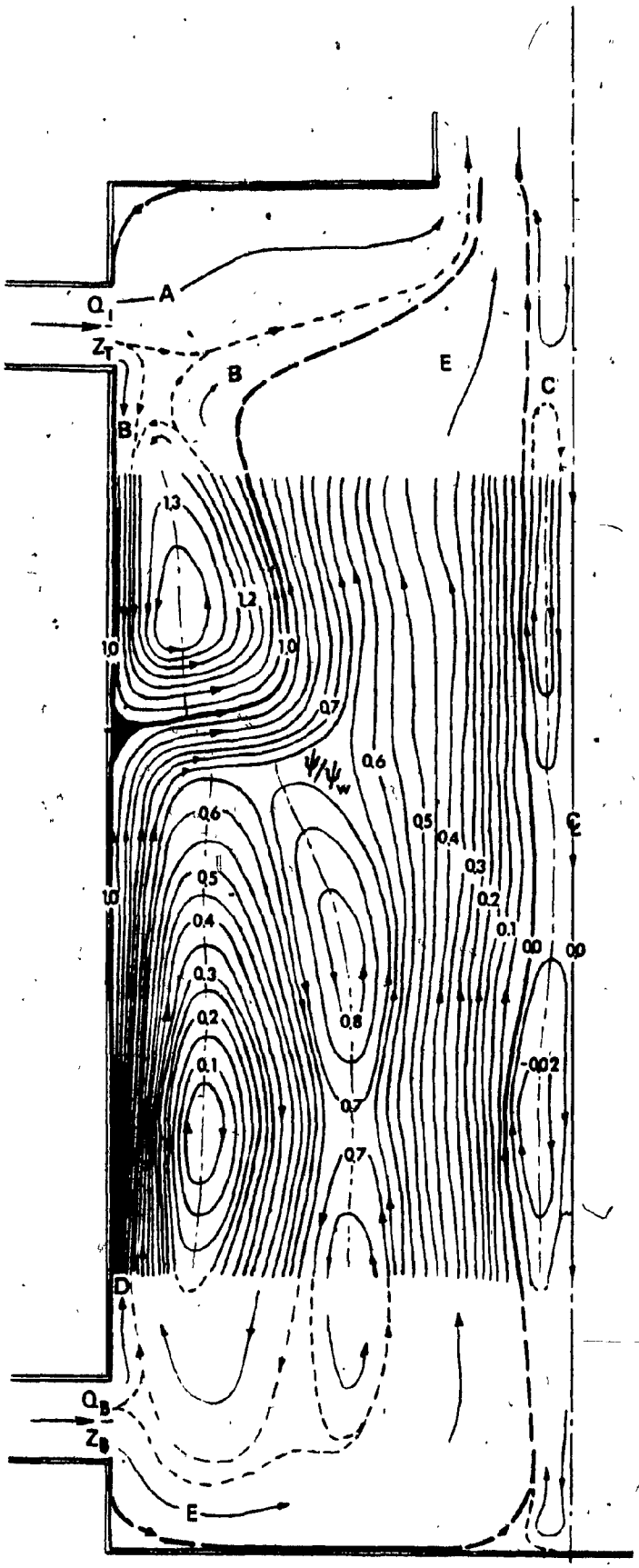

Fig. 6.3 Double vortex structure; Q_B/Q_T = 1.22
Air flow rate: 2.83 SCMM

extending from more than the half radius distance up to the periphery of the chamber.

The flow pattern of the double vortex can be considerably altered by varying the relative strength of the two single vortices. When the top inlet air flow rate is low, the top vortex is completely confined to the top end of the chamber; it moves toward the exit without being able to descend below its inlet level, Fig.6.4. Under these conditions, the single vortex flow pattern with bottom inlet is dominant along the whole length of the vortex chamber, and the localized radial velocity stream is suppressed to the top end of the chamber.

When the relative strength of the top vortex is increased, it becomes predominant and begins to descend along the side wall towards the bottom end of the chamber, (see Fig. 6.3, and then 6.5). Finally, when the strength of the top vortex has been increased sufficiently, the bottom vortex is completely suppressed to the bottom flat plate, Fig. 6.6, and is forced to flow radially inwards. At this extreme case the bottom vortex has access to the exit of the chamber only through the central annular space formed between the top vortex flow and the reversed atmospheric flow zone along the chamber axis.

As the top vortex is extended along the whole length

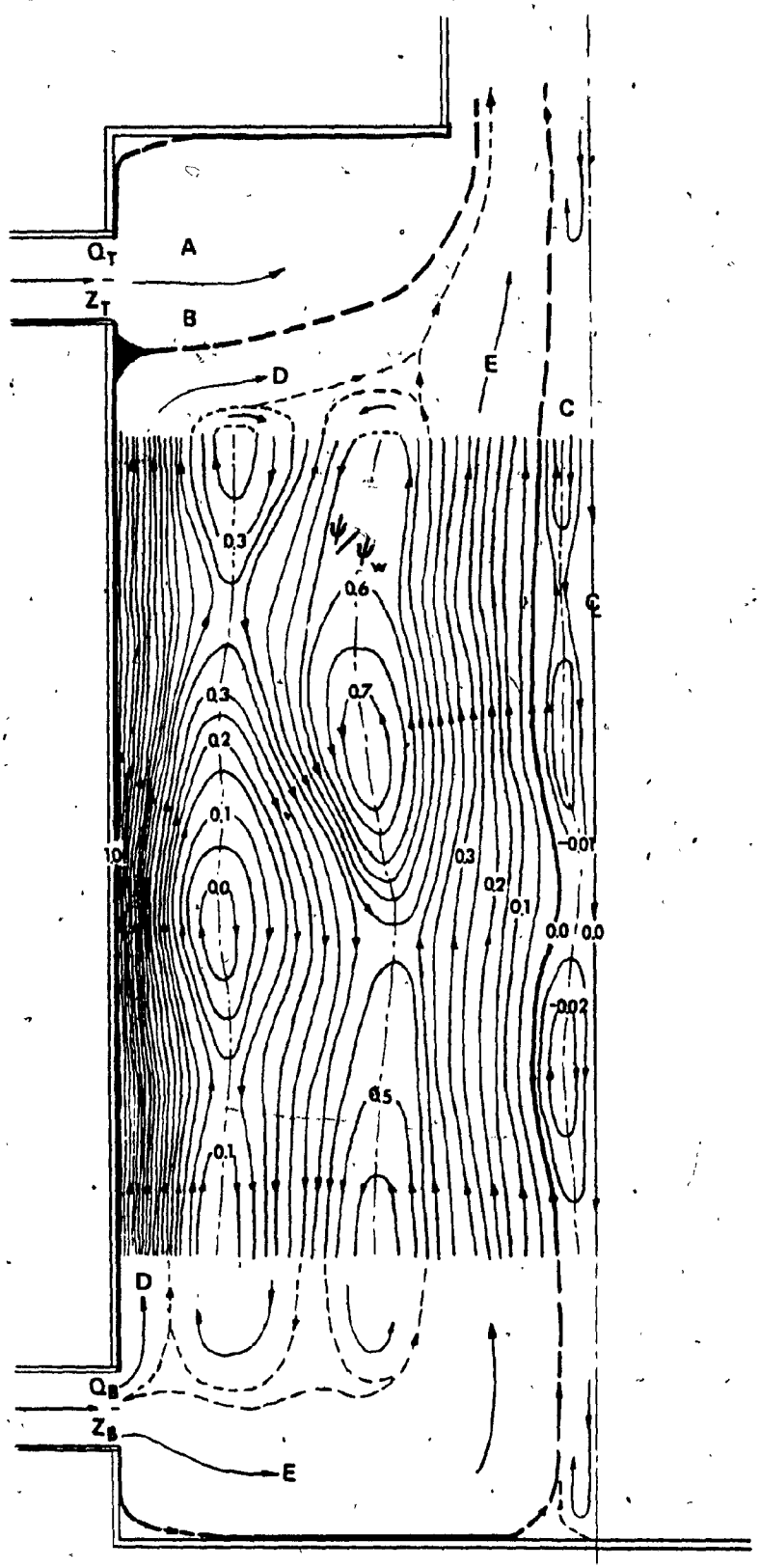

Fig. 6.4 Double vortex structure with prevailing bottom flow. Q_B/Q_T = 1.5. Air flow rate: 2.83 SCMM (100 SCFM)

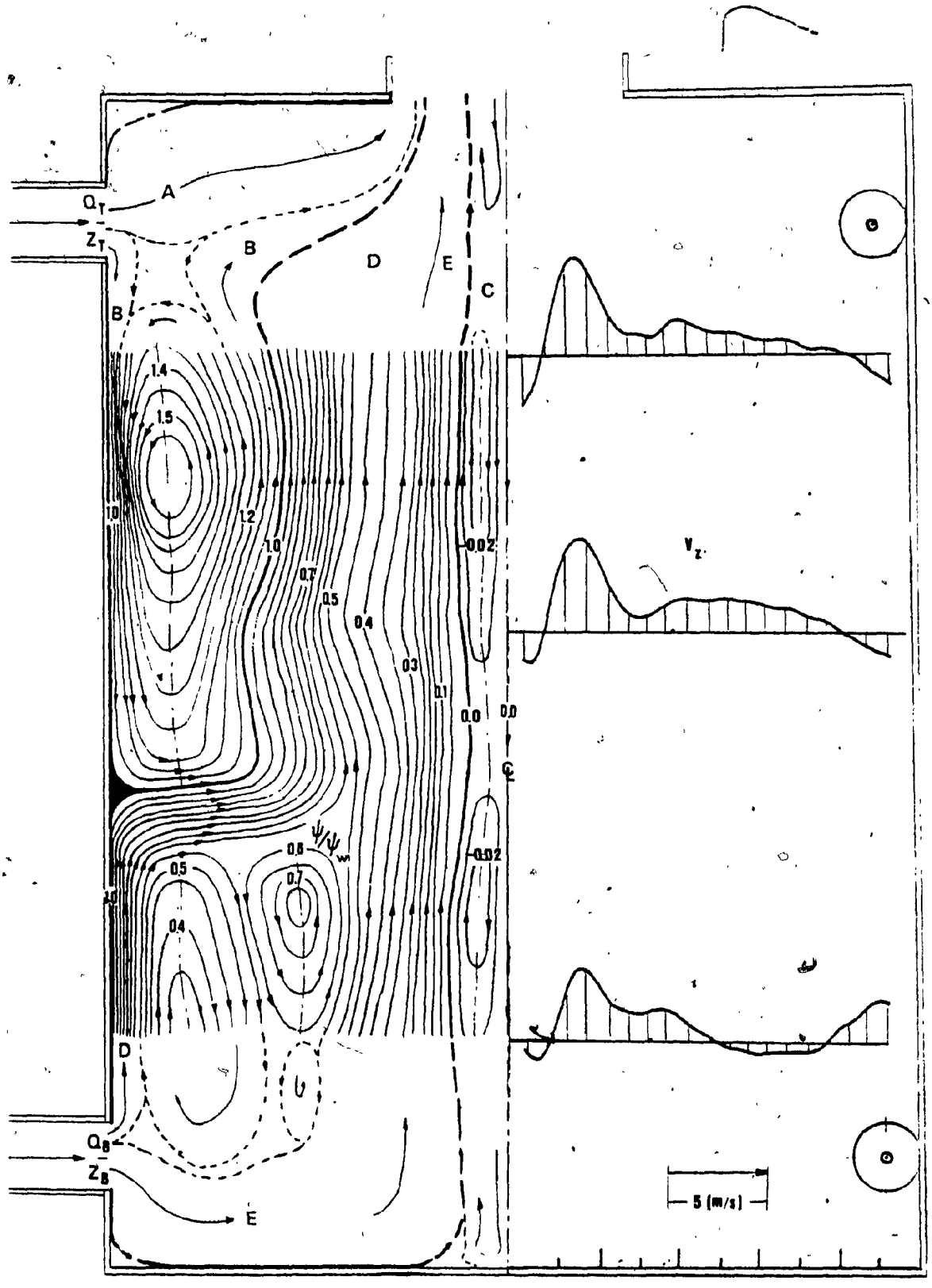

Fig. 6.5 Double vortex structure. Q_B/Q_T = 1.
Air flow rate 2.83 SCMM

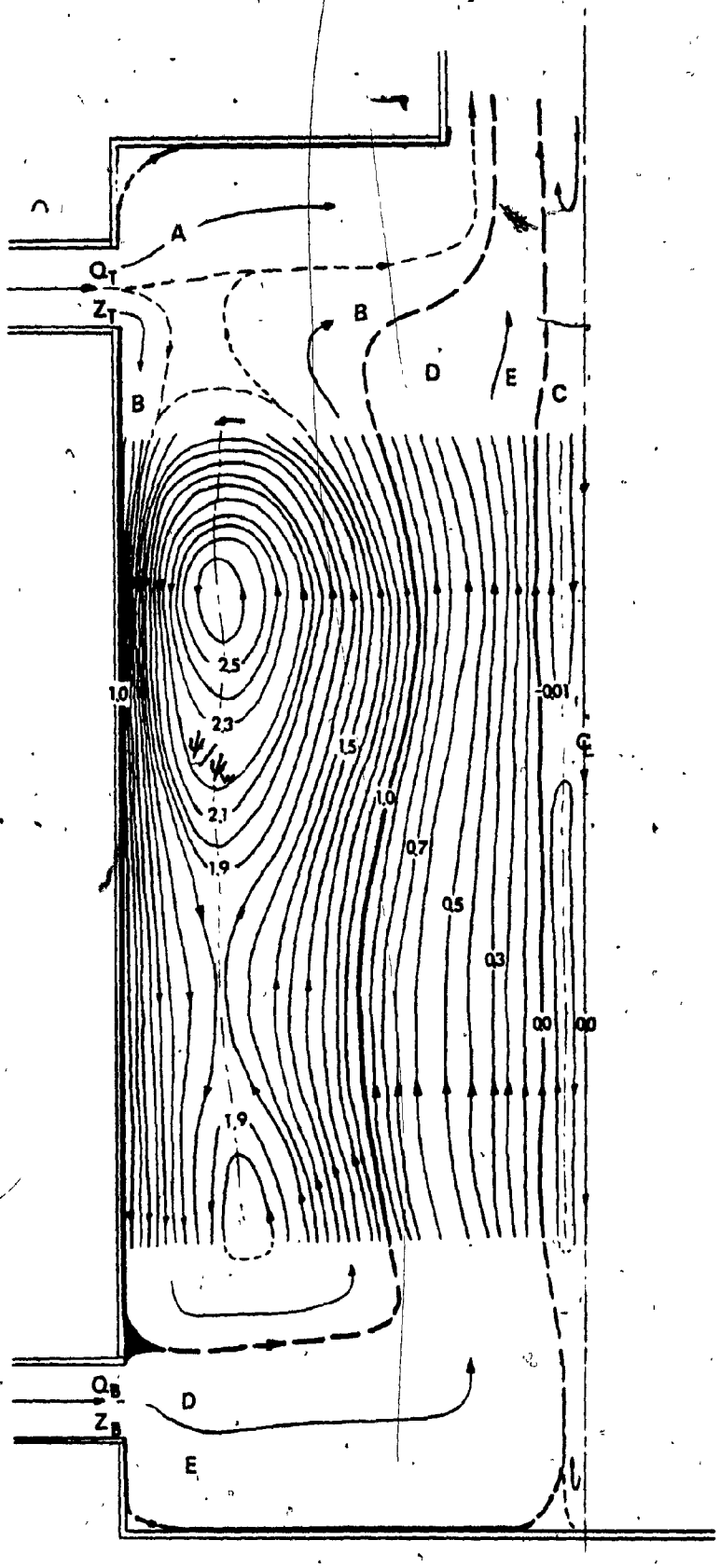

Fig. 6.6 Double vortex structure with top flow prevailing. Air flow rate 2.83 SCMM (100 SCFM). Q_B/Q_T = 0.67

of the chamber, the secondary vortex flow induced by the descending and ascending parts of stream B, narrows in the middle radius and is finally separated into two vortices, Fig. 6.6. In vortex chambers of higher aspect ratios ($2<L/D$), however, more than two secondary vortex cores are expected to be formed.

The experiments showed that the two peripheral flows (B and D), of the top and bottom vortices, and the localized inward radial velocity region, will form at some level of the chamber between the top and bottom inlets, only when the relative strength of the two single vortices is close to unity. For the particular model examined here, the extreme values of the relative strength (Q_B/Q_T) were found to be limited to $0.67 < Q_B/Q_T < 1.5$. When the bottom vortex flow rate is decreased below its limiting value, the top single vortex structure, extends along the whole length of the chamber, as it is allowed more space within the chamber to expand in the radial direction. As a result, the two vortex cores of the secondary flow merge into one, and the top inlet single vortex flow pattern is obtained, (see Figure 6.1).

From the point of view of application of the double vortex flow pattern in the furnace engineering technology the unique and most important feature of the double vortex system is its ability to create a localized fuel residence

zone, at some distance away from the end walls, where suspension burning could take place. An additional feature of the above system is that the fuel residence zone could be shifted along the height of the chamber by only changing the ratio of the top to bottom air flow rate. The calibration for determining the position of the localized radial velocity zone due to the variation of the relative vortex strength, is shown in Figure 6.7.

The development of a mathematical model for the determination of the solid particles dynamic equilibrium for isothemal and for combustion conditions is presented in reference 27. The minimum (critical) particle size retained in the residence zone was determined. The dependence of the critical size of the particles on important flow and fuel parameters, such as particle density, air velocity and temperature, were examined in order to provide guidelines for the design of a double vortex combustion chamber (or a dust separator).

6.6 Visualization of the Double Vortex Structure

Visualization of the vortex flow field is very difficult, especially in the present case where the flow medium is air. The major difficulty is due to the fact that a strong centrifugal force field is generated by the swirling flow and a visible medium that would follow the

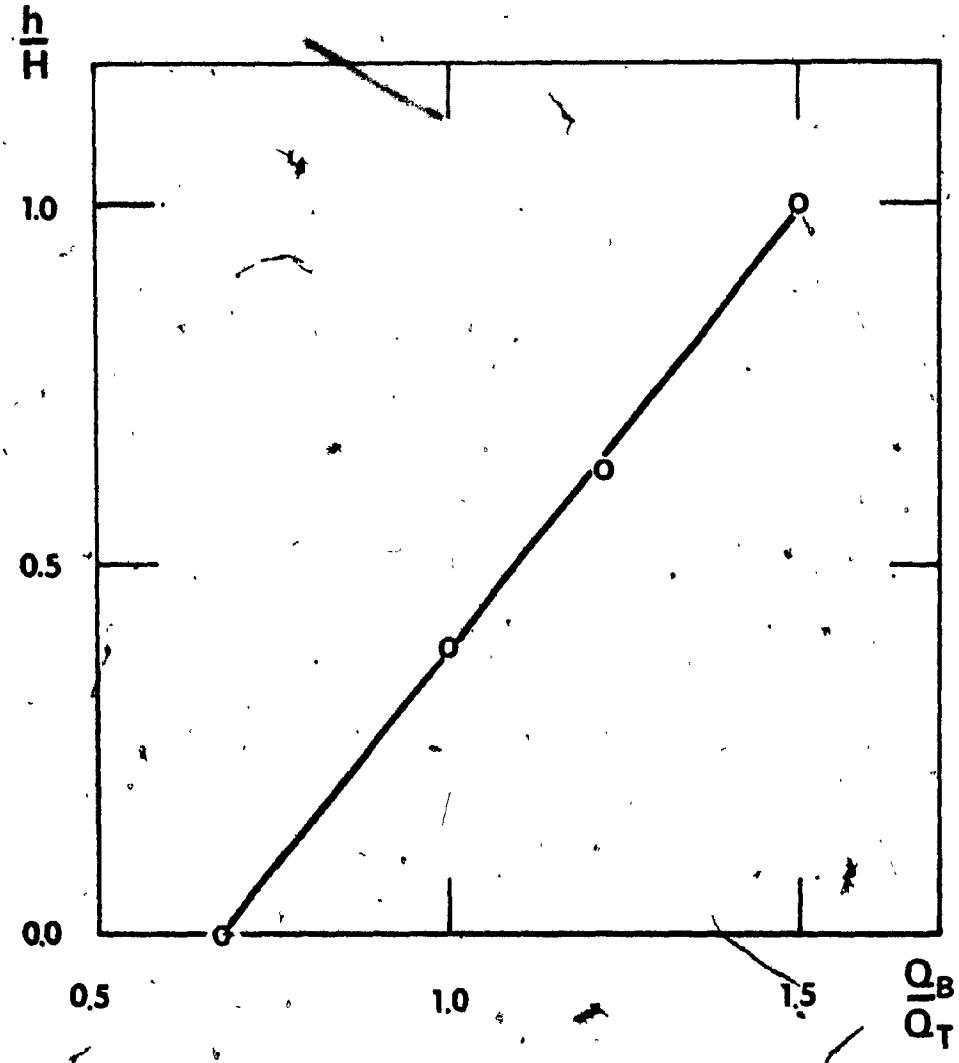

Fig. 6.7 Vertical position of the localized radial velocity zone versus the bottom to top flow ratio.

air flow path (i.e. the streamlines) is not available. Any medium with higher density than that of the air, would separate to the periphery of the chamber. A colored medium of the same density as that of the air would be more appropriate. Even in this case, the peripheral flow would always block the view of the internal features of the vortex flow. In addition, the diffusion process would blur the vision of any distinct local flow pattern in a very short time. Any attempt to perform visualization experiments, therefore, would only result in a very general, rather qualitative picture of the flow.

6.6.1 Smoke Visualization

White smoke, being quite suitable and readily available, was used for the visualization of the double vortex flow pattern. The smoke was produced by a smoke generating candle that was inserted in the bottom supply pipe upstream of the inlet ports.

When the concentration of the smoke was very low, the core of the vortex flow was barely visible. As more smoke was introduced into the chamber, a more meaningful pattern could be seen. The smoke started to ascend along the periphery of the chamber, carried by stream D of the bottom vortex, but it was prevented from dominating the whole length of the chamber, by the descending stream B of

the top vortex, (Plate 6.1). At the point along the side wall where the two vortices met, the smoke was transported radially inward to merge with stream E, and it was consequently carried to the exit nozzle, (see top part of Plate 6.1). This behaviour was exactly as anticipated according to the double vortex description in the previous section.

The smoke picture was sustained for only a short time period because the smoke was trapped by the secondary flow of the top vortex, mainly by diffusion to the lower concentration areas, and it appeared to exist along the whole length of the chamber (Plate 6.2). The localized radial velocity area, however, was vaguely visible at about the middle length of the chamber. When the smoke was introduced at the top inlet, the results were not satisfactory because none of the internal parts of the vortex flow were visible along the whole length of the chamber.

Plate 6.1 Smoke Visualization of the Double Vortex Air Flow Pattern

Plate 6.2 Double Vortex Smoke Pattern after Smoke Diffusion

CHAPTER 7

7.1 Conclusions

The objective of the present investigation was to obtain the experimental flow field of the confined, double (and single) vortex flow inside a cylindrical cyclone chamber, in view of its application in the combustion engineering field.

The 5-channel omnidirectional, Pitot static pressure probe was found to be well suited for use in obtaining the velocity and the static pressure distributions. Although not as powerful as the DLA or HWA flow measuring techniques, this instrument was found to provide satisfactory accuracy at low cost.

The experimental results showed that the flow situation for the tangential velocity component was well approximated by a "Rankine Vortex". The radial location of the maximum tangential velocity, which occurred at the common boundary of the potential and the forced flow zones, was found to be virtually independent of the volumetric air flow rate through the cyclone chamber. It was found that this radial position was much affected by the exit nozzle size.

The highest static pressure was found to occur at the side wall of the chamber. It dropped to subatmospheric values within the vortex core region near the axis of the chamber. A semi-analytical expression, based on the radial position of the maximum tangential velocity, the tangential velocity power exponent, and the static pressure at the side wall of the chamber, was derived. It was found to approximate the experimentally obtained static pressure distribution very closely.

The axial velocity profiles measured for different vortex configurations, all revealed mass entrainment flow zones that extended almost along the whole height of the cylindrical chamber. A reverse axial flow (secondary flow) was also found to exist along the chamber axis.

The radial velocity was found to be very small and subject to measurement errors. It was possible, however, to obtain the radial velocity profiles by using the experimental results of the axial velocity and applying the concept of mass flow continuity in an annular control volume. Results showed that the major part of the radial flow must have occurred near the end walls of the chamber.

A unique radial flow zone was found to be formed in

the middle height of the chamber, for the double vortex configurations, when the two single vortices, the top and bottom, were of comparable strength ($Q_B/Q_T=1$). This zone could be shifted to different levels of the chamber by varying the relative strength of the two interacting vortices.

It is expected that the findings of the present work will contribute to the better understanding of the mechanisms governing the complex fluid flow inside cylindrical vortex chambers.

7.2 Future Work

Many aspects of the confined vortex flow still remain unanswered. With regard to the single and double cyclone configuration, investigated herein, detailed measurements close to the end wall boundary layers should be performed in order to verify the postulated flow pattern at these regions. The investigations should also be extended to the free vortex flow outside the chamber exit plane for different exit nozzle geometries.

Since the radial distance of the maximum tangential velocity is very important for describing the flow, and for making predictions, such as of the static pressure and the tangential velocity profiles, its dependence on the other

structural parameters besides the exit nozzle size, should be investigated.

The effect of the wall roughness on the vortex flow decay within the cyclone chamber, should be examined. Thus, results could be obtained that would be usuful for performance calculations in real combustion systems, where higher wall roughness and structural irregularities are expected. Any qualitative changes of the fluid flow pattern due to the presence of the solid fuel particles at the fuel residence zone, should also be investigated.

The present study together with the follow-up work, if completed, would offer a more comprehensive picture of the basic confined vortex flow.

LIST OF REFERENCES

1. Holman, J. P., and Razgaitis R. A.,"Fluidized Vortex Incineration of Waste", Technical Report prepared for U.S. Enviromental Protection Agency, series EPA- 600/2- pp. 76- 225, Departments of Civil and Mechanical Engineering, Southern Methodist University, 1976.

2. Roberts, A.,"The Combustion of Pulverized Fuel in Vortex Chamber", Doctoral Thesis, University of Sheffield, 1968.

3. Mack, L.,"The Laminar Boundary Layer on a Disk of Finite Radius in a Rotating Flow, Part I" J.P.L. Technical Report No.32-224, 1969.

4. Smithson, J.K.,"Characteristics of Free and Confined Vortex Flow", Ph.D. Thesis, Department of Fuel Technology and Chemical Engineering, Sheffield University, 1969.

5. Lewellen, W.S.," Magnetohydrodynamic Vortex Power Generation", Report for Air Force Ballistic Missile Division Air Research and Development Command, USAF, March 1961.

6. Kerrebrock, J.L., and Meghreblian, R.V.," Vortex Containment for the Gaseous-Fission Rocket", J. Aerospace Sci., 28 1961, p. 710.

7. Lewellen, W.S.,"A Review of Confined Vortex Flows", NASA CR-1772, July 1971.

8. Lafferty, J.F. and Hammitt, F.G.,"Experimental Investigation for a Two-Phase Vortex", ANS Trans., 362-363, 1967, pp. 10.

9. Lafferty, J.F. et al,"Velocity Distributions in Two-Phase Vortex Flow", J. Basic Eng., 368-372 September, 1968, pp. 90.

10. Kwok, C.K., Lee, P.M., and Lin, S.,"An Analytical Investigation of a Vortex Flowmeter", ISA Transaction, Vol.14, No.2, 1975

11. Howell, W.J.,"Cyclone Furnace Firing", Babcock-Wilcox and Goldie-McCulloch Limited, Bulletin 59-2.

12. Mills, R.G. and Desmon, L.G.,"Operating Experience in the Suspension Burning of Waste Materials in Cyclone Incinerators", Energy Ltd., Proceedings of 1972 ASME National Incineration Conference.

13. Swithenbank, J., "2000 Years More Oil", Journal of Fluids Engineering, Transactions of ASME series I 96, No.1 March 1974, p. 2.

14. Cohan, L.J. and Fernandes, J.H."The Heat Value of Refuse", Mechanical Engineering 90, No.9, September 1968 pp. 47-51.

15. Murthy, S.N.B., "Survey of Some Aspects of Swirling Flows", Aerospace Research Laboratories Report ARL-71-0244, November 1971.

16. Bank, N., and Gauvin, W.H.,"Measurements of Flow Characteristics in a Confined Vortex Flow", The Canadian Journal of Chemical Engineering, Vol.55, 1977, p. 397

17. Bank, N.,"Measurements of Flow Characteristics in the Confined Vortex Flow", M.Eng. Thesis, Department of Chemical Engineering, McGill University, 1975.

18. Reydon, R.F., and Gauvin, W.H.,"Theoretical and Experimental Studies of Confined Vortex Flow", The Canadian Journal of Chemical Engineering, February 1981, pp. 14-23.

19. Raydon, R.F.,"Theoretical and Experimental Studies of Confined Vortex Flow", M.Eng. Thesis, Department of Chemical Engineering, McGill University, 1978.

20. Syred, N., and Beér, J.M.,"Combustion in Swirling Flows: A Review". Combustion and Flame, No.23, 1974.

21. Lander, C.H.,"Improvements in and Relating to Carrying out Chemical and Physical Processes", B.P. 338, 108, 1929.

22. Hurley, T.F.,"Some Factors Affecting the Design of Small Combustion Chamber for Pulverised Fuel", J. Inst. Fuel, April, 1931, p. 43.

23. Krepec, T., and Kwok, C.K.," Preliminary Investigations of a Double Vortex Combustion Chamber," 1981 Fall meeting of Combustion Institute, Eastern Section, Pittsburgh, U.S.A.

24. Angus, D., United States Patent No. 4,002,127, January 11, 1977.

25. Krepec, T., and Kwok, C.K., " Problems Encountered in the Development of a Double Cyclone Furnace". 16-th South-Eastern Seminar on Thermal Sciences in 1982 in Miami, Florida, U.S.A.

26. Georgantas, A., Krepec, T., Kwok, C.K., " Flow Pattern

Investigations in a Model of a Double Vortex Combustion Chamber", Presented in 1982 Spring Technical meeting of Combustion Institute, Canadian Section, Banff, Alberta.

27. Georgantas, A., Krepec, T., Kwok, C.K., "Investigation of Double Vortex Structure and its Ability to Retain Fuel Particles in a Cyclone Combustion Chamber", Presented in 1983 Fall Technical meeting of the Combustion Institute, Eastern Section, Providence, Rhode Island.

28. Kelsall, D.G.," A study of the motion of Solid Particles in a Hydraulic Cyclone", Trans. Inst. Chem. Engrs., 30, 1952, pp. 87-108.

29. Kendall, J.M.Jr., "Experimental Study of a compressible Viscous Vortex", JPL Tech. Report No. 32-290 (June), 1962.

30. Savino, J.M., and Keshock, E.G., "Experimental Profiles of Velocity Component and Radial Pressure Distributions in a Vortex Contained in a Short Cylidrical Chamber," NASA TND-3072, October 1965.

31. Kwok, C.K.,Thinh , D.N., and Lin, S., "An Investigation of Confined Vortex Flow Phenomena", Trans., ASME, Basic Eng., Paper No.72- Flcs- 3g, Sptember 1972.

32. Kendall, J.M., Jr.,"Experimental Study of Tubulence in a Driven Vortex", Tech. Report No.32- 290, Jet Propulsion Laboratory, California Institute of Technology, June 1962.

33. Baluev, E.D, and Troyankin, Y.V.,"Study of the Aerodynamic Structure of Gas Flow in a Cyclone", Thermal Engineering, Vol.14, 1967, p.84.

34. Lyakhovskii, D.N.,"Article in: Problems of Aerodynamics and Heat Transfer in Boiler-Furnace Engineering". (Voprosy aerodiamiki i teploperedachi v kotel' no-topochnoi tekhnike), Cosenergoizedat, 1958.

35. TSI Incorporated,"Laser Velocimetry System", U.S.A.

36. DISA Electronik,"Hot-Wire and Hot-Film Anemometry", Harlev, Denmark, 1970.

37. Bryer, D.W., and Pankhurst, R.C.,"Pressure-Probe Methods for Determining Wind Speed and Flow Directions", National Physics Laboratory, 1971.

38. Goldstein, S.,"A Note on the Measurement of Total Head and Static Pressure in a Turbulent Stram", Proc. Roy. Soc. (A), 1936, 155,570.

39. Yuan S.W., "Foundations of Fluid Mechanics", Prentice-Hall, Inc., Englewood Cliffs, N.J., 1967.

40. United Sensor, "Directional Probes... 3-Dimensional", Boulletin 5, Issued April 30, 1974.

APPENDICES

APPENDIX A

CALIBRATION OF THE ROTAMETERS USED TO MEASURE THE AIR SUPPLY TO THE TRANSPARENT CYCLONE CHAMBER

Three rotameters were utilized to measure the required air flow rates; one for the top air supply and the other two for the bottom, Fig. 4.3. The readings of these rotameters had to be corrected for the operating pressure and temperature, as well as for the molecular weight of the fluid being metered. The following formula was used to make the above corrections:

$$Q_{act} = Q_{sc}\sqrt{\frac{M_{sc}}{M_{act}} \times \frac{P_{sc}}{P_{act}} \times \frac{T_{act}}{T_{sc}}} \qquad (A.1)$$

where, M_{sc}, P_{sc} and T_{sc} are the molecular weight, pressure and temperature of the fluid, respectively, during the manufacturer's calibration, and $M_{act}, P_{act}, T_{act}$ are the respective quantities at the operating conditions for the experemental set-up as shown in Figure 4.3.

The following types of rotameters were used:

a) For the top inlet air supply:

Rotameter A

Manufacturer : Brooks

Float type : S-12-RU-221

Tube size : R-12-25-5

Scale reading : 0-2.07 SCMM N_2 at 21.1°C, 1 atm.

No appreciable variation in temperature was noted while tested with a thermometer, and the correction formula A.1 reduced to:

$$Q_{act} = Q_{sc}\sqrt{\frac{0.966}{P_{act}}} \qquad (A.2)$$

The calibration procedure is outlined in Table A.1 and the results are plotted in Figure A.1.

b) For the bottom inlet air supply:

Rotameter B

Manufacturer : Fisher

Float type : 1-GNSV GT 69T60

ROTAMETER A

ROTAMETER SCALE READING, Q_{scale} (SCTM) [70°F, 14.7psia]	BACK PRESSURE - GAGE		Q_{act} (CMM)	Q (SCMM) [0°c, 1 atm]
	cm Hg	Psig		
70	8.3	1.60	1.85	1.90
60	6.2	1.20	1.61	1.61
50	4.8	0.93	1.35	1.33
40	3.7	0.72	1.09	1.06
30	2.7	0.52	0.82	0.79
20	2.0	0.39	0.55	0.52
10	1.7	0.33	0.28	0.26

TABLE A.1 Calibration of Rotameter A

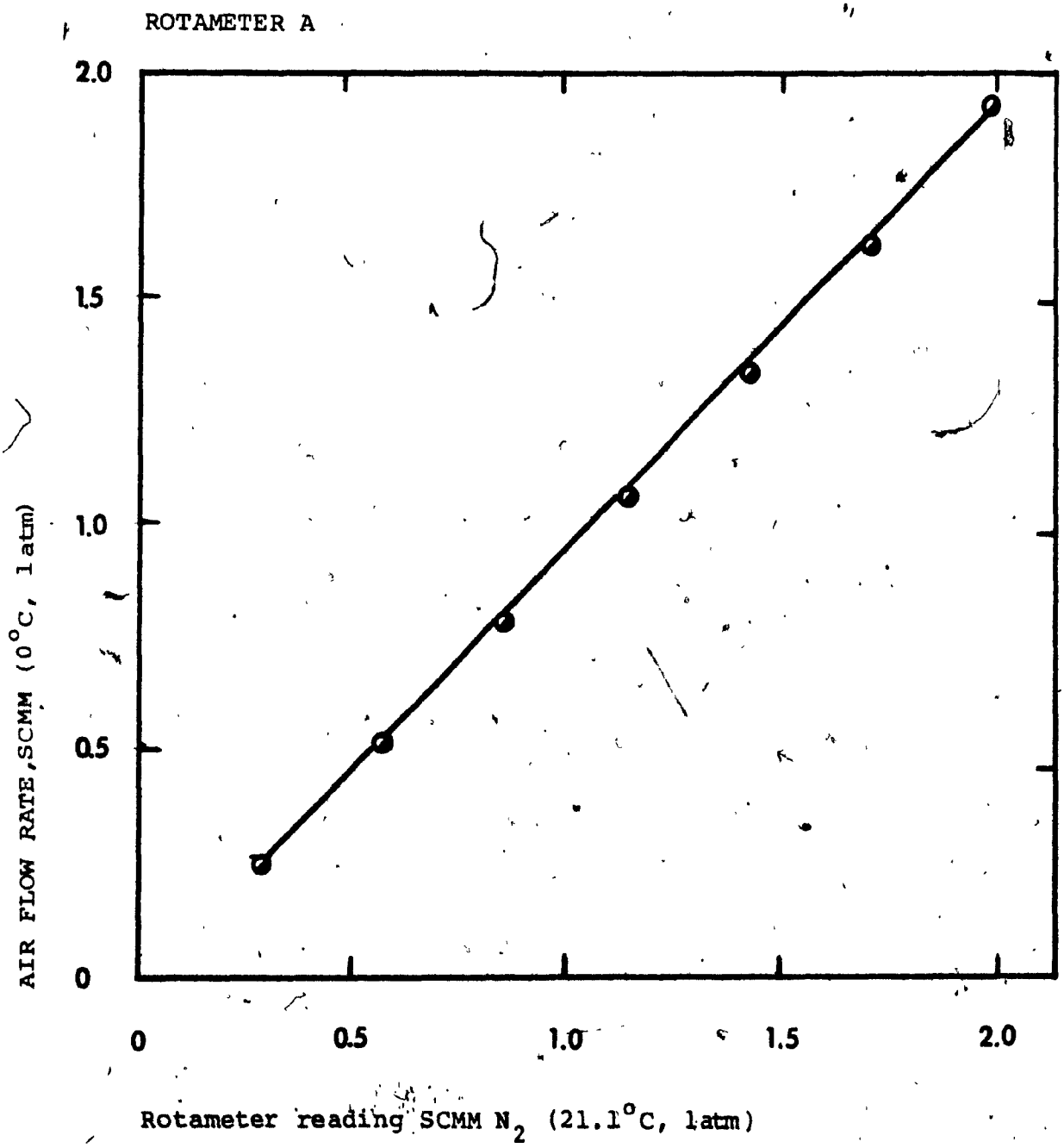

Fig. A.1 Top inlet air flow rate; Calibration curve

Scale reading : (0-100)% of total flow

calibrated with liquid SP.SR.1.0

at 21.1°C, 1 atm.

100% of total flow=9.5 USGPM

For this rotameter it was necessary to convert from liquid to gas flow. The conversion formula for a stainless steel float is:

SCFM Air Equivalent = 4.12x (GPM water SP.GR. 1.0)

at 21.1°C, 1 atm.

For 100% of liquid flow, air equivalant is:

(4.12)(9.5) = 39.14 SCFM=1.11 SCMM

As a result, a side scale should be attached to the tube with a maximum reading of 1.11 SCMM aligned to the 100% reading of the existing scale. Such a side scale was available and its reading was in SCFM of air flow at 70 F and 14.7 psia. This scale was corrected, however, according to Equation A.1:

$$Q_{act} = Q_{sc}\sqrt{\frac{1.0}{P_{act}}} \qquad (A.3)$$

Rotameter C

Manufacturer : Fisher

Float type : 1-GNSVGT 68T60

Scale reading : 0-0.71 SCMM air at 21.1 C, 1 atm.

Correction Formula,

$$Q_{act} = Q_{sc} \sqrt{\frac{1.0}{P_{act}}} \qquad (A.4)$$

The air flow rates of rotameters B and C were combined together and a single calibration curve that indicated the total bottom air flow rate versus the reading of rotameter C was produced, see Table A.2 and Figure A.2.

Side scales were made and affixed on rotameters A and C in order to obtain the direct reading of the top and bottom air flow rates.

ROTAMETERS B and C in Parallel

ROTAMETER SCALE READING, Q_{scale} (SCFM) [70°F, 14.7Psia]		BACK PRESSURE - GAGE (cm Hg)		Q_{act} (CMM)		Q (SCMM) [0°C, 1atm]	
ROT B	ROT C	ROT B	ROT C	ROT B	ROT C	ROT B	ROT C
33.5	37	13.3	13.3	0.87	0.96	0.93	1.05
29.5	33	10.4	10.4	0.78	0.88	0.83	0.92
25.5	29	8.2	8.2	0.69	0.78	0.71	0.80
21.5	25	6.2	6.2	0.58	0.68	0.59	0.68
17.5	21	4.7	4.7	0.48	0.58	0.47	0.57
13.5	17	3.6	3.6	0.37	0.47	0.37	0.46
9.0	13	2.6	2.6	0.25	0.36	0.24	0.35

ROTAMETER C SCALE READING (SCFM), [70°F, 14.7Psia]	37	33	29	25	21	17	13
TOTAL BOTTOM AIR FLOW RATE (SCMM) [0°C, 1atm]	2.0	1.75	1.51	1.27	1.04	0.83	0.59

TABLE A.2 Calibration of Rotameters B and C

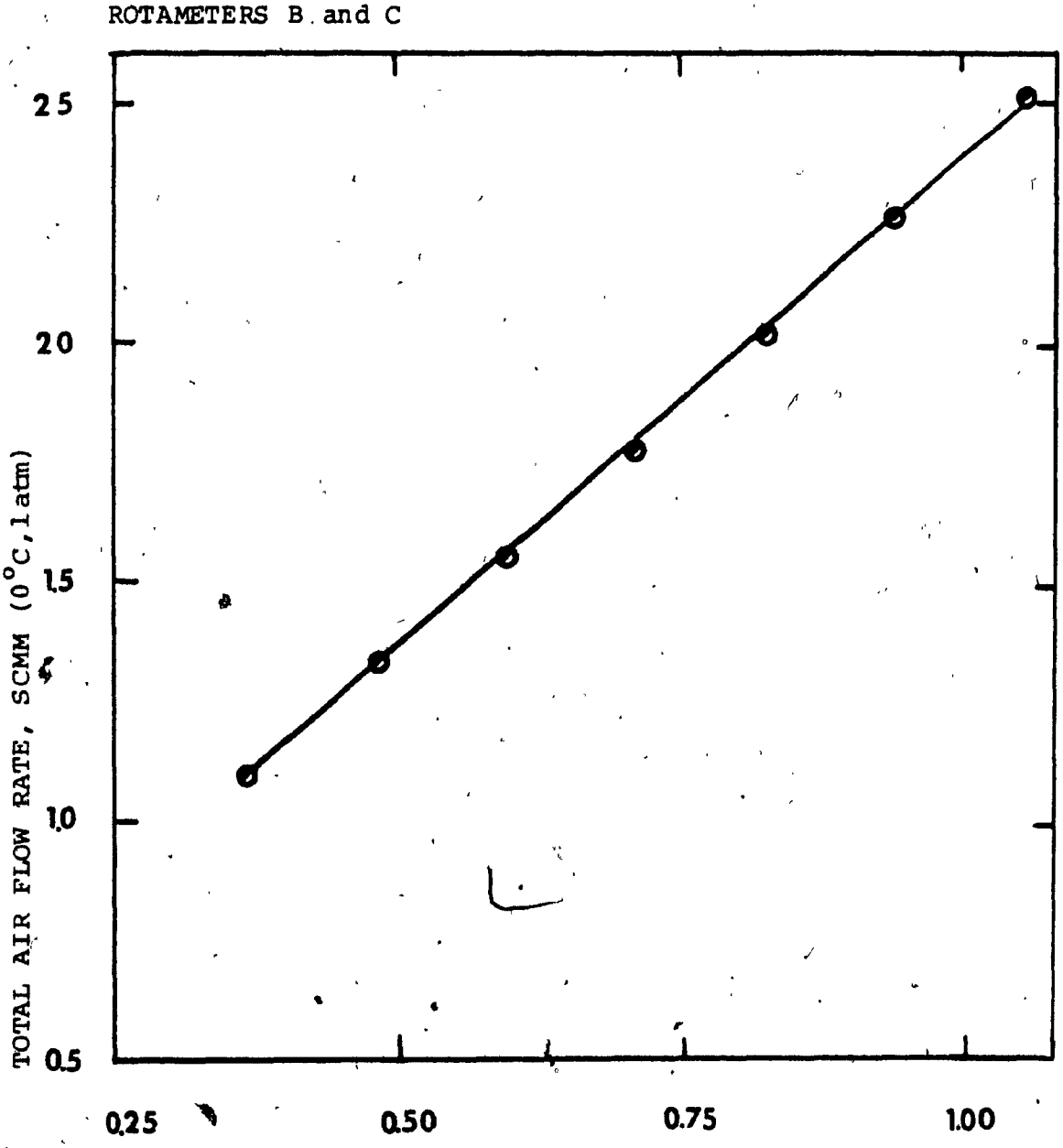

Fig. A.2 Bottom inlet air flow rate; Calibration curve for the combined air flow rate of rotameters B and C

APPENDIX B

```
C*****************************************************************
C*
C*  THIS PROGRAM  PERFORMS THE DATA REDUCTION AND PLOTS THE RESULTS
C*  OF THE EXPERIMENTAL INVESTIGATION IN A  TRANSPARENT CYCLONE CHAMBER.
C*  THE PROGRAM READS THE VELOCITY AND PRESSURE COEFFICIENTS AS WELL AS
C*  THE YAW AND PITCH ANGLES OBTAINED FROM A 5-CHANNEL PITOT-STATIC
C*  PRESSURE PROBE, AND CALCULATES THE VELOCITY COMPONENTS AND THE
C*  STATIC PRESSURE DISTRIBUTIONS WITHIN THE CYCLONE CHAMBER.
C*
C*****************************************************************
      PROGRAM PROBE (INPUT,OUTPUT,TAPE5=INPUT,TAPE6=OUTPUT,
     +VDATA,TAPE4=VDATA)
C===============================================================
C
C                    L E G E N D
C                    -----------
C
C===============================================================
C
C  DATA(J,1)   =  P1-P(ATM)
C  DATA(J,2)   =  P1-P2
C  DATA(J,3)   =  YAW ANGLE
C  DATA(J,4)   =  PITCH ANGLE
C  DATA(J,5)   =  TOTAL PRESSURE COEFFICIENT
C  DATA(J,6)   =  VELOCITY PRESSURE COEFFICIENT
C  DYNAMIC     =  DYNAMIC PRESSURE
C  TOTID       =  P1
C  ZER         =  P1-PT
C  TOTAL       =  TOTAL PRESSURE
C  STATIC      =  STATIC PRESSURE
C  STATG       =  STATIC PRESSURE, GAGE
C  DENSTY      =  DENSITY
C  VELTOT      =  ABSOLUTE VELOCITY
C  VELRAD      =  RADIAL VELOCITY COMPONENT
C  VELTAG      =  TANGENTIAL VELOCITY COMPONENT
C  VELAX       =  AXIAL VELOCITY COMPONENT
C  FLOW        =  VOLUMETRIC AIR FLOW RATE (INTEGRATED FROM
C                 THE AXIAL VELOCITY PROFILE)
C  QACT        =  VOLUMETRIC AIR FLOW RATE AS RECORDED FROM THE ROTAMETERS
C
C===============================================================
      DIMENSION DATA(30,30),DYNMIC(30),ZER(30),TOTID(30),TOTAL(30),
     +STATIC(12),DENSTY(12),VELTOT(12),VELRAD(12),VELTAG(12),VELAX(12)
      DIMENSION STATG(12),STAT(51),SG(51,6),STAT1(51)
      DIMENSION STAT2(51),STAT3(51),STAT4(51)
      DIMENSION STAT5(51),STAT6(51)
      DIMENSION VELT(51),VELR(51),VELA(51),RRRRR(51)
      DIMENSION VELR1(51),VELR2(51),VELR3(51),VELR4(51),
     +VELR5(51),VELR6(51)
      DIMENSION VELA1(51),VELA2(51),VELA3(51),VELA4(51),
     +VELA5(51),VELA6(51)
```

```
      DIMENSION VELT1(51),RRRR(51),VELT2(51),VELT3(51),VELT4(51),
     +VELT5(51),VELT6(51)
      DIMENSION ERAD(6,11),ERADD(12),EVELR(51),EVR(51,6),EVELR1(51)
      DIMENSION EVELR2(51),EVELR3(51),EVELR4(51),EVELR5(51),EVELR6(51)
      REAL RR(11),VT(51,6),VR(51,6),VA(51,6)
C=======================================================================


C  CALCULATIONS AT SIX AXIAL LEVELS OF THE CHAMBER
C=======================================================================
      DO 15 I=1,6
      ER=0.0
      QBOT=100.0
      QACT=1.077*QBOT
      RLGTH=17.62
      PI=2.0*ATAN2(1.0,0.0)
C=======================================================================
C  CULCULATIONS AT 11 OR 23 RADIAL STATIONS AT EACH AXIAL LEVEL
C=======================================================================
      DO 22 J=1,11
      READ (4,20)(DATA(J,L),L=1,6)
      DYNMIC(J)=0.0361*DATA(J,2)*DATA(J,6)
      ZER(J)=0.0361*DATA(J,5)*DYNMIC(J)
      TOTID(J)=(DATA(J,1)+408)*0.0361
      TOTAL(J)=TOTID(J)-ZER(J)
      STATIC(J)=TOTAL(J)-DYNMIC(J)
      STATG(J)=STATIC(J)-(408.0*0.0361)
      DENSTY(J)=(1.584/10000.)*STATIC(J)
      VELTOT(J)=SQRT(288.0*DYNMIC(J)/DENSTY(J))
      VELRAD(J)=VELTOT(J)*SIN(DATA(J,4)/57.296)
      VELTAG(J)=VELTOT(J)*COS(DATA(J,4)/57.296)*SIN(DATA(J,3)/57.296)
      VELAX(J)=VELTOT(J)*COS(DATA(J,3)/57.296)*COS(DATA(J,4)/57.296)
      R=(J)/2.
      RR(J)=R
      ERROR=VELAX(J)*R+ER
      ER=ERROR
   22 CONTINUE
C-----------------------------------------------------------------------
C  CALCULATION OF THE VOLUMETRIC AIR FLOW RATE BASING ON THE AXIAL
C  VELOCITY PROFILE
C-----------------------------------------------------------------------
      ERR=0.5*ERROR+VELAX(1)*0.125**2.
      FLOW=(3.14/144.)*ERR*60.
      PDIFF=ABS(QACT-FLOW)*100./((QACT+FLOW)/2.)
C-----------------------------------------------------------------------
C  NON-DIMENSIONALIZATION OF RESULTS FOR PLOTTING
C-----------------------------------------------------------------------
      IF(I.EQ.1)GOTO 50
      GOTO 70
   50 RNORMS=STATG(11)
      RNORMT=VELTAG(11)
      RNORMA=QACT/(PI*(5.875)**2.0*(1.0/144))*(1.0/60.0)
   70 CONTINUE
      DO 33 K=1,11
```

```
      R=(K)/2.
      STATG(K)=STATG(K)/RNORMS
      VELTAG(K)=VELTAG(K)/RNORMT
      VELAX(K)=VELAX(K)/RNORMA
      VELRAD(K)=VELRAD(K)/(QACT/(2.0*PI*(0.5/12))*(1.0/RLGTH/12))
   33 CONTINUE
C-----------------------------------------------------------------------
C  CUBIC SPLINE METHOD FOR THE INTERPOLATION OF EXPERINENTAL RESULTS
C-----------------------------------------------------------------------
      CALL CUSPLN(11,RR,VELTAG,RRRRR,VELT)
      CALL CUSPLN(11,RR,STATG,RRRRR,STAT)


      CALL CUSPLN(11,RR,VELRAD,RRRRR,VELR)
      CALL CUSPLN(11,RR,VELAX,RRRRR,VELA)
C-----------------------------------------------------------------------
C  PREPARATION OF RESULTS FOR PLOTTING AT SELECTED AXIAL STATIONS
C-----------------------------------------------------------------------
      DO 54 MM=1,51
      VA(MM,I)=VELA(MM)
      VR(MM,I)=VELR(MM)
      VT(MM,I)=VELT(MM)
      SG(MM,I)=STAT(MM)
   54 CONTINUE
      DO 1000 IK=1,51
      VELT1(IK)=VT(IK,1)
      VELT2(IK)=VT(IK,2)
      VELT3(IK)=VT(IK,3)
      VELT4(IK)=VT(IK,4)
      VELT5(IK)=VT(IK,5)
      VELT6(IK)=VT(IK,6)
      STAT1(IK)=SG(IK,1)
      STAT2(IK)=SG(IK,2)
      STAT3(IK)=SG(IK,3)
      STAT4(IK)=SG(IK,4)
      STAT5(IK)=SG(IK,5)
      STAT6(IK)=SG(IK,6)
      VELR1(IK)=VR(IK,1)
      VELR2(IK)=VR(IK,2)
      VELR3(IK)=VR(IK,3)
      VELR4(IK)=VR(IK,4)
      VELR5(IK)=VR(IK,5)
      VELR6(IK)=VR(IK,6)
      VELA1(IK)=VA(IK,1)
      VELA2(IK)=VA(IK,2)
      VELA3(IK)=VA(IK,3)
      VELA4(IK)=VA(IK,4)
      VELA5(IK)=VA(IK,5)
      VELA6(IK)=VA(IK,6)
      RRRRR(IK)=RRRRR(IK)/6.
  100 CONTINUE
C-----------------------------------------------------------------------
   15 CONTINUE
```

```
C-----------------------------------------------------------------
C  READING OF EMPIRICAL RADIAL VELOCITY PROFILES AND
C  PREPARING THEM FOR PLOTTING
C-----------------------------------------------------------------
      READ(4,71)((ERAD(I,K),I=1,5),K=1,11)
      DO 73 I=1,11
 73   ERAD(6,I)=ERAD(5,I)
      DO 74 I=1,6
      DO 76 K=1,11
      R=K/2.0
      ERADD(K)=ERAD(I,K)/(QACT/(2.0*PI*5.815/12)*(1.0/RLGTH/12))
 76   CONTINUE
      CALL CUSPLN(11,RR,ERADD,RRRRR,EVELR)
      DO 77 MM=1,51
 77   EVR(MM,I)=EVELR(MM)
      DO 78 IK=1,51
      EVELR1(IK)=EVR(IK,1)


      EVELR2(IK)=EVR(IK,2)
      EVELR3(IK)=EVR(IK,3)
      EVELR4(IK)=EVR(IK,4)
      EVELR5(IK)=EVR(IK,5)
      EVELR6(IK)=EVR(IK,6)
      RRRRR(IK)=RRRRR(IK)/6.0
 78   CONTINUE
 74   CONTINUE
C-----------------------------------------------------------------
C  PLOTTING OF RESULTS USING PLOTT-10 SUBROUTINES
C-----------------------------------------------------------------
      CALL INITT(120,5,6,0,0)
      CALL BINITT
      CALL NPTS(51)
      CALL STEPS(5)
      CALL SIZES(1.0)
      CALL SLIMX(200,825)
      CALL SLIMY(50,775)
      CALL XFRM(3)
      CALL YFRM(3)
      CALL XMFRM(3)
      CALL YMFRM(3)
C-----------------------------------------------------------------
C  PLOTTING OF STATIC PRESSURE AT SELECTED AXIAL STATIONS
C-----------------------------------------------------------------
      CALL SYMBL(1)
      CALL DLIMY(-1.0,1.5)
      CALL CHECK(RRRRR,STAT1)
      CALL DSPLAY(RRRRR,STAT1)
C     CALL SYMBL(4)
C     CALL CPLOT(RRRRR,STAT4)
      CALL SYMBL(3)
      CALL CPLOT(RRRRR,STAT6)
      CALL FRAME
      CALL TINPUT(IV)
C-----------------------------------------------------------------
C  PLOTTING OF TANGENTIAL VELOCITY AT SELECTED AXIAL STATIONS
C-----------------------------------------------------------------
```

```
      CALL SYMBL(1)
      CALL DLIMY(0.0,2.0)
      CALL CHECK(RRRRR,VELT1)
      CALL DSPLAY(RRRRR,VELT1)
      CALL SYMBL(4)
      CALL CPLOT(RRRRR,VELT3)
      CALL SYMBL(3)
      CALL CPLOT(RRRRR,VELT6)
      CALL FRAME
      CALL TINPUT(IV)
C-----------------------------------------------------------------
C  PLOTTING OF AXIAL VELOCITY AT SELECTED AXIAL STATIONS
C-----------------------------------------------------------------
      CALL SYMBL(1)
      CALL DLIMY(-3.0,3.5)
      CALL CHECK(RRRRR,VELA1)
      CALL DSPLAY(RRRRR,VELA1)
      CALL SYMBL(4)
      CALL CPLOT(RRRRR,VELA4)

      CALL SYMBL(3)
      CALL CPLOT(RRRRR,VELA6)
      CALL FRAME
      CALL TINPUT(IV)
C-----------------------------------------------------------------
C  PLOTTING OF RADIAL VELOCITY AT SELECTED AXIAL STATIONS
C-----------------------------------------------------------------
      CALL SYMBL(1)
      CALL DLIMY(-1.0,1.5)
      CALL CHECK(RRRRR,VELR1)
      CALL DSPLAY(RRRRR,VELR1)
      CALL SYMBL(4)
      CALL CPLOT(RRRRR,VELR4)
      CALL SYMBL(3)
      CALL CPLOT(RRRRR,VELR6)
      CALL FRAME
      CALL TINPUT(IV)
C-----------------------------------------------------------------
C  PLOTTING OF EMPIRICAL RADIAL VELOCITY AT SELECTED AXIAL STATIONS
C-----------------------------------------------------------------
 101  CONTINUE
      CALL SYMBL(1)
      CALL DLIMY(-10.0,10.5)
      CALL CHECK(RRRRR,EVELR1)
      CALL DSPLAY(RRRRR,EVELR1)
      CALL SYMBL(4)
      CALL CPLOT(RRRRR,EVELR4)
      CALL SYMBL(3)
      CALL CPLOT(RRRRR,EVELR6)
      CALL FRAME
      CALL TINPUT(IV)
      CALL FINITT(0,700)
  20  FORMAT(6F10.3)
  71  FORMAT(10X,5F10.4)
      STOP
      END
```

```
      SUBROUTINE CUSPLN(N,X,A,Z,F)
C*********************************************************************
C*
C*     CUBIC SPINE NATURAL BOUNTRY ALGORITHM
C*     CONSTRUCTS THE CUBIC SPINE INTERPOLANT FOR F
C*
C*********************************************************************
C
C                    L E G E N D
C
C*********************************************************************
C
C      F(X)=FUNCTION F IF AVAILABLE
C      XA=ALPHA,XB=B, XU=MU, XZ=Z
C
C*********************************************************************
      DIMENSION X(11),A(12),B(12),C(12),D(12),H(12),XA(12),XB(12)
     1,XU(12),XZ(12),Z(51),F(51)
      M=N-1
      DO 23 I=1,M
23    H(I)=X(I+1)-X(I)
C---------------------------------------------------------------------
C     STEP 1
C---------------------------------------------------------------------
      DO 24 I=2,M
24    XA(I)=3*(A(I+1)*H(I-1)-A(I)*(X(I+1)-X(I-1))+A(I-1)*H(I))/
     1(H(I)*H(I-1))
C---------------------------------------------------------------------
C     STEP 2
C---------------------------------------------------------------------
      XB(1)=1.0
      XU(1)=0.0
      XZ(1)=0.0
C---------------------------------------------------------------------
C     STEP 3
C---------------------------------------------------------------------
      I=2
C---------------------------------------------------------------------
C     STEP 4
C---------------------------------------------------------------------
4     XB(I)=2*(X(I+1)-X(I-1))-H(I-1)*XU(I-1)
      XU(I)=H(I)/XB(I)
      XZ(I)=(XA(I)-H(I-1)*XZ(I-1))/XB(I)
C---------------------------------------------------------------------
C     STEP 5
C---------------------------------------------------------------------
      I=I+1
C---------------------------------------------------------------------
C     STEP 6
C---------------------------------------------------------------------
      IF(I.LT.N) GO TO 4
C---------------------------------------------------------------------
C     STEP 7
C---------------------------------------------------------------------
```

```
      XB(N)=1.0
      XZ(N)=0.0
      C(N)=XZ(N)

C-----------------------------------------------------------------
C     PROCESS IS COMPLETE
C     STEP 8
C-----------------------------------------------------------------
      J=N-1
C-----------------------------------------------------------------
C     STEP 9
C-----------------------------------------------------------------
9     C(J)=XZ(J)-XU(J)*C(J+1)
      B(J)=(A(J+1)-A(J))/H(J)-H(J)*(C(J+1)+2*C(J))/3
      D(J)=(C(J+1)-C(J))/(3*H(J))
C-----------------------------------------------------------------
C     STEP 10
C-----------------------------------------------------------------
      J=J-1
C-----------------------------------------------------------------
C     STEP 11
C-----------------------------------------------------------------
      IF(J.GE.1) GO TO 9
C-----------------------------------------------------------------
C     STEP 12
C-----------------------------------------------------------------
      Z(1)=.50
      KM=0
      DO 1 I=1,10
      DO 2 K=1,5
      KM=KM+1
      F(KM)=D(I)*(Z(KM)-X(I))**3.0+ C(I)*(Z(KM)-X(I))**2.0+B(I)
     +*(Z(KM)-X(I))+A(I)
      Z(KM+1)=Z(KM)+.10
2     CONTINUE
1     CONTINUE
      F(51)=A(11)
      RETURN
      END
```